Characterization of Materials for Civil Engineering
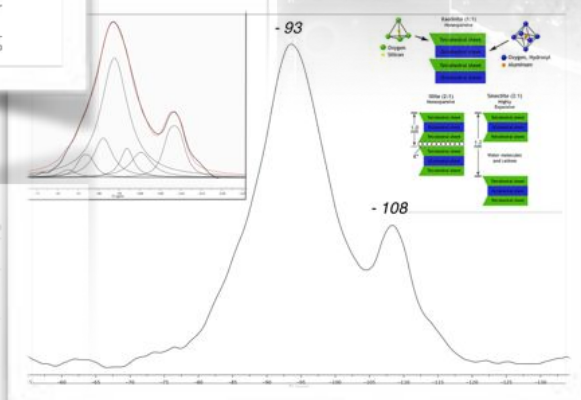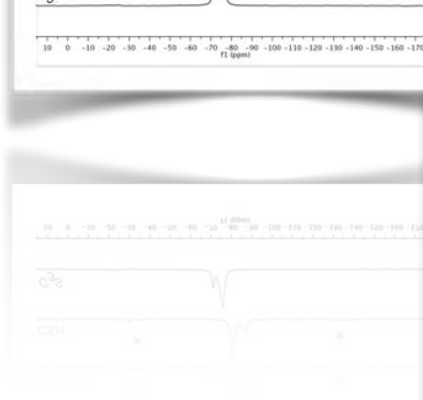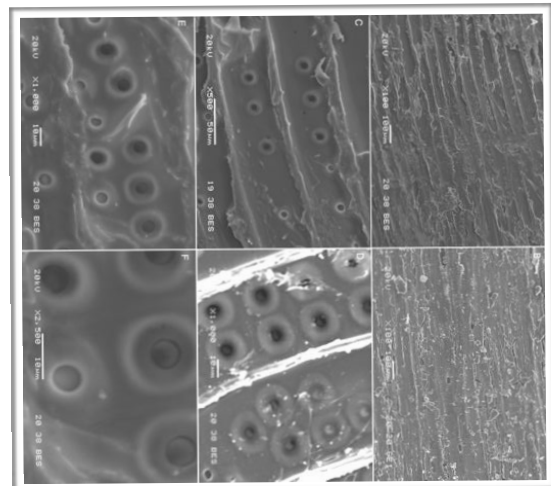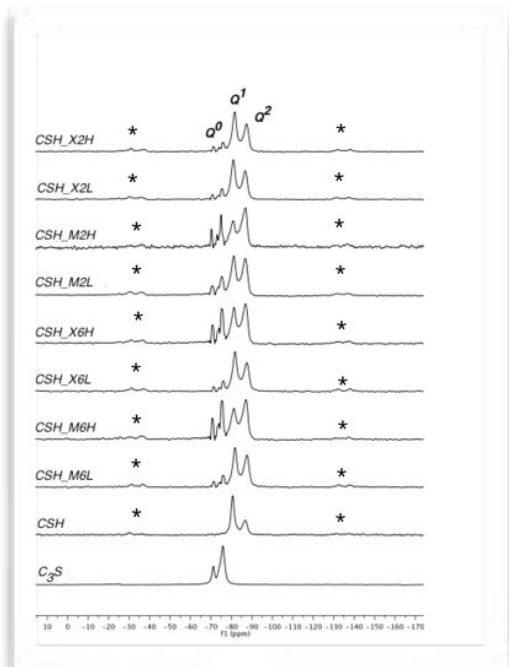
Elisa Cappelletto

CHARACTERIZATION OF MATERIAL FOR CIVIL ENGINEERING

Elisa Cappelletto

E-mail: cappellettoelisa@hotmail.it

Approved by:

Prof. **Rosa di Maggio**, Advisor
Department of Civil, Environmental and
Mechanical Engineering,
University of Trento,Italy.

Ph.D. Commission:

Prof. **Giovanni Straffelini**,
Department of Industrial Engineering
University of Trento, Italy.

Dr. **Michele Remo Chierotti**,
Department of Chemistry
University of Torino, Italy.

Dr. **Paola Fermo**,
Department of Department of Analytical,
Inorganic and Organometallic Chemistry.
University of Milan, Country.

Dr. **Marco Scoponi**,
Institute of Organic Synthesis and
Photoreactivity (ISOF)
CNR, Bologna.

University of Trento,
Department of Industrial Engineering

April 2014

Table of Contents

3. **<u>Solid State NMR characterization of Cement base materials</u>**

LIST OF FIGURES

LIST OF TABLES

X

X

XI

LIST OF ABBREVIATIONS

ATR	*Attenuated Total Reflectance*
APTES	*Aminopropyltriethoxysilane*
C$_3$A	*Tricalcium aluminate*
C$_3$S	*Tricalcium silicate*
CSH	*Calcium silicate hydrate*
C$_4$AF	*Tetracalcium alumino-ferrite*
CIE	*Commission Internationelle Eclairage*
DCA	*Dynamic Contact Angle*
DOC	*Degree of Condensation*
DP	*Degree of Polymerization*
EDS	*Energy-dispersive X-ray spectrometer*
EMC	*Equilibrium Moisture Content*
EtA	*Ethanolamine*
FT-IR	*Fourier Transform Infrared Spectroscopy*
HT-DSC	*High-Temperature Differential Scanning Colorimetry*
M$_2$DES	*Dimethyldiethoxysilane*
M$_3$MES	*Trimethyl monoethoxysilane*
MAS	*Magic Angle Spin*
MBA	*N,N'-methylenebisacrilamide*
MCL	*Mean silicate Chain Length*
MTES	*Methyltriethoxysilane*
MLRav	*Average mass loss rate*
NMR	*Nuclear Magnetic Resonance*
OC	*Occhito sediment*
OPC	*Ordinary Portland Cement*
PAA	*Poly(amidoamine)*
PCEs	*Polycarboxylic esters*
PFOS	*Perfluorooctyltriethoxysilane*
PhTES	*Phenyltriethoxysilane*
RA	*Arithmetic Average*
RH	*Relative Humidity*
SA	*Sabeta sediment*
SEM-EDS	*Scanning electronic microscopy with Energy-dispersive X-ray spectroscopy*
SP	*Single Pulse*
TEOS	*Tetraethoxysilane*
THR	*Total Heat Released*
T.I.	*Time of ignition*
TFPS	*Trifluoropropylehoxysilane*
VIECA	*Vibrationally Induced Equilibrium Contact Angle*
XRD	*X-ray Diffraction*

Declaration for a thesis with publication

This thesis contains four publications. The PhD student's scientific contribution is summarized below.

	Title	Authors	Journal	PhD student's contribution
1	**Hydrophobic siloxane paper coatings: the effect of increasing methyl substitution**	**Elisa Cappelletto**, Emanuela Callone, Renzo Campostrini, Fabrizio Girardi, Simona Maggini, Claudio della Volpe, Stefano Siboni, Rosa Di Maggio.	*Journal of Sol-Gel Science Technologies*	The PhD student prepared the samples and conducted the following analyses: SEM, FT-IR, NMR, contact angle measurement, colorimetric testing of samples. The PhD student wrote the article. The co-authors contributed to the article with corrections and advice
2	**Wood surface protection with different alkoxysilanes: a hydrophobic barrier**	**Elisa Cappelletto**, Simona Maggini, Fabrizio Girardi, Giovanna Bochicchio, Barbara Tessadri, Rosa Di Maggio	*Cellulose*	The PhD student prepared the samples and conducted the following analyses: SEM, FT-IR, NMR, contact angle measurement. The PhD student wrote the article. The co-authors contributed to the article with corrections and recommendations
3	**Comb-Shaped Polymers as Nanostructure Modifiers of Calcium Silicate Hydrate: A ^{29}Si Solid-State NMR Investigation**	**Elisa Cappelletto**, Silvia Borsacchi, Marco Geppi, Francesca Ridi, Emiliano Fratini, Piero Baglioni	*Journal of Physical Chemistry C*	The PhD student conducted NMR investigations and wrote a large part of the article.
4	**Thermally treated clay sediments as geopolymer precursors**	B. Liguori, Claudio Ferone, Irene Capasso, F. Colangelo, R. Cioffi, **Elisa Cappelletto**, Rosa di Maggio	*Applied Clay Science*	The PhD student conducted NMR analyses and contributed to the writing of the article.

CHAPTER I

1. General Introduction

Materials are the heart of engineering, which can be defined as the creative and rational use of materials for practical purposes. Materials have had an essential role in the development of civil engineering: from the beginning of human evolution, man has used many different materials to build houses, bridges, roads and countless other structures to make his life easier. Ancient populations used the raw materials at their disposal, such as stone, clay and timber. Over the centuries, the search for new materials became increasingly important to respond to changing human needs, and men learned how to use clay to form artificial stones, cements and concretes, for instance. While hands-on familiarity rooted in tradition and crafting expertise initially drove these human activities, in modern times the need for a scientific understanding of materials prompted the birth of the *material science* discipline. Material science studies the composition, behavior and properties of materials to solve problems associated with their use. Engineering and material science work together to create functional, durable and beautiful structures.

Among the materials used in civil engineering constructions, wood and cement have had the most important role over the centuries and they are still the main components of our infrastructures.

Timber was used as a building material even by primitive man, and a few ancient temples, palaces and bridges built of wood can still be seen today. In the 20th century, although materials such as concrete had become competitive, wood retained its significant role in building. The main problem with the use of wood as a construction material concerns its possibly limited lifetime. Wood is characterized by a limited resistance to moisture and fire, the two elements responsible for the destruction of most wooden buildings in the past.

Cement, and consequently concrete, is the most often used material today. The term "cement" is now used to mean a modern binder, the so-called Portland cement, patented in England in 1824. Similar binding materials were already being used from very early on ancient Mesopotamia, Egypt, Greece and Rome. Modern cement formulations have changed a great deal and can be adapted to their intended use and the surrounding environment.

This thesis is divided into two main parts. The first part (Chapter II) deals with the study of protective treatments for cellulosic materials. The aim is to investigate different treatments and, after broadly characterizing them, to suggest the system capable of improving the durability of the material.

In the second part (Chapter III), two different cementitious formulations are studied using Nuclear Magnetic Resonance (NMR) spectroscopy. In the first case, the aim is to study changes in the nanostructure due to the use of certain additives; in the second, the focus is on the formation of a geopolymer suitable for use as an alternative binder in concrete blends.

CHAPTER II

Characterization of Coatings for cellulose base materials

2.1 Introduction

Wood has many excellent properties, such as a high tensile strength, a high elastic modulus and an aesthetically pleasing appearance, and it has consequently been used in many applications. But it also has various disadvantages due to its organic nature: it can be destroyed by the long-term effects of oxygen, light and water under atmospheric conditions. Only few old wooden buildings have survived to the present day. Wood consequently needs to be modified to enhance its durability.

This chapter starts with a brief overview on the structure and properties of this material, which is necessary to clarify the mechanisms of wood degradation. The state of art in the field of wood protection is outlined in the section *Wood modification: treatments to improve the properties of wood*. After these general considerations, the protective systems studied for this thesis are presented in the *Wood modification with alkoxysilanes* and subsequent sections.

Chapter II is completed with two articles published in scientific journals:

1) *Hydrophobic siloxane paper coatings: the effect of increasing methyl substitution*, Sol-gel Technologies (2012).

> This research work was financed by a Provincia Autonoma di Trento project, PAT-CENACOLI (Nanostructured metal oxide and inorganic-organic hybrid coatings for cellulose and lignin, paper and wood, for preservation against fungi and chemical attack, and as a flame retardant).
>
> Protective treatments were initially applied to pure cellulose, which is the main component of paper and wood, and an extensive characterization of these samples led to the choice of the best treatments to apply to wood, which is a more complex system.
>
> The results obtained with other treatments are presented here for the first time (*fluorinated and phenyl functionalized coatings*).

2) *Wood surface protection with different alkoxysilanes: a hydrophobic barrier, Cellulose (2013)*

> *Leaching and biological testing* are discussed here for the first time.

The chapter includes the NMR study of a new system for protecting wood patented by Prof. Predieri's research group.

2.2 Wood cell structure and chemical composition

The structure of wood can be examined on different levels, from the macroscopic to the microscopic. We focus on the cellular structure and chemical composition of wood. The cell wall of wood is composed of a number of layers classed as primary (P) and secondary (S) layers. The secondary layer is further divided into layers S1, S2 and S3. The primary layer consists of microfibrils, which are essentially randomly oriented. The secondary layer forms subsequently, with each of the sub-layers exhibiting different patterns in the way the microfibrils are oriented. The space between the microfibrils is occupied by hemicelluloses and lignin (Figure 1).
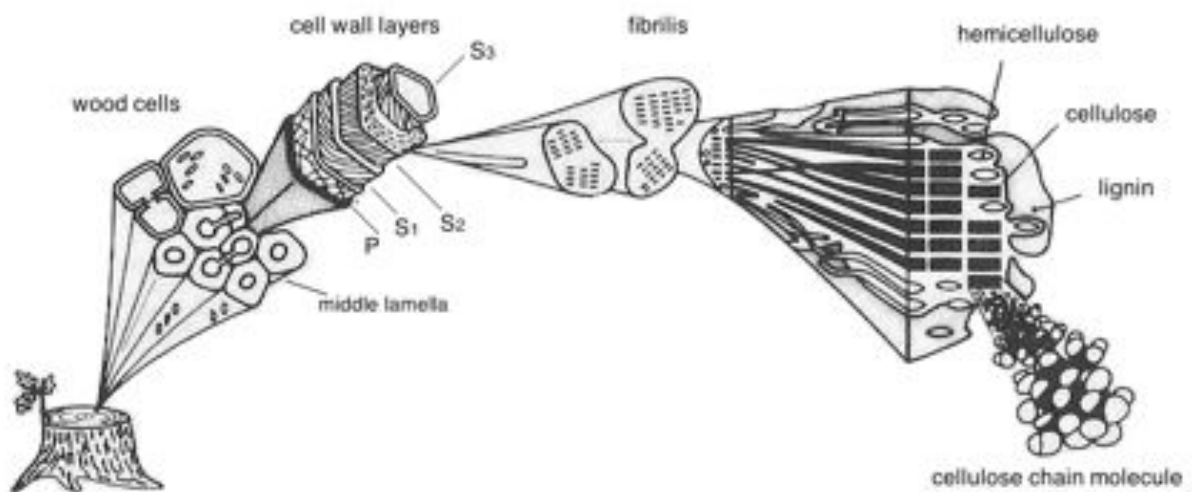
Figure 1. A schematic of the structure of the wood cell wall, showing the middle lamella, the main cell wall layers and the associated micro fibrillar orientation.

Many of the properties of wood are determined by its polymeric chemical constituents, which vary depending on tree species, geographic location, climate and soil conditions. Wood is essentially composed of cellulose (from 40 to 55% of the total cell wall mass), hemicelluloses (25-40%), lignin (18-33%), and extractives (<10%).

Cellulose is a linear polymer formed by linear chains of D-glucose linked by ß-1,4-glycoside bonds (Figure 2). The degree of polymerization in wood (the number of glucose units per cellulose molecule) ranges between 8000 and 10000, depending on the species [**Campanella** (2007)]. Cellulose has a strong tendency for the hydroxyl groups of adjacent chains to form intermolecular hydrogen bonds, which give rise to the highly-ordered arrangement of molecular chains in microfibrils and fibrils (crystalline structure).

Crystalline regions alternate with amorphous ones, and the non-crystalline zones absorb more water than the crystalline areas because they contain more hydroxyl groups with no intermolecular linkage.
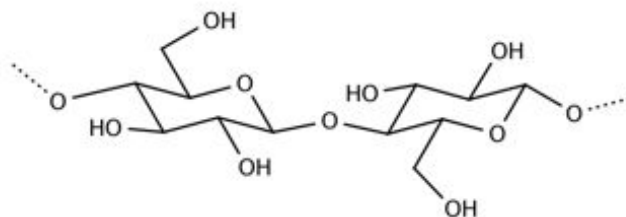
Figure 2. The molecular structure of cellulose, cellobiose.

Like cellulose, hemicelluloses are polysaccharides, but they are composed of a number of different sugar units. The hemicelluloses are generally less ordered than cellulose, and some of the OH groups are naturally acetylated (Figure 3). Because of the generally amorphous nature of hemicelluloses, they react more readily and are less thermally stable than cellulose or lignin.
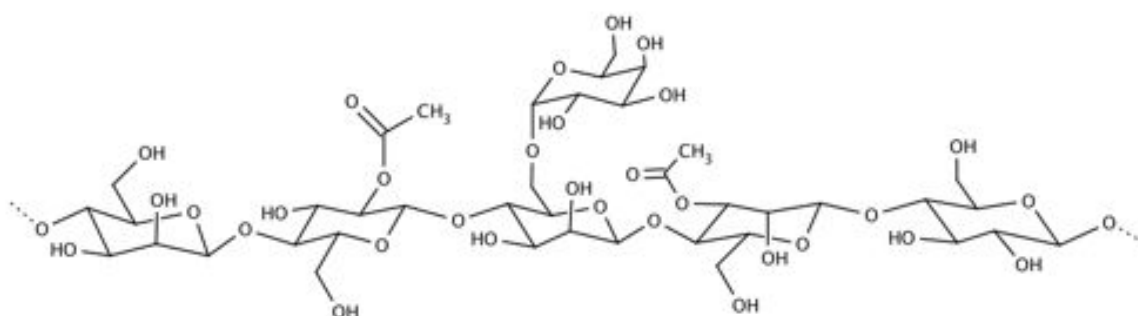
Figure 3. The molecular structure of a hemicellulose (O-acetylgalactoglucomannan).

Lignin is a highly amorphous phenolic polymer of indeterminate molecular weight. Polymerization of the phenylpropane monomer units (p-coumaryl alcohol, coniferyl alcohol, and sinapyl alcohol) (Figure 4) produces a random three-dimensional network via a free-radical mechanism.
There is no definitive structure to lignin. This polymer is responsible for cell wall stiffness and also serves to bond individual cells together in the middle lamella region. Lignin has a lower OH content than the polysaccharide components.
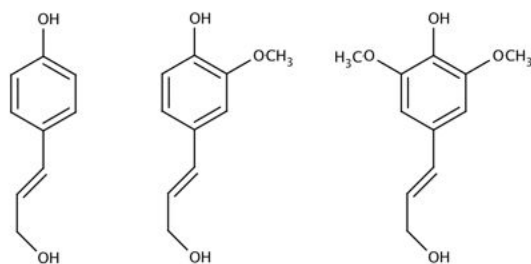
Figure 4. The molecular constituents of lignin: p-coumaryl alcohol, coniferyl alcohol, and sinapyl alcohol.

Extractives are low-molecular-weight organic substances that can be extracted from wood using solvents. They can influence the wood's color, hydroscopicity, smell and strength. Conifer extractives are divided into three categories: terpenoids, fatty acids and phenolic compounds.

2.2.1 *Larix decidua Mill* and *Pinus sylvestris L.* characteristics

Two different tree species were considered in the present work, *Larix decidua Mill.* and *Pinus sylvestris L.* Both species belong to the Pinophyta division, which includes the majority of trees commonly known as conifers. Most conifers are evergreen trees and shrubs, with the exception of four genera, including Larch (*Larix*), which lose their leaves in autumn (deciduous conifers). The wood of conifers is known as softwood. The genus *Larix* includes ten species that are widely distributed across the cooler regions of the northern hemisphere. Larch was already used as a construction material in Ancient Rome and it is still used extensively in the building industry (to build houses, roofing, bridges, etc.). This wood is usually appreciated for its good mechanical properties and its appealing color and texture, as well as for the durability of its heartwood. European larch has a marked genetic variability due to its wide distribution and this is reflected in highly variable wood properties. In general, the genus has a high content of extractives in its heartwood, the concentration of which correlates strongly with its resistance to decay. Treatments were performed on *Larix decidua* (European Larch) from the Trentino Alto Adige (Italy): this wood has a lower concentration of phenolics and lignin than other larch species. *Larix decidu*a from the Southern Alps is quite stiff.
Pinus sylvestris L. (Scots pine, from Val di Susa, Italy) was used for fire resistance tests, as required by the standards. Timber from Scots pine is widely used as softwood in buildings in Nordic countries. Its heartwood is classified as moderately-to-weakly resistant to decay, while the sapwood is classified as perishable.
The treated wood blocks were obtained from sapwood, as is usually recommended by the European standards for assessing the efficacy of preservatives. Sapwood is less durable than heartwood.

2.3 Wood properties

Wood is characterized by a great variability in its properties, which differ from one tree species to another and also within a given tree. This can pose some problems when it comes to studying the material.

2.3.1 The wood-water relationship and dimensional stability

Wood is a hygroscopic material due to the hydroxyl groups of the polymeric constituents. Wood responds to its environment, changing in dimension in response to changes in atmospheric relative humidity (RH). Dry wood absorbs moisture until it is in equilibrium with the surrounding atmosphere, while saturated wood placed in an atmosphere with a lower RH loses moisture until equilibrium. The flux of water molecules through the cell wall causes dimensional changes that are anisotropic and greatest in the tangential direction. Dimensional instability can cause problems when wood is used in service situation for structural purposes, so the purpose of wood modification is often to improve the dimensional stability of the natural material.

2.4 Wood degradation

Natural wood exposed to adverse conditions can be degraded by several factors, including humidity, ultraviolet energy, heat, fungi and insects.

2.4.1 Abiotic degradation

In general, wood exposed to outdoor climate is liable to complex combinations of chemical, mechanical and energy reactions.
When wood is used outdoors, its moisture content changes with variations in the humidity and temperature of the environment. This process can be reversed, and alternate cycles of shrinking and swelling can cause cracking in the material. Wood is liable to degradation by the UV component of the solar spectrum; phenolic hydroxyl groups, the aromatic skeleton, double bonds and carbonyl groups are all good light absorbers. Combined with moisture, temperature and oxidative agents, UV light contributes to depolymerizing both lignin and cellulose [**Evans** (1992)]. This degradation can causes discoloration, surface roughening and an increased susceptibility to other degradation phenomena.

2.4.2 Biological degradation

Wood is susceptible to degradation by biological organisms such as insects, fungi, molds and bacteria. Microbiological attacks occur when the conditions are right. Fungi, for example, degrade wood in the

presence of water, oxygen and a source of nutrients, by generating enzymes that disrupt the cell wall polymer components. These enzymes can be divided into two main families: polysaccharide-degrading enzymes and lignolytic enzymes. Fungal attacks are distinguished as brown, white and soft rot, according to the appearance of the wood after degradation. Bacteria can degrade wood in wet or moist conditions, while insects can attack wood even if it has a low moisture content.

2.5 Wood modification: treatments for the improvement of wood properties

Wood is a perishable material, so treatments are needed to enhance its longevity in service. The term "wood modification" can be applied to all processes involving the action of a chemical, biological or physical agent on the material with a view to enhancing its properties.

The aim of these treatments is to improve its resistance to decay or dimensional stability, or to protect it against ultraviolet light.

In the past, such undesirable properties of the natural material as dimensional instability or biodegradation were overcome by using the more durable tropical hardwoods, thereby contributing to tropical deforestation. With the declining availability of naturally durable species, the industry has begun to use less durable raw materials, and consequently to apply protective treatments. The modern timber preservation industry began to develop in the Thirties of the Nineteenth century when Berthell developed a method for the impregnation of timber under pressure using creosote and tar oil [**Hill** (2007)]. This solution was used to treat sleepers and poles for the rapidly-expanding railway industry. The real breakthrough came in the 20th century, however, with the development a very broad spectrum of preservative systems. In the last fifty years, wood modification has been the object of a great deal of academic research. In recent years, more attention has been paid to environmental issues and health, and laws have been passed to regulate the use of certain toxic substances in wood-preserving treatments. In fact, hazardous agents were long used in this field, beginning in the 1930s when copper-chrome-arsenic (CCA) systems were widely employed for their excellent preservative properties, but such treatments release arsenic and chromium into the environment, becoming dangerous for people exposed to them. Nowadays, systems containing toxic metals are being banned, or their use is being restricted, and the trend of wood preservation methods is moving towards the use of low-toxicity metals and chlorine-free organic biocides.

As mentioned earlier, research on protective treatments for wood has increased considerably, on both the academic and the industrial fronts, in the last century. This has led to the development and use of a number of systems that can be classified in different ways. In general, the modifications obtained can be defined as "active" or "passive", the former involving changes to the chemical nature of the wood, while the latter does not alter the material's chemistry. The different methods can also be classified according to the part of the wood affected by the treatment, which may be confined to the surface or completely impregnate the wood's

structure (bulk modification). Surface modifications can involve applying a chemical, physical or biological agent to the wood's surface to obtain a desired improvement in performance. Surface coatings, e.g. varnishes, waxes or natural oils, have been used since ancient times. Penetrating treatments can be troublesome due to the difficulty of ensuring that the reagent is evenly distributed throughout the material. These systems impregnate the bulk material with a chemical, or a combination of chemicals, that then reacts to form a material that is locked within the cell walls. Unlike surface modification, a good impregnation treatment requires the use of pressure (vacuum) to ensure the penetration of the reactants inside the intracellular spaces. There is not necessarily a clear separation between surface and penetrating methods, however, and the same chemical agents have often been used in both cases.

Most of the treatments cited in the literature are "active" chemical modification methods, in which case chemical reagents are applied that react with the wood's polymeric constituents through a covalent bond (the reaction involves the hydroxyl groups of the cell wall polymers). To be effective, it is essential for the chemical treatments to be non-leachable in service conditions.

In recent years, a great variety of compounds have been used for wood modification, including anhydride, acid chlorides, carboxylic acid, isocyanate, aldehydes, lactones and epoxides [**Militz** (1997), **Norimoto** (2001), **Donah** (2004)]. These processes involve the use of reagents, solvents or catalysis that are not easy to handle on a large scale, hindering their commercialization in many cases.

The most effective technologies used are heat treatment, acetylation, furfurylation, and treatments with silica, silicones and silanes. The thermal modification of wood has long been recognized as a potentially useful method for improving its dimensional stability and increasing its resistance to decay. Chemical changes to the wood's structural polymers due to heat treatments include, for instance, an increase in the relative amount of crystalline cellulose and lignin bond rearrangements, with the subsequent formation of a more condensed structure. This process improves the material's dimensional stability and makes it less hygroscopic, but heat-treated wood also suffers a loss of mechanical strength, and impact and abrasion resistance, so it is not suitable for some applications. Thermal wood modification has nonetheless been successfully commercialized in Europe for decades, e.g. ThermoWood, the registered trademark owned by the Finnish ThermoWood Association (Finland).

Acetylation consist in the substitution of wood hydroxyl groups with acetyl hydrophobic groups, thereby reducing moisture content exchange because acetylated wood is far less susceptible to shrinkage and swelling in the presence of varying atmospheric conditions. Acetylation has also proved effective in protecting against biodegradation and weathering. This process has some disadvantages, however, relating to reaction variables that affect the reproducibility of the results, i.e. sample pre-treatment, reaction medium, temperature, pressure and clean-up procedure (in this reaction, acetic acid is produced as a by-product and it is important to remove this as well as any unreacted acetic anhydride at the end of the process). Wood acetylation is a rather complex process and, together with its high cost (it is more expensive than other wood modification processes), this has delayed its commercialization. **Evans** (2003) and **Kiguchi** (1995) cited a commercial acetylation process developed by the Daiken Wood Industry of Japan (the product was called alpha-Wood), and a UK company has been working to develop wood acetylation on a large scale in recent years [**Hill** (2007)].

Wood treatments based on nanoparticle silica sols (nanosols) have recently been developed and there are some interesting publications on the modification of wood with silica compounds [**Mai** (2004), **Malthing** (2008)]. Wood treated in this way shows a better resistance to liquid water sorption, photochemical degradation [**Temiz** (2006)], and combustion [**Yamagushi** (2002)].

As for the use of biocides, the list of lawful treatments has changed drastically in the last few years. In the past, the main active ingredients of preservative formulations were: mercury, copper, arsenic, organometal compounds, carbamates and benzimidazole derivatives [**Shultz** (2008)]. Most of these chemicals have now been banned by the European Community because of their persistence in the environment and high toxicity for the human body. Some copper compounds, quaternary ammonium compounds, and boron compounds are still allowable in certain concentrations. Since the introduction of these restrictions, the use of silver-based systems has been encouraged, as they are safe and cost-effective preservatives. Several studies have demonstrated that silver ions are selectively toxic for certain classes of microorganism (prokaryotic) [**Bae** (2010)].

2.5.1 Wood modification with alkoxysilanes

The chemicals investigated in this research work were chosen with a view to improving the hydrophobic behavior of wood. The surface wettability of wood is a crucial issue, especially when the material is exposed to the outdoors. As mentioned previously (see the sections on "*The wood-water relationship and dimensional stability*" and *"Abiotic degradation"*), one of the drawbacks of wood is its dimensional instability under different humidity conditions, and its hydrophilic behavior is due to the hydroxyl groups of the constituent polymers. In addition to posing problems of shrinkage and swelling, the moisture content also influences the material's resistance to decay, which is better when the moisture content is lower [**Hill** (2007)], and this joins forces with other factors in degrading the natural material. Treatments that modify the hydrophilic behavior of wood are very important.

Silicone polymers have been studied with a view to changing the wettability characteristics of wood [**Sebe** (2001)]. Silicones consist of alternating silicon-oxygen-silicon chains, with various organic substituents attached to the silicon atoms and reactive groups situated at the ends of the chain (Figure 5).
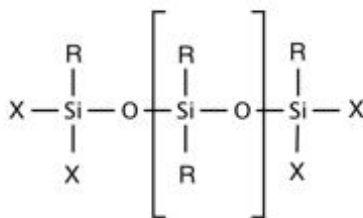
Figure 5. The generic structure of a silicone.

Water-based silicone systems have already been applied to concrete since the 1960s. Taking this into account, **Hager** (1995) and **Lukowsky** (1997) treated wood with silicone microemulsions and found that a good water repellency could be achieved. The disadvantage of these systems is a high molecular weight, which precludes any possibility of cell penetration.

The organosilanes investigated in this thesis have two different kinds of organic group attached to the silicon atom. Some are "inert", while the others may react with the cell wall polymers, with other silane molecules or with co-additives [**Militz** (2004)]. Hydrolysis of the alkoxy groups produces silanols, which then react with the cell wall (Figure 6).

In the literature there are several reports on the use of organosilane compounds to protect wood; methyltrimethoxysilane, tetraetyoxysilane, n-propyltrimethoxysilane, vinyltrimethoxysilane, 3-isocianatopropyltriethoxysilane are just some of the most studied options [**Saka** (1992), **Hill** (2004), **Goethals** (1994)]. These studies have generated conflicting results, probably due to the different treatment protocols used.
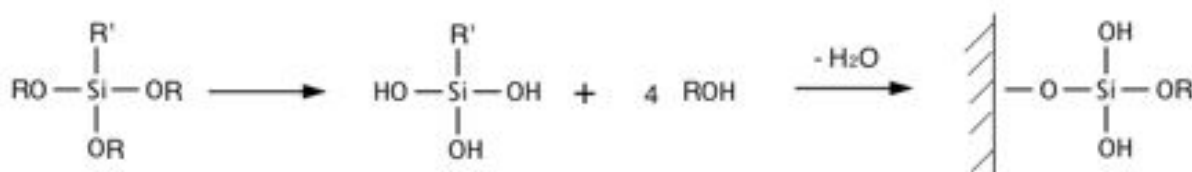
Figure 6. The proposed reaction of a hydrolyzed mono-organo trialkoxysilane with cell wall polymers, R' is an inert organic group.

Organosilanes have been used in aqueous solutions, or dissolved in alcohol or other solvents such as acetone. These chemicals have been applied to surfaces or used as impregnating agents, and using wood samples that have undergone different pre-treatment, i.e. silanes have been applied to blocks conditioned in a controlled-humidity environment or to wet wood. Some studies also report using thermal treatments after their application (curing process). The above-cited works focused mainly on the degree of penetration of the reagents and their ability to reduce the treated surfaces' hydrophobicity. Generally speaking, the chemicals penetrate deeper into the cell walls if the wood is conditioned, in which case organosilanes are able to improve some physical properties of the wood, such as water repellency [**De Vetter** (2010)], photochemical degradation, weathering [**Donath** (2007)] and shrinkage [**Donath** (2004)].

Despite the abundance and variety of the bibliography, no in-depth studies have been conducted to analyze the use of protective treatments. In the present work, different organofunctionalized alkoxysilanes were investigated at macroscopic and microscopic level to study the final performance with changing the hydrophobic group (Table 1).

Abbreviation	Chemical	Formula
T	Tetraethoxysilane	$Si(OC_2H_5)_4$
M	Methyltriethoxysilane	$CH_3Si(OC_2H_5)_3$
M2	Dimethyldiethoxysilane	$(CH_3)_2Si(OC_2H_5)_2$
M3	Trimethylethoxysilane	$(CH_3)_3Si(OC_2H_5)$
PFOS	1H,1H,2H,2H-Perfluorooctyltriethoxysilane	$C_{14}H_{19}F_{13}O_3Si$
TFPS	(3,3,3-Trifluoropropyl)trimehoxysilane	$C_6H_{13}F_3O_3Si$
PhTES	Phenyltriethoxysilane	$(C_6H_5)Si(OC_2H_5)_3$

Table 1. List of the precursors.

The chemicals can be divided into three families according to the nature of their hydrophobic (inert) group, i.e. methyl, fluoroalkyl and phenyl functionalized silanes. These precursors were polymerized using a sol-gel method and deposited on the surface of wood blocks using dip-coating process.

2.5.1.1 Sol-gel deposition of alkoxysilane coatings

The alkoxysilane monomers can be polymerized by means of the sol gel process, which is widely used to make advanced materials in a variety of shapes: porous structures, thin fibers, dense powders and thin films. Sol-gel technology has a long history; the first treatments date back to the 1930s, when Geffcen and Berger used a sol-gel process to deposit oxide layers on industrial glass. Several sol-gel processes have been proposed over the years, but the use of this technology began to grow exponentially as of the early 1980s. The first International Conference on Glasses and Glass Ceramics Obtained from Gels was held in Padova, Italy in 1981. The development of this technology is still far from complete, and the opportunities for varying the parameters and precursors enable a wide range of materials to be obtained. In recent decades, the scientists' attention has focused on developing organic-inorganic hybrid or nanostructured materials.

In general, the sol-gel process implicates the transition of a solution from a liquid "sol" (a stable dispersion of colloidal particles or polymers in a liquid medium) into a solid "gel" phase (a three-dimensional continuous network enclosing a liquid phase) (Figure 7). The sol-gel method can be divided into the following steps: a) preparing a homogeneous solution either by dissolving precursors in a solvent (an organic solvent and/or water; b) adding a suitable reagent (water with or without an acid/base) to convert the homogeneous solution into a sol; c) aging with the formation of the gel; c) shaping; and v) thermal treatment or sintering.

Sol-gel processes can be classified by: a) the use of water (aqueous or non-aqueous sol-gel processes); b) the nature of the precursors (inorganic metal salts, metal organic compounds, or transition metal oxides); c) the drying process used (aerogels are obtained in hypercritical conditions, xerogels in ambient conditions) (Figure 7).
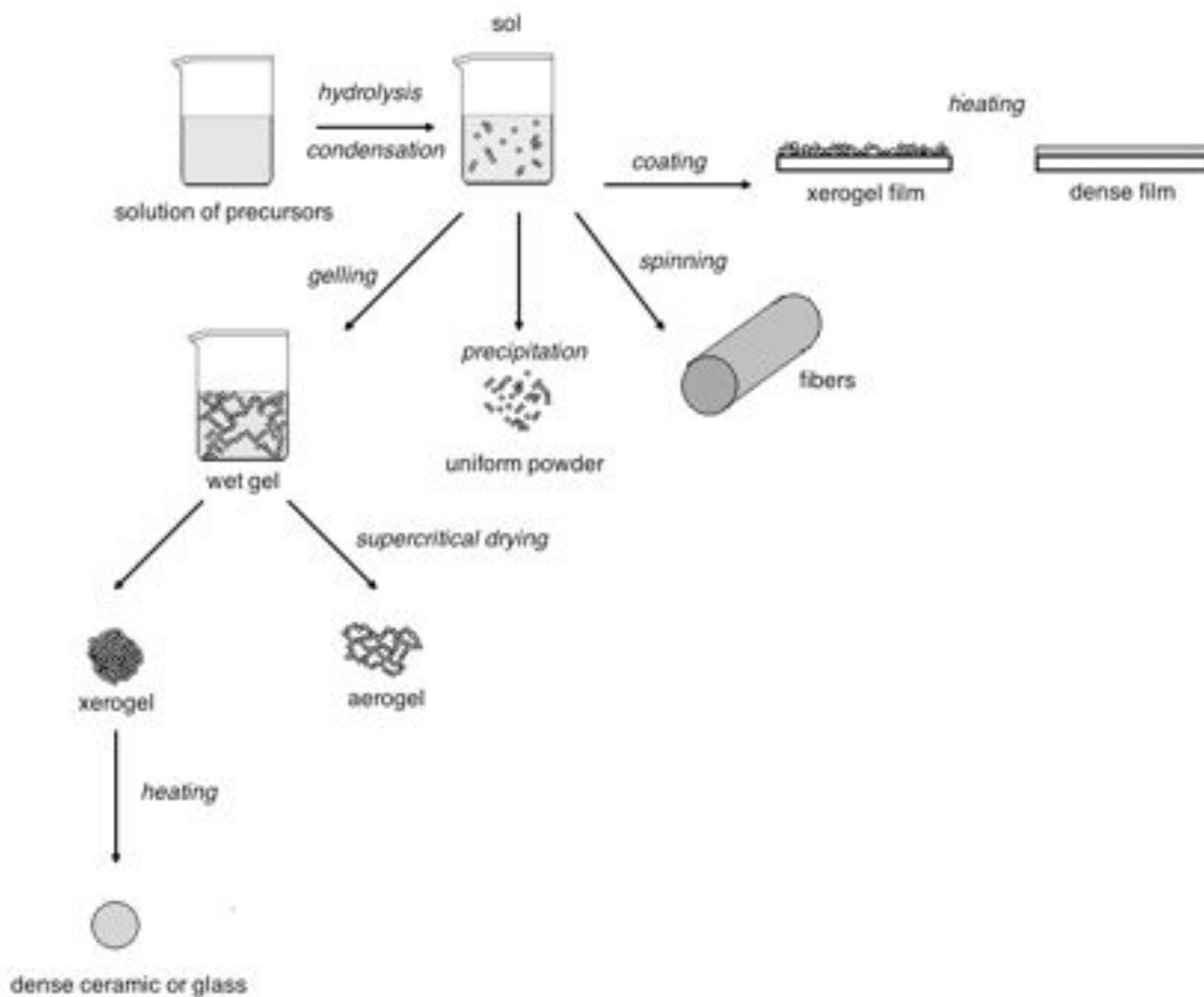
Figure 7. Various steps in the sol-gel process to control the final morphology of the product.

In this thesis, surface treatments were produced using a sol-gel process starting from different organofunctional alkoxysilanes. The sol-gel conversion involves two main reaction types: hydrolysis and condensation (Figure 8).

During hydrolysis, the alkoxide groups (-OR) are replaced under the nucleophilic attack of the oxygen atom in a water molecule, with the release of alcohol and the formation of a hydroxide. Subsequent condensation reactions involving the silanol groups produce siloxane bonds (Si-O-Si). Because the water and alkoxysilane

are immiscible, an alcohol is normally used as a homogenizing agent; we added ethanol to our formulation. The amount of water added in the hydrolysis step determines whether or not the alkoxides are completely hydrolyzed, and which oligomeric intermediate species are formed. The amount of water also strongly influences the hydrolysis and condensation kinetics, e.g. the gelling time decreases with a lower water content: TEOS [**Milea** (2011)]. In the present work, water was added in stoichiometric amounts vis-a-vis the ethoxy groups (OEt/H_2O = 1) to ensure their complete hydrolysis.

The pH of the solution and the type of catalyst influence sol-gel synthesis [**Brinker** (1988)]. Acid catalysis is characterized by a rapid hydrolysis step, with the formation of linear molecules (chain polymers) and microporous gels (pores < 20 Å). Under alkali-catalyzed conditions, the condensation step is faster than hydrolysis, and spherical particles and mesoporous gels (pores > 20 Å) are obtained. The rate of silicon alkoxide hydrolysis is lowest at pH = 7 and increases exponentially at both lower and higher pH, in contrast with the rate of condensation, which is lowest at pH = 2 and highest at around pH = 7 [**Coltrain** (1992) **Milea** (2011)].

Both acid (pH=5) and base catalysis (pH=8) were used to prepare alkoxysilane solutions, which were aged for 4 h to obtain liquid sols for deposition by dip-coating.
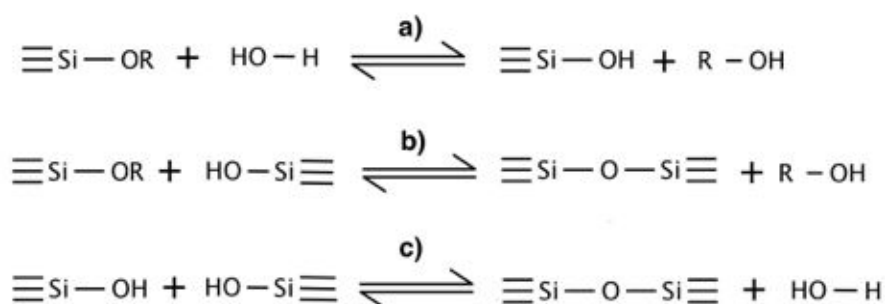
Figure 8. Main reactions in the sol-gel process using metal organofunctional alkoxysilanes.
a) hydrolysis, b) alcohol condensation and c) water condensation.

2.4.1.2 Dip coating process
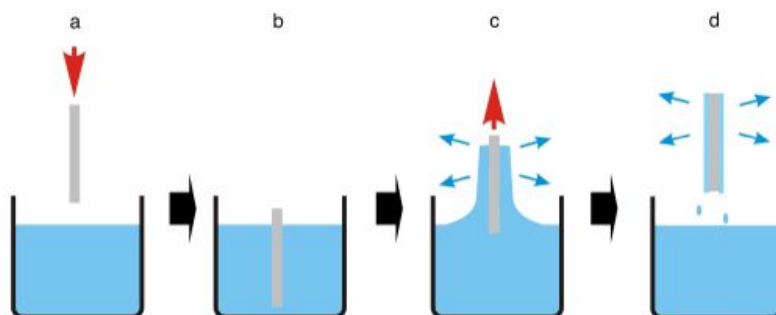
Figure 9. Fundamental steps of the dip coating process.

All the sol-gel treatments described in this thesis were deposited by dip-coating. Among the available deposition techniques, dip-coating is the most widely used in both industrial and laboratory applications because it is simple and inexpensive, and it enables good-quality coatings to be obtained. The dip-coating process can be separated into 4 stages: a) the substrate is immersed in a solution at a constant speed; b) it remains fully immersed for a given period of time (dwell time); c) it is withdrawn, again at a constant speed; d) the coated samples are then dried in atmospheric conditions, or in an oven to favor solvent evaporation (Figure 9). The sample's immersion and extraction should be managed at a constant speed to ensure uniformity of the final film. The rate of extraction also influences the final thickness of the film, which can be calculated with the Landau-Levich equation:

$$h = \frac{0{,}94 \cdot (\eta \cdot v)^{2/3}}{\gamma_{LV} \cdot (\beta \cdot g)^{1/2}}$$

where h is the thickness of coating, η is the viscosity, v is the withdraw speed, γ_{LV} is the surface tension, β is the density and g is the gravity. As you can see from the equation, the thickness of the film depends on the speed of extraction, thick coatings are obtained with high speeds. Also, high viscosity solutions involve greater difficulty of sliding between floors and an increase in thickness. Problems of uniformity of the thickness along the surface can happen due to variations in speed or oscillations of the substrate during the immersion phase or extraction from the solution. Finally the homogeneity of the film depends on that of substrate. Tests were made to optimize the speed of extraction in order to obtain thin films. All coatings were obtained with a withdraw speed of 0.66 mm/s using a homemade dip-coater available in the laboratory. Taking into account that the treated substrates are extremely porous (especially the pure cellulose), reference was made to the amount of deposited material per unit of surface area.

2.6 Hydrophobic siloxane paper coatings: the effect of increasing methyl substitution

Elisa Cappelletto, Emanuela Callone, Renzo Campostrini, Fabrizio Girardi, Simona Maggini, Claudio della Volpe, Stefano Siboni, Rosa Di Maggio.

Abstract

Paper is an organic material widely used in cultural heritage and mainly composed of cellulose mixed with lignin, hemicellulose and small amounts of additives. This paper deals with siloxane coatings on pure cellulose paper, applied by sol–gel dipping in sols prepared with different siloxane precursors (tetraethoxysilane, methyl triethoxysilane, dimethyl diethoxysilane, trimethyl monoethoxysilane). The coated samples were characterized using various techniques (Fourier Transform Infrared Spectroscopy FT-IR, Nuclear Magnetic Resonance NMR and Scanning Electron Microscopy and Energy Dispersive Spectroscopy SEM–EDS), measuring their mechanical properties, flame resistance and contact angles, and a colorimetric test. The coated samples' behavior was more hydrophobic the higher the methyl number of siloxane precursor, regardless of the coating's thickness. Increasing the thickness improved the mechanical and thermal properties. The thickest coatings were obtained using a double coating process and a basic catalyst for the hydrolysis step, but this latter condition facilitated the formation of surface agglomerates, which make the paper too stiff and yellow.

Introduction

For many centuries, paper has been the main mean of communication and knowledge transmission worldwide, making it very important to preserve old paper documents. Prior to the second half of the nineteenth century, paper was made with rags, using hemp, flax and cotton fibers, and adding sizing compounds, so that the paper was essentially composed of cellulose. Later on, wood pulp came to be commonly used as a raw material and the resulting paper contains cellulose mixed with lignin and hemicellulose. All these materials are easily degraded by insects, fungi, acids, enzymes, bacteria, moisture, oxidative agents and ageing. Several published studies have focused on the conservation of paper, suggesting different solutions: the use of protective coatings made by organic and inorganic compounds has often been proposed, but there is a shortage of thorough analyses that take every aspect of paper coatings into account. Paper-based materials deteriorate mainly due to cellulose degradation, which can have several causes. The cellulose matrix can be divided into crystalline domains, which are highly-resistant ordered areas, and amorphous domains that can easily be degraded by chemicals (acid hydrolysis, oxidative agents, light, air, pollution), or by physical or biological attacks (e.g. micro-organisms such as bacteria and fungi) [**Nicolas** (1974), **Xu** (2009)]. Decades of scientific research have focused on how paper deteriorates and different

solutions have been proposed, including: controlling storage conditions (fluctuations in relative humidity, exposure to light and pollutants, and temperature); and using protective treatments made of various materials with anti-microbial or flame-retardant properties. Some of the substances studied for protecting cellulosic materials are: epoxy glues; various polymers (e.g. polyaniline and polyurethanes), used alone or with encapsulated low moecular-weight molecules (quaternary ammonium salts) or nanoparticles (typically heavy metals such as silver, copper or zinc); and inorganic treatments such as carboxylate-alumoxanes or silica coatings [**Abdelmouleh** (2004), **Kandelbauer** (2010), Fir (2007), **Klemencic** (2010), **Maneerung** (2008), **Son** (2006), **Bath** (2006), **Klibanov** (2007), **Martin** (2007), **Malthing** (2004), **Haufe** (2005), **Hou** (2009), **Xie** (2009)]. Despite the abundance and variety of the bibliography, no in-depth studies have been conducted to analyze all aspects of the use of protective paper coatings. Previous works have generated some interesting recommendations, but the pictures they present often seem incomplete, since they only concern particular aspects of the usage of such coatings. Hence our decision to produce a number of samples, changing some of the synthesis parameters, and to analyze them extensively using different experimental methods. Based on what has been done so far, and knowing that protective coatings must have certain characteristics (they must be non-toxic for mammals, repellent for fungi and other micro-organisms, fire-resistant, inexpensive, stable and environment-friendly; and they must not alter the basic properties of the substrate), our interest focused on the use of functionalized silicon alkoxides synthesized using the sol–gel method. This type of coating has been widely tested on glass, stone and plastics. In some cases it has also been studied on cellulose fibers, but no studies on its application on paper or wood have been conducted to date [**Sheen** (2009]. The use of these compounds as protective coatings on cellulose materials is of interest because the sol–gel process enables inorganic materials to be deposited starting from a solution at room temperature [**Belleville** (2010), **Schmidt** (1988), **Mackenzie** (2003)], making it suitable for coating degradable materials, like paper, that usually have a limited thermal stability. The cellulose content ensures considerable amounts of hydroxyls on the surface that could be involved in reactions with the silanols produced during the conventional sol–gel process, linking the organic substrate to the inorganic coating (Figure 10).

Figure 10. Scheme of reaction cellulose-silanols.

Among the great variety of commercial functionalized silanes available, ethoxysilanes bearing 1–3 methyl (the smallest hydrophobic functional group) were considered in this work because they are inexpensive and easy to use. Increasing the number of methyls should make them more hydrophobic [**Guo** (2007)], preserving the paper against fungi and providing flame-retardant properties at the same time. To analyze how the siloxane matrices bearing methyl groups behaved on paper both at molecular and macroscopic level, and their degree of condensation, several techniques were used to characterize the coatings (scanning electron microscopy, infrared spectroscopy, solid-state NMR, contact angle measurement, and colorimetric, mechanical and flame resistance tests).

Experimental part

Materials

All chemical reagents were purchased from Sigma-Aldrich (Italy) and used without further purification. Blue ribbon Whatman filter paper was used as material to coat. Sols with a nominal SiO_2 concentration of 100 g/L were prepared by dispersing the appropriate amount of precursor (tetraethoxysilane, TEOS, methyltriethoxysilane, MTES, dimethyldiethoxysilane, M_2DES, or trimethyl monoethoxysilane, M_3MES) in absolute ethanol at room temperature under stirring. Then HCl 0.05 M, or NH_4OH 1 M was added dropwise as catalytic agent [**Huang** (2009)] in stoichiometric amounts with respect to the ethoxy groups (OEt/H2O = 1) to ensure their complete hydrolysis. The sols were aged for 4 h then used for dip coating. When M_3MES was used, it was not added acid water or catalyst in order to prevent the formation of volatile dimer species [**Hook** (1996)]. Paper sheets, 500x500x0.12 mm, were cut and dip coated (immersion time 90 s for single layers, 60 s for double layers, withdraw speed v). After the first dipping, the samples were conditioned at room temperature for 1 h. When a second dipping was planned, the coated samples were conditioned in the oven at 60 °C for 30 min. All samples were stored at room temperature. Table 2 shows a complete list of the studied samples.

Sample ID	Composition of 1st layer (HCl as catalyst)	Composition of 2nd layer (HCl as catalyst)	Catalyst of sol for 2nd layer	Weight of coating per unit of surface area (mg/cm²)
cM	MTES			1.2
cM2	M_2DES			0.3
cM3	M_3MES			0.2
cT	TEOS			1.4
cTT	TEOS	TEOS	HCl	3.8
cTM	TEOS	MTES	HCl	3.1
cTM2	TEOS	M_2DES	HCl	1.7
cTM3	TEOS	M_3MES	HCl	0.9
cTMb	TEOS	MTES	NH_4OH	4.1
cTM2b	TEOS	M_2DES	NH_4OH	3.0
cTM3b	TEOS	M_3MES	NH_4OH	2.5

Table 2. List of cellulose samples

Measurements

Scanning electron microscopy (SEM) scans were obtained using a JEOL JSM 5500 Scanning Electron Microscope and the microanalysis was conducted using an energy dispersive X-ray spectrometer (EDS). Samples were covered by galvanic gold deposition with a current of 5 mA for 45 s. FT-IR spectra were recorded in transmission mode in the 4000–400 cm^{-1} interval on a Nicolet Avatar 330 spectrometer (256 scans, 4 cm^{-1} resolution). At this regard, the coated paper were cut, mixed and ground with a standard amount of KBr in order to obtain transparent pellets under pressure. ^{29}Si and ^{13}C NMR spectra were recorded with a Bruker Avance 400 WB spectrometer with a carrier frequency of 400.13 MHz (^{1}H). Samples were packed in 4 mm zirconia rotors and spun at 6.5 kHz. ^{29}Si Single Pulse (SP) spectra were obtained with a 4.3 ls pulse length, a 15 s scan delay, and 2 k scans with a proton decoupling power of 47 kHz. Q8M8 was used as the external secondary reference. ^{13}C NMR spectra were acquired with a 3.36 ls pulse length, a 7.5 s scan delay, and 3 k scans with a proton decoupling power of 51 kHz. Adamantane was used as the external secondary reference. Roughness was measured with a Hommelwerke Wave System profilometer with a TLK100 tip, using a scan length of 50 mm, 8,000 readings and a 0.8 mm cut-off. The drop method was used to measure contact angle. The drop volume of water was 3 lL and the static contact angle was measured with the aid of a camera immediately after the drop's deposition, processing the images with IMAGE j software (for details of this method see [**Della Volpe** (2006)]). Then the equilibrium contact angles were measured using the VIECA (Vibrationally Induced Equilibrium Contact Angle) technique, i.e. a sonic vibration of appropriate frequency, waveform and duration is applied and should induce a further relaxation of the drop to a configuration with a lower free energy, making the contact angle come much closer to the true thermodynamic contact angle. This approach cannot be applied to plain paper because of its permeability, so this measurement was obtained using the Wilhelmy balance method (DCA technique, dynamic contact angle) and the corresponding runs were analyzed using a particular numerical method capable of correcting the liquid absorption by applying a Washburn-like function, as explained elsewhere [**Brugnara** (2006)]. The water used for the tests was purified in a Millipore MilliQ device with UV control, showing a constant electrical resistivity of 18.2 MXcm and a surface tension of 72.7 mJ/m2 at 20 °C. All data were collected at a room temperature of 26 ± 2 °C. The mean of five measurements was calculated for each type of sample. The elastic modulus (E), elongation at fracture (ef) and ultimate strength (rf) were measured at room temperature on rectangular samples (15x1x0.125 mm) using a Seiko TMA EXSTAR SS6300 in tension mode with an elongation rate of 1 mm/min. High-Temperature Differential Scanning Colorimetry (HT-DSC) analyses were performed with a HT-DSC SETARAM, in O2 with 10 °C/min heating rate. Fire tests were conducted with a home-made apparatus according to UNI 8456. All the tests were repeated three times and then the morphology of the burnt samples was studied using SEM. Colorimetric tests were performed according to the CIEL*a*b system on the basis of the standard 43/93 ''Colorimetric measurements of opaque surfaces'', using the portable Konica Minolta CM 2600d spectrophotometer with the 10° detector and the D65 primary source. The color coordinates were measured according to the CIE 1976 (Commission Internationelle Eclairage) parameters to quantify the colorimetric variations produced by the protective film deposited on the paper. The parameters are L*, a* and b*, where: L* denotes the brightness of the color on a gray scale from 0 (black) to 100 (white); a* is the red/green color component, with values around zero (green being

negative and red being positive); b* stands for the blue/yellow component (blue being negative and yellow positive); a* + b* refers to the dominant wavelength, and therefore to the purity and saturation of the color. E* is the sum of the three parameters indicating the position of the color in the specific colorimetric space, so ΔE* represents the deviation from the original value due to the coating, as a cumulative effect.

Results

Electron microscopy findings

Plain paper is made of very long intertwined cellulose fibers with no filler and has a discontinuous surface (Figure 11). Given that it is extremely rough and is not a perfect flat surface, the coating is not homogeneously thick and follows the profile of cellulose fibers (Figure 11).
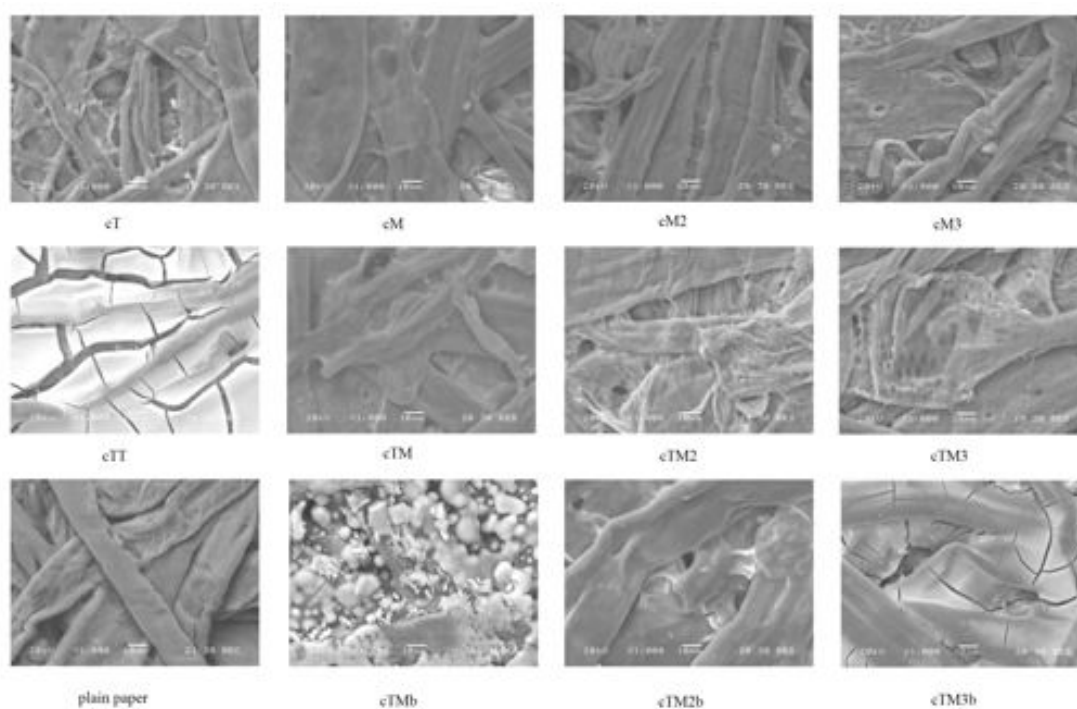
Figure 11. SEM micrographs of all the samples.

Therefore the thickness of coating cannot be measured accurately by usual methods, therefore an indirect method has been considered: the quantity of deposited material (reported in Table 1 as weight per unit of surface area [mg/cm^2]). The thinnest coatings generally do not noticeably modify its surface morphology. The paper's fibrous microstructure is still detectable underneath the coating, though the sheets look smoother than uncoated paper due to the ''filling'' or ''masking'' effect of the siloxane matrix (Figure 11). As shown in Table 1, the mass of cM2 and cM3 is really low compared with the others, thus these coatings cannot provide a significant coverage due to the nature of their precursors, which are unable to undergo effective

condensation. Under the thickest coatings (cTT, cTMb, cTM2b and cTM3b), none of the features of the substrate remain visible; there is only a network of cracks, or a granular silica deposit (as in the cTMb sample) due to flocculation and the growth of grains. These coated samples also become very fragile and stiff to the touch. The EDAX analyses (Figure 12) confirm a homogeneous distribution of the Si atoms all over the samples. In particular, cross sectional analyses (Figure 12d, e, f) reveal silicon atoms under the paper's surface, confirming the penetration of the silane solution even into the bulk of the substrate.
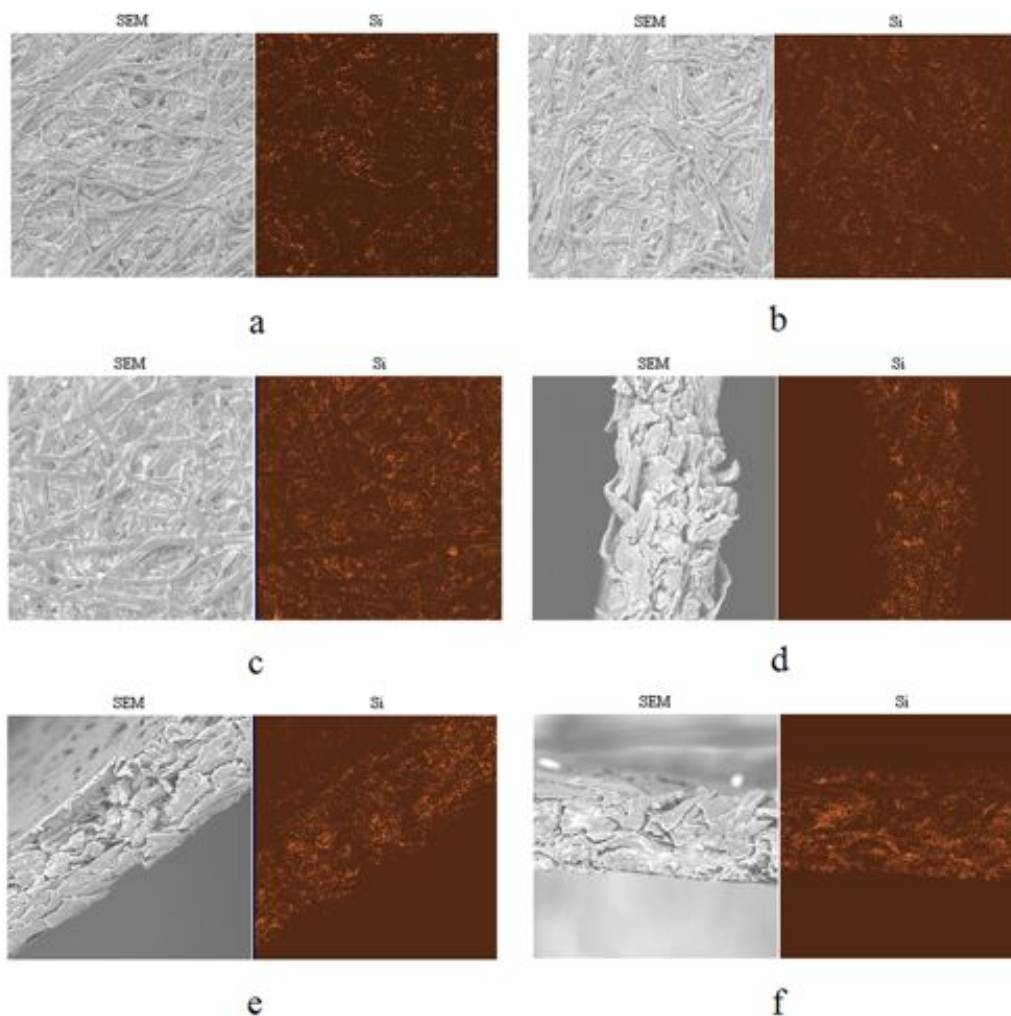
Figure 12. Si distribution maps of some representative samples: a and d cT; b and e cTM2; c and f cTM2b.

Spectroscopic observations

Solid-state NMR

Si units were labeled according to the usual chemical notation: Q^n, T^n D^n and M^n where capital letters refer to the number of Si–O– bonds and n is the number of oxo-bridges. Figure 13 shows the ^{29}Si NMR spectra and Table 3 the assignments, the relative amounts of each species and the related degree of condensation (DOC), which appears to be very high for all samples. In the double-layer samples, TEOS accounts for about 80 % of the coating (mainly forming Q^4 and Q^3 species), while only 20 % consists of methyl substituted silane. Both TEOS and M$_2$DES are poorly condensed in the double-layer samples, where the Q^4 units account for less than 40 % in all cases, while they are about 60 % in cT. There are only D^2 species in the cM2 sample, which account for 83 % of the second layer in cTM2.
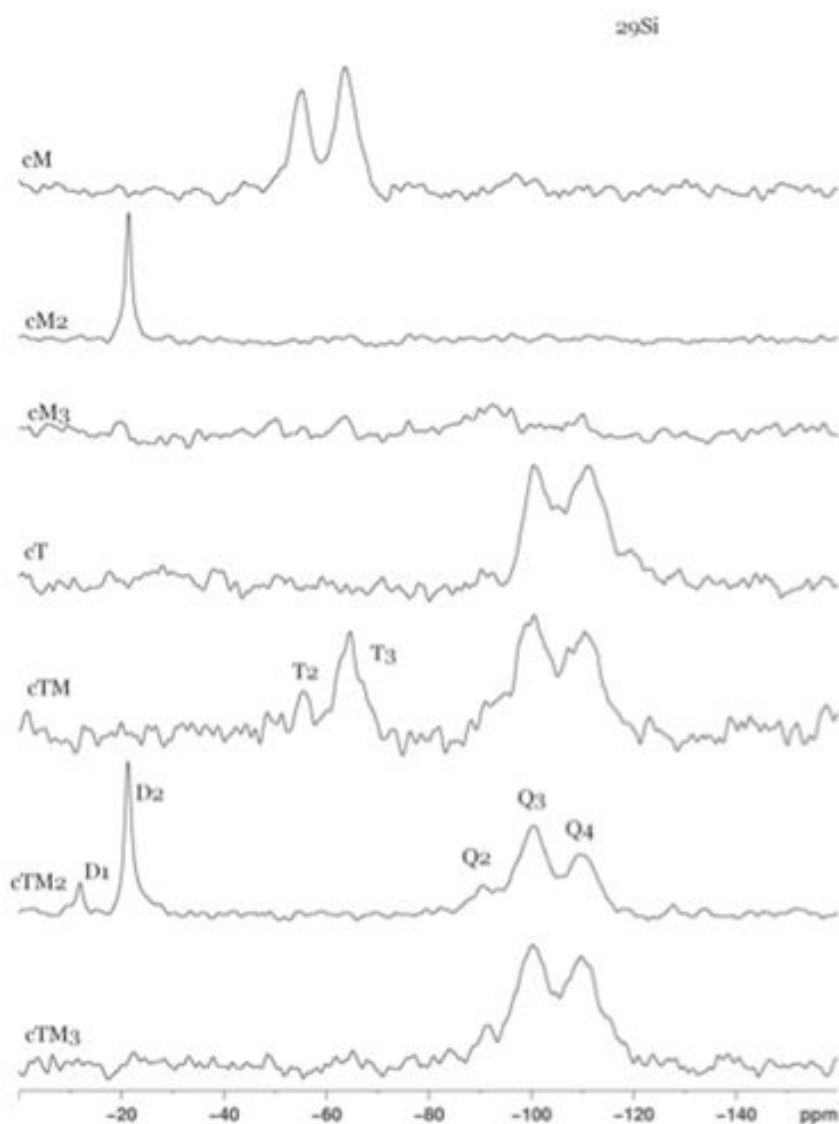
Figure 13. ^{29}Si SP spectra of paper coated with single and double layers of silanes.

Fully condensed T^3 species account for 58 % in the cM sample, while around 80 % of the second layer of cTM is T3, irrespective of the acid or alkaline conditions of the hydrolysis. As discussed before, cM3 shows no signals attributable to M units due to the absence of self-condensation. The spectra and data obtained for the samples hydrolyzed in alkaline conditions are actually similar to those obtained after acid catalysis. Whatman paper consists of crystalline and paracrystalline cellulose domains, and this gives rise to different neighboring peaks in the ^{13}C spectrum on NMR [**Atalla** (1999), **Girardi** (2011), **Wickholm** (1998)]. The ^{13}C spectra of all the samples (not shown here) demonstrate that the coating does not affect the paper's structure, since all the spectra are similar apart from the signal of the CH$_3$ group bonded to silicon found in the case of methyl functionalized alkoxysilane.

Sample	Structure unit	ppm	Relative area %	DOC
cM	T^2	-53.0	41.6	86.1
	T^3	-63.0	58.4	
cM2	D^2	-19.0	100.0	100
cM3	M	+9.0		
cT	Q^2	-91.0		
	Q^3	-98.4	39.5	90.1
	Q^4	-109.1	60.5	
cTM	T^2	-53.3	5.2	87.9
	T^3	-62.6	18.6	
	Q^2	-89.8	1.8	
	Q^3	-98.5	37.9	
	Q^4	-108.5	36.5	
cTM2	D1	-9.7	2.9	80.9
	D^2	-19.3	14.7	
	Q^2	-88.3	17.2	
	Q^3	-98.2	36.2	
	Q^4	-107.5	29.1	
cTM3	Q^2	-90.1	20.1	79.2
	Q^3	-99.3	42.9	
	Q^4	-108.0	37.0	

Table 3. Quantitative analysis of the ^{29}Si NMR peaks.

The amount of material deposited can be calculated from the relative intensities: the MTES layer accounts for about 71 % of the cM sample and 59 % of the cTM sample, whereas M_2DES represents 44 and 35 %, respectively, of the cM2 and cTM2 samples.

Infrared spectroscopy
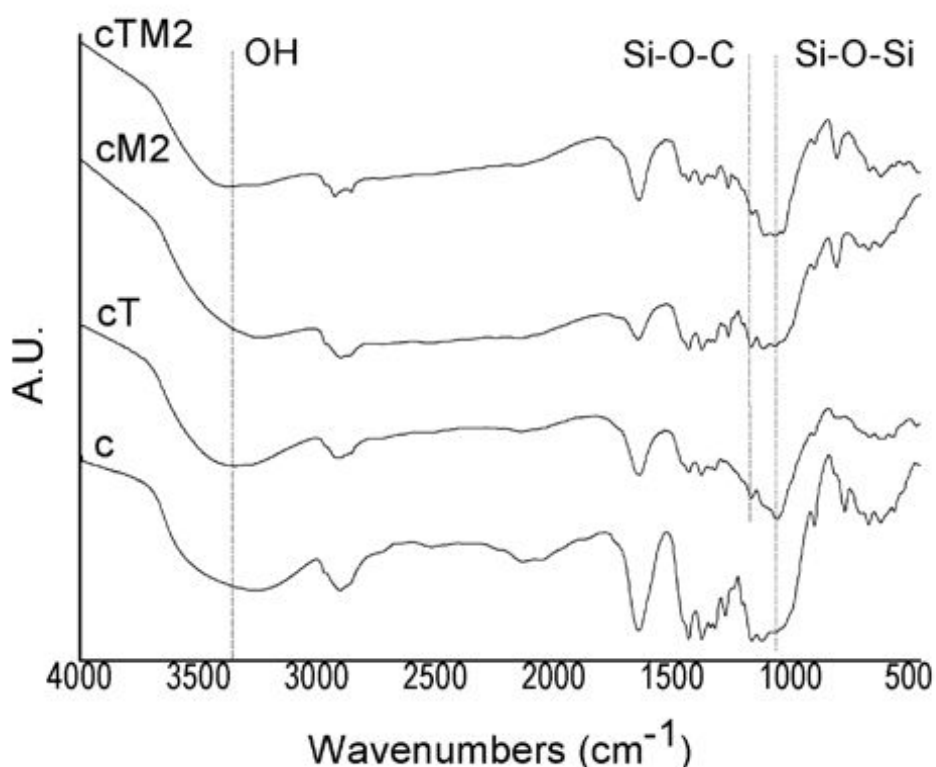
Figure 14. FT-IR spectra of plain paper (c), samples cT, cM2 and cTM2.

Figure 14 shows the FT-IR spectra of several samples and plain paper. The spectra of the coated samples are fairly similar, whatever the type of catalyst (acid or alkaline) used during hydrolysis. The typical bands of cellulose and siloxane bonds are detectable, though they largely overlap. The broad band of O–H stretching centered at 3379 cm^{-1} and the band of OH deformation at 1637 cm^{-1} confirm their involvement in the H bond due to adsorbed water [**Jung** (2005)]. The intensities of both the signals decline after coating, because the sol displaced the water. The bands due to siloxane coating are at: 800 cm^{-1} (Si–O–Si symmetric stretching), 1070 cm^{-1} (Si–O–Si asymmetric stretching), 1270 cm^{-1} (Si–CH$_3$ symmetric deformation), 1108 cm^{-1} (stretching Si–O–R, R = ethoxy group) [**Kannangara** (2008)]. A broad band is observed in the range of 1000–1200 cm^{-1} due to the O–H bending of primary and secondary hydroxyl groups of cellulose.

This prevents a clear attribution of the signals corresponding to the Si–O–Si and Si–O–C bonds in the same range, apart from the stretching frequency at 1180 cm-1 of Si–O–C unit, where the carbon atom belongs to the cellulose glucose unit [**Abdelmouleh** (2004)]. This last confirms the chemical interaction between the siloxane coating and the cellulose.

Contact angle measurement

Contact angle (CA) measurements were used to assess the wettability of the coated sample as well as the hermodynamic parameters and the surface roughness at the interface between the coating and the water [**Kannangara** (2006) (2008)]. The paper roughness appears very similar before and after coating, with a mean Ra (arithmetic average of absolute values) of 5–6 lm, a value that can certainly influence wettability. The difference in the contact angle results can thus be attributed to different chemical bonds on the surfaces. The contact angle of plain paper is 48.8°, and could only be measured using the Wilhelmy balance method [**Brugnara** (2004)], after correcting for liquid absorption, because the paper is highly hydrophilic. Both sessile static and equilibrium contact angles were measured for the coated samples, though the former is less accurate because it is unable to indicate the true capacity of he film to prevent water from spreading when the surface is heterogeneous and/or rough, as in the present case. The sessile static angle simply corresponds to the highest possible contact angle value, being a measure of the most hydrophobic portion. The equilibrium contact angle, measured with the VIECA technique, provides the experimental value as close as possible to the Young angle and is consequently more reliable [**Della Volpe** (1997) (2000) (2002), **Brugnara** (2004)].
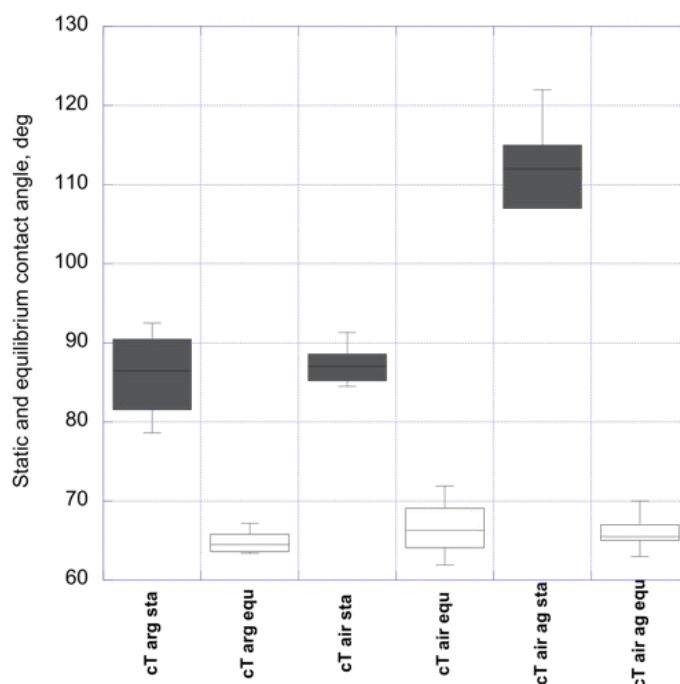
Figure 15. Static and equilibrium contact angles of the cT sample in different atmospheric and measurement conditions (ar argon, air air, sta static angle, equ equilibrium angle, ag aged sample).

Figure 15 shows the static and equilibrium angles of cT samples prepared in argon or air and analyzed immediately after their preparation, which show no major differences; on the other hand, the static value appears significantly higher for the samples left in standard laboratory ambient conditions and labeled as ''aged''. Since the static angle is closer to the advancing state, i.e. closer to the most hydrophobic portions of the surface, an increase in this angle suggests a decrease in the surface energy of the aged samples due to impurities. Comparing the data of all the ''aged'' samples (Figure 16a,b), the coatings increased the hydrophobic nature of the paper, as expected, though some hydrophilic regions remained on the surface.
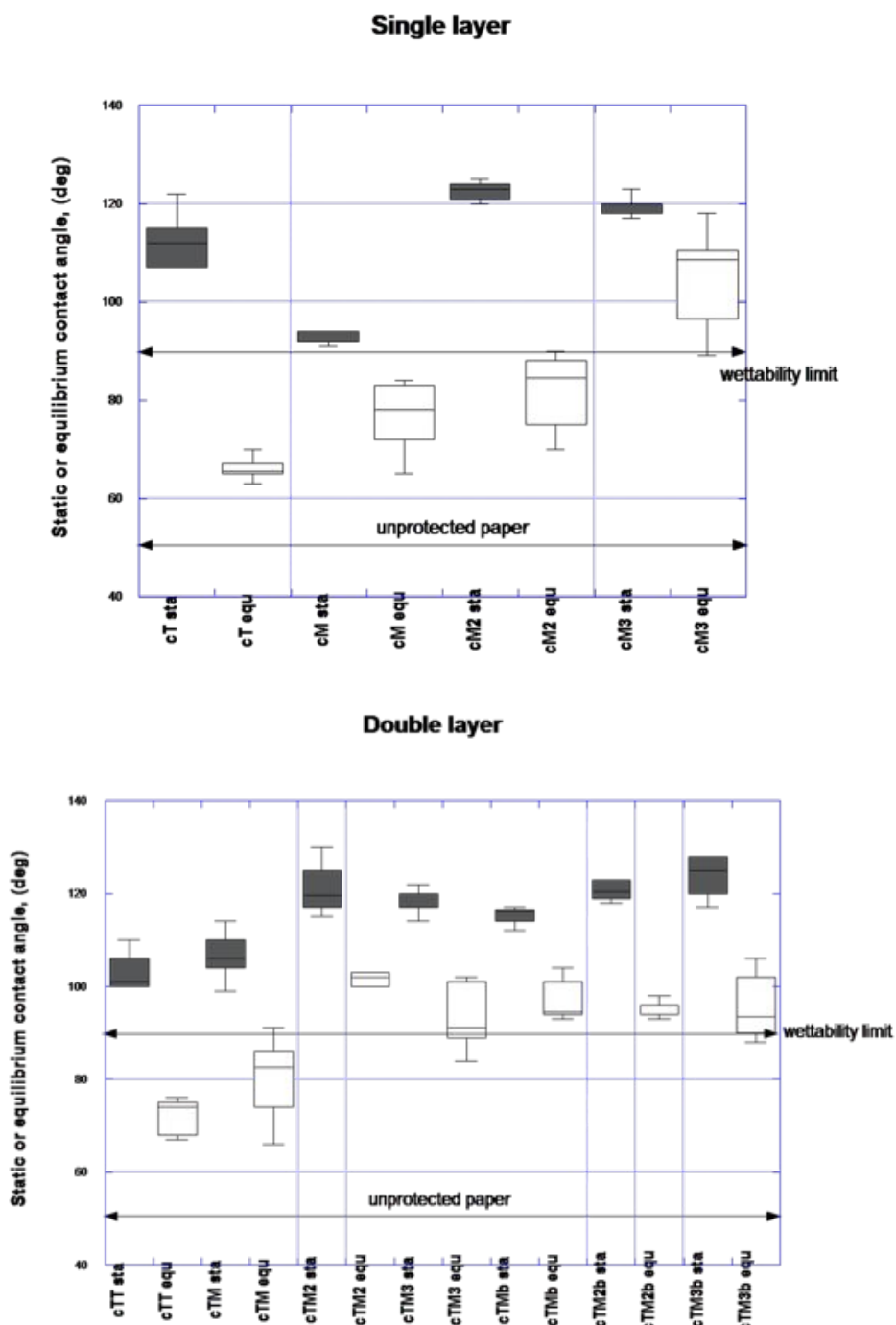
Figure 16. Static and equilibrium contact angles of samples coated with single (a) and double layers (b) (grey = static angle, white = equilibrium angle).

25

The equilibrium contact angles of the samples with single-layer coatings are below 90° (the limit for the material to be considered hydrophobic) (Figure 16a), except for the cM3 sample, which had both static and equilibrium values above the wettability limit. The equilibrium contact angles recorded for the samples with a double-layer coating were greater, except for cTT and cTM. This general trend is probably due to the second layer, which significantly reduces roughness. The contact angle also increases with the number of hydrophobic methyl groups (TEOS \ MTES \ M₂DES \ M₃MES).

Mechanical properties

The stress–strain behavior of the uncoated and coated paper was measured in terms of tensile deformation; all the samples were tested up to failure. Figure 17 shows the Young modulus (E), fracture strength (rf), strain at fracture (ef), and energy loss (Z), all measured in the machine direction. A single coating of MTES, M₂DES or M₃MES is not enough to improve the paper's mechanical properties due to the low weight increase.
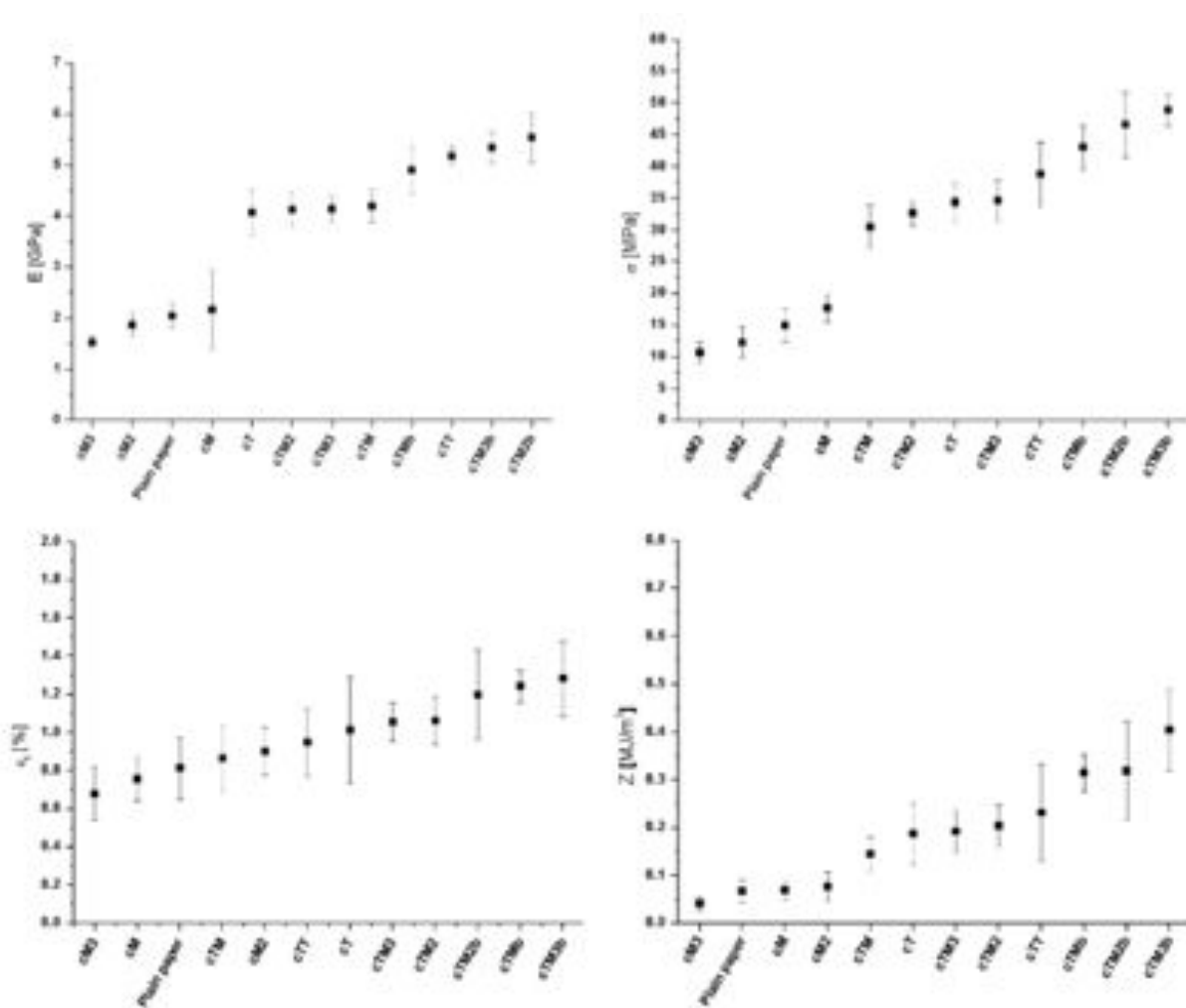
Figure 17 Young's modulus (E), fracture strength (rf), strain at fracture (ef), and energy loss (Z), all measured in the direction of the machine.

Among the single coatings, only cT seems to improve the properties by comparison with the untreated paper. In all the samples coated with a double layer, however, there were significant changes in the paper mechanical properties, such as a higher elastic modulus and fracture strength, suggesting that the mechanical properties are better, the greater the thickness of the coating. The data also indicate that the samples prepared with alkaline catalysis generally behave better than the others. The cTM3b sample shows the highest energy loss due to the higher values not only of E and r, but also of ef. Elongation relates to the paper ability to comply with the applied load, while tensile strength reflects bonding between fibers and generally declines in aged paper. In this respect, the coating process may even contribute to restoring the paper mechanical resistance [**Havlinova** (2009)]. On the other hand, the marked increase in the elastic modulus of the samples prepared with alkaline catalysis makes them very stiff for some applications.

Thermal and flame retardant properties

As illustrated in Figure 18, the plain paper in air shows a strong exothermal peak at about 361°C, attributed to charring and oxidation of the products of the thermal decomposition of cellulose [**Jain** (1985), **Gaan** (2009)]. The char is oxidized at about 462 °C, releasing heat again. All the samples have a different thermal pattern from plain paper, with peaks that are more pronounced and broader [**Girardi** (2011)]. All the coatings make the second peak shift to higher temperatures because the residual silica slows down the combustion process (Table 4). The above results would indicate that the coating enhances the paper's thermo-oxidative stability, especially in the high-temperature region. On the other hand, the first peak remains almost unchanged in almost all cases, although a shift to lower temperatures indicates combustion/charring of the most volatile fraction of the coating. It is worth noting that the cTMb, cTM2b and cTM3b samples not only show a low total mass loss, like the cTT sample, but also correspond to the lowest mass loss values during charring, and therefore to the highest char residue. The char yield increases with the weight of the coating and can be correlated with its flame retardant properties. Increasing char formation reduces the production of combustible gases. The high char yields imply that fewer volatile substances were being released from the resins during heating. Because volatiles fuel combustion in a material in the event of a fire, a more limited release of volatiles implies a lower flammability. The flammability of our samples was assessed according to the Italian standard UNI 8456. The plain paper burns completely in 6 s when exposed to fire and becomes dark brown due to residual graphitic carbon, while the time it takes for the flame to spread increases noticeably for all the coated samples, up to 15 s for the cTT sample, which also retained its shape [**Stejskal** (2005), **Salgaonkar** (2004), **Bodart** (2008)]. As soon as the siloxane matrix has formed, it acts as a barrier to oxygen diffusion, reducing the flammability of the coated paper.
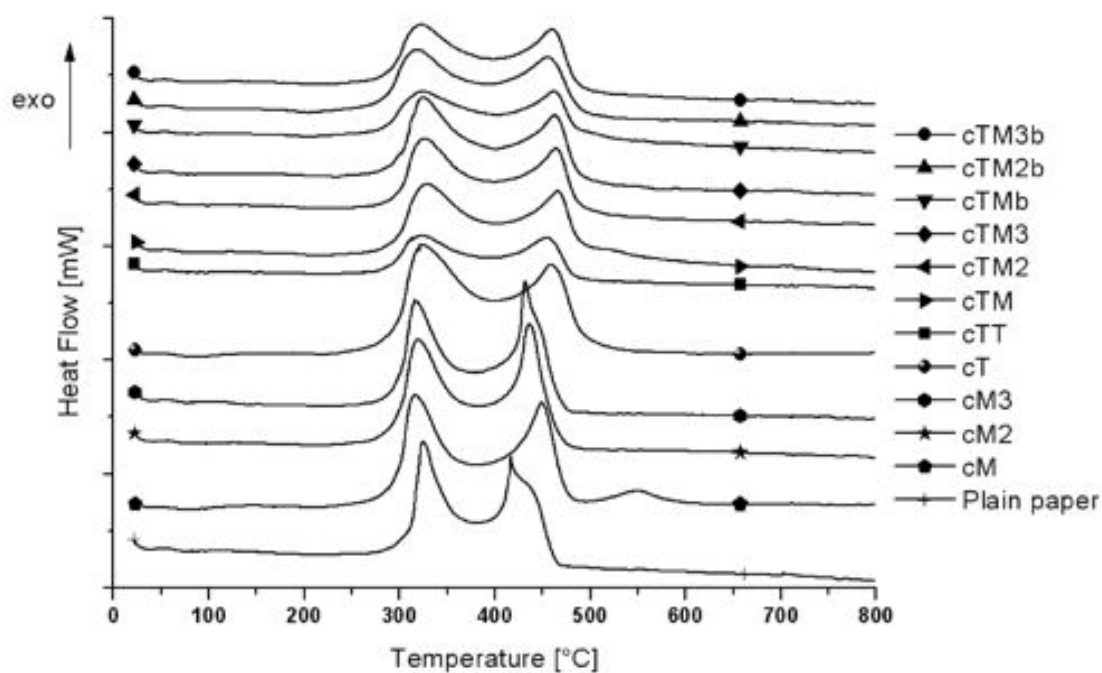
Figure 18. HT-DSC curves in the oxygen of untreated and coated paper samples.

Sample ID	Max temperature of 1st peak(°C)	Max temperature of 2nd peak(°C)	Δm (total) (%)	Δm (1st peak) (%)
Plain Paper	324	417	63	48
cM	316	449	52	39
cM2	319	436	62	44
cM3	316	432	63	47
cT	322	458	52	38
cTT	324	455	39	28
cTM	329	466	50	36
cTM2	326	464	53	38
cTM3	326	464	53	37
cTMb	324	463	43	17
cTM2b	319	456	48	17
cTM3b	324	460	48	16

Table 4. Maximum temperatures of the first and second peaks on the HT-DSC curves in oxygen; total and first-peak weight loss.

Colorimetry

A protective treatment should not alter the visual appearance and original color of the underlying paper. A colorimetric measurement was obtained at three different points on the surface of each sample, the average values and differences vis-a`-vis the reference (ΔE) were studied. A value of 1.5 for ΔE is usually considered the maximum allowable variation because it is below the level perceivable by the human eye [**Larsson** (1999)]. Assuming that $\Delta E^* = [(\Delta E^*)^2 + (\Delta a^*)^2 + (\Delta b^*)^2]^{1/2}$, individual variations can be considered for the three parameters, where L*, a* and b* are described in the experimental part. For the brightness measurements, the ΔL* values obtained were negative, meaning that all the coated samples are less bright than the original paper. There were no effects on the red/green scale, so the parameter a* remains virtually unchanged. The most significant variations were recorded for the parameter b*, i.e. surface yellowing: for samples coated with alkaline double layers, there is a clear shift towards yellow. Figure 19 shows the trend for Δb* and ΔE*. In general, the ΔE* value for the samples coated with single layers is quite low, below the 1.5 limit. This value increases slightly in the case of double layers produced in acid catalysis, and it exceeds the limit in the case of double layers of coating produced in alkaline catalysis, which presumably modifies the structure of the cellulose.

Figure 19. Δb (white bars) and DE* (black bars).*

29
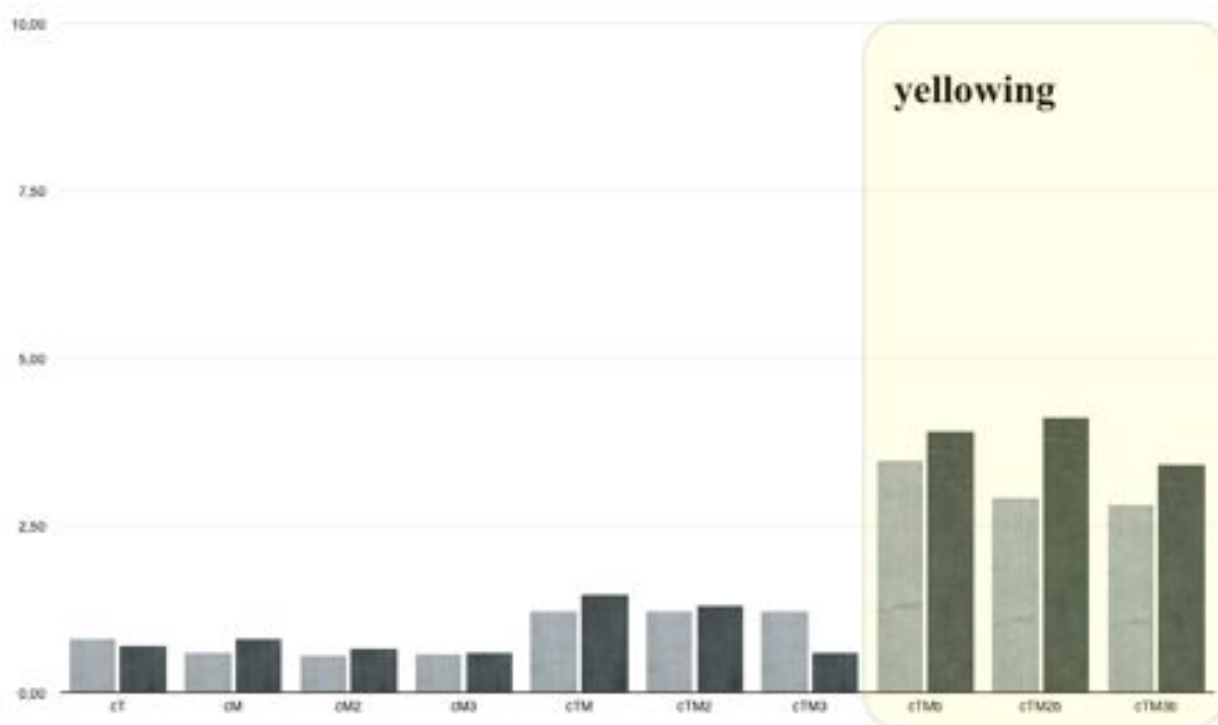
Discussion and conclusions

With a view to producing uniform hydrophobic paper coatings, we used sols with different methyl-functionalized alkoxysilanes. The rationale was to coat the paper with hydrophobic methyl groups, outwardly exposed to the environment. The samples prepared for our experiments are classifiable according to the number of layers deposited on the paper's surface and type of catalyst used for the precursor sols. The EDAX analyses showed that the inorganic material covered the cellulose fibers quite well, consolidating their structure and interconnections. The structure of the cellulose network was still visible under the coating (as shown by SEM micrographs) on the single-layer and cTMx samples, but not on the cTT and cTMxb samples. Since the MTES layer is heavier than in the case of M_2DES or M_3MES, the amount of material deposited must correlate with the silane's ability to form siloxane bonds, and is therefore inversely proportional to the degree of methyl functionalization. In all the FT-IR spectra, the expected overlap between the siloxane and cellulose bands, along with the small peak at 1180 cm^{-1} assigned to Si–O-cellulose interaction, support the conviction that the second layer is stably anchored to the first or to the cellulose by oxygen bonds; it does not simply adhere to them. The degree of silica matrix condensation was quite high for all the samples, with both single and double layers of coating. The highest DOC were recorded especially for the cT cM and cM2, because homocondensation produces a highly regular matrix whereas the steric hindrance of the methyl groups can restrict co-condensation in the double-layer samples. The DOC of the double-layer coatings derives from the contributions of TEOS (around 80%) and methyl silanes (around 20%): there are Q species deriving from TEOS than those coming from the precursor of the second layer. The lower percentage of Q^4 species recorded for the double-layer coatings also indicated that they are less condensed than the single-layer coatings. Finally, the nature of the precursor M_3MES prevented condensation in the cM3 samples. Analyzing the ^{13}C NMR spectra indicated that the coatings do not alter the cellulose [**Larsson** (1999)], so this type of coating can be proposed for preserving ancient historical documents. Some of the other key requisites for restoring our cultural heritage, such as breathability, the ink solubility of the coating, or the reversibility of the treatment, will be the object of further studies. The color variation is virtually negligible for all the single layers, but more noticeable for the cTMx samples and unacceptably high for cTMxb, making their surface appear yellow. The yellowing of the paper is due to the agglomerates scattering on the surface: although these agglomerates are large, they are unable to create the superhydrophobic ''lotus'' effect. Comparing the CA values, the hydrophobicity and the degree of methyl substitution on the silane precursor were found to be directly proportional: $\theta cT < \theta cTM < \theta cTM2 < \theta cTM3$. The increase in the methyl groups makes the coating more hydrophobic, reducing moisture absorption and defending against fungi and insects. The contact angles of all the coated samples are higher than for the plain paper, but the differences seem to relate more to the evenness of the coating than to its composition. There is a difference between the static and equilibrium contact angles, however: the coating is hydrophobic when all the angles exceed the 90° limit, and this was the case for cM3 and all the samples coated with double layers except for cTT and cTM. There are different reasons for this result. In the cM3, cTM2 and cTM3 samples it is merely the consequence of the uniform, outward-facing methyl groups, while in cTMxb it is due mainly to the grainy surface when the static contact angle is measured, and to the surface roughness when the

equilibrium angle is measured. This also explains why the discrepancy between the two values is smallest for cTMxb, indicating that the surface is stably hydrophobic due to the high percentage of surface coverage. The mechanical properties of the samples with single coatings are similar to those of the original paper, except for cT, which became noticeably stiffer (twice as stiff as the untreated paper). All the mechanical properties not only the elastic modulus, but also the fracture strength, strain at fracture and consequent toughness improve with a second layer, especially in the case of the cTT or cTMxb samples, thanks to the larger amount of coating on the substrate. The stiffening of the samples is mainly attributable to the amount of TEOS left on the substrate, which reacts with the cellulose's OH groups, creating strong bridges between the coating and the fibers. This may yield a ''welding'' of the fibers to one another, inhibiting slip-page between fibers and thereby enhancing the effective elastic modulus. The use of more diluted sols of TEOS is therefore advisable to preserve the material's flexibility. The thermal analyses on the coated samples show that silica coatings are glassy materials practically unaffected by fire, which delay flame propagation and char formation. These coatings enable the samples to retain their shape after burning and serve as flame retardant treatments meeting an important requirement for paper that might come into contact with fire.

2.6.1 Fluorinated and Phenyl functionalized coatings: a comparison

Chemicals characterized by different hydrophobic groups were studied.

1H,1H,2H,2H-Perfluorooctyltriethoxysilane (PFOS), (3,3,3-Trifluoropropyl)trimethoxysilane (TFPS) and Phenyltriethoxysilane (PhTES) were employed as precursors.

These chemicals are widely used to obtain superhydrophobic coatings on various substrates such as aluminum alloy, silicon and glass substrates or cellulosic materials. The molecules have low surface energy groups that can reduce the energy surface of substrate. In general, coatings obtained starting from these precursors are characterized by very low surface energy and therefore high contact angles (>120°). In the literature, the contact angles were commonly measured with the sessile method, it is therefore reasonable to assume that these values differ from the true contact angle as discussed above.

The purpose of this part of the research is to investigate these protective treatments through various techniques focusing mainly on their hydrophobic behavior. The results will be analyzed in the light of those obtained with the methylated compounds.

Experimental part

Materials

Sample ID	Composition of 1st layer	Composition of 2nd layer	Weight of coating per unit of surface area (mg/cm
cTTFPS	TEOS	TFPS	8
cTPFOS	TEOS	PFOS	10
cTPhTES	TEOS	PhTES	6

Table 5. List of the samples:fluorinated and phenyl alkyl precursors.

Silica polymers were synthesized by sol-gel as discussed previously. The chemicals were dispersed in absolute ethanol at room temperature under stirring, then the acidic solution (HCl 0.05 M) was added dropwise as catalytic agent [21] in stoichiometric amounts with respect to the ethoxy groups. The aged sols were applied on cellulosic substrate (Whatman filter paper) by dip coating. Taking into account the results reported in the above article, double layer samples were prepared. After the second dipping, the coated substrate were conditioned in the oven at 60 °C for 30 min. Table 5 shows a complete list of the studied samples.

Measurements

Technical specifications of the measures can be found into the section "Measurements" of the scientific pubblication.

Results

The fibres of substrate are still visible after the treatment with different silane (Figure 20). The siloxane matrix fills the spaces between the fibers as previous coatings and the EDS analysis confirm the homogeneous distribution of the Si atoms all over the sample (Figure 21) .
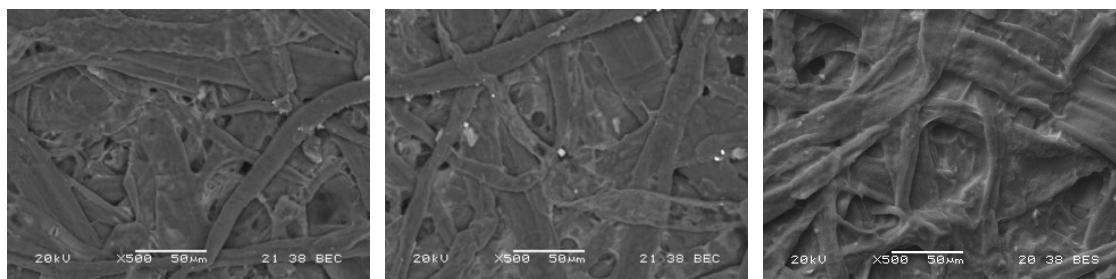
Figure 20. SEM micrograhs (x500): left) cTTFPS; centre) cTPFOS; right) cTPhTES.
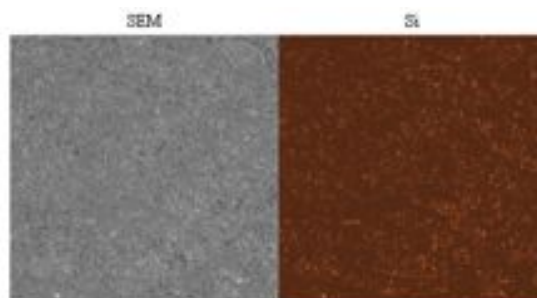
Figure 21. EDS map. Silicon distribution on surface.

Infrared spectra (Figure 22) show the typical siloxane resonances, very strong bands in the region 1130-1000 cm^{-1}. The asymmetricalpresents of fluorinated compounds is due to the peaks at 1145 1235 1430 cm-1. The vibrations attributed at CF$_2$ and CF$_3$ groups appear at 1450 cm^{-1}, 1235 cm^{-1}, and 1430 cm^{-1} in the spectrum of cPFOS (the spectrum of cTTFPS is very similar). Carbon–carbon double bond vibration of the phenyl group is visible at 1475 and 1600 cm^{-1}.
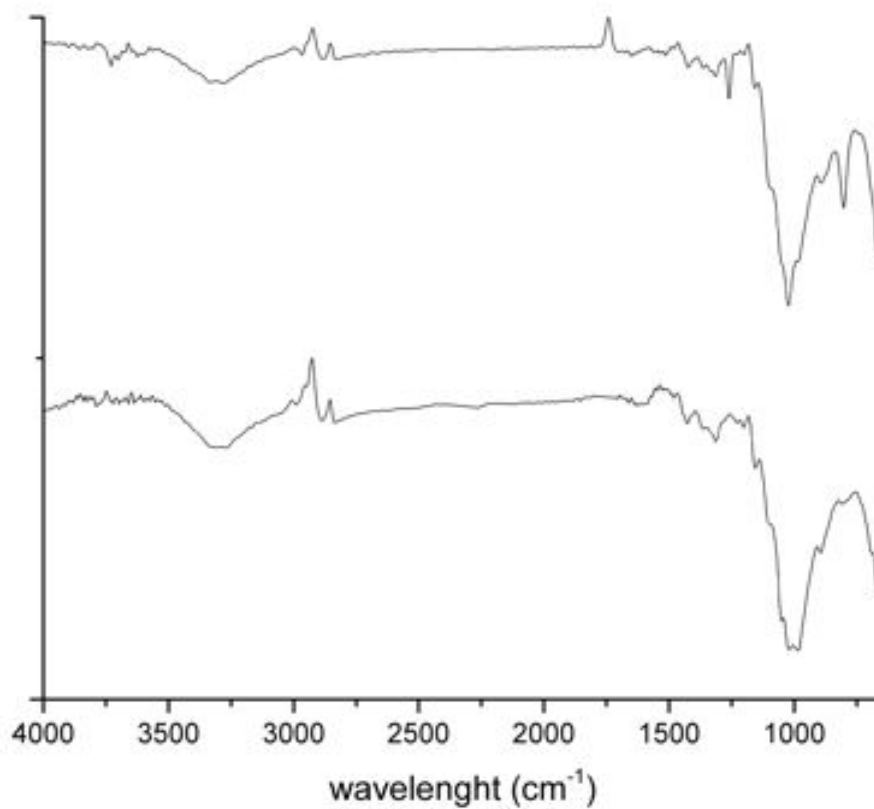
Figure 22. IR spectra: cTPhTES, above. cTPFOS, bottom.
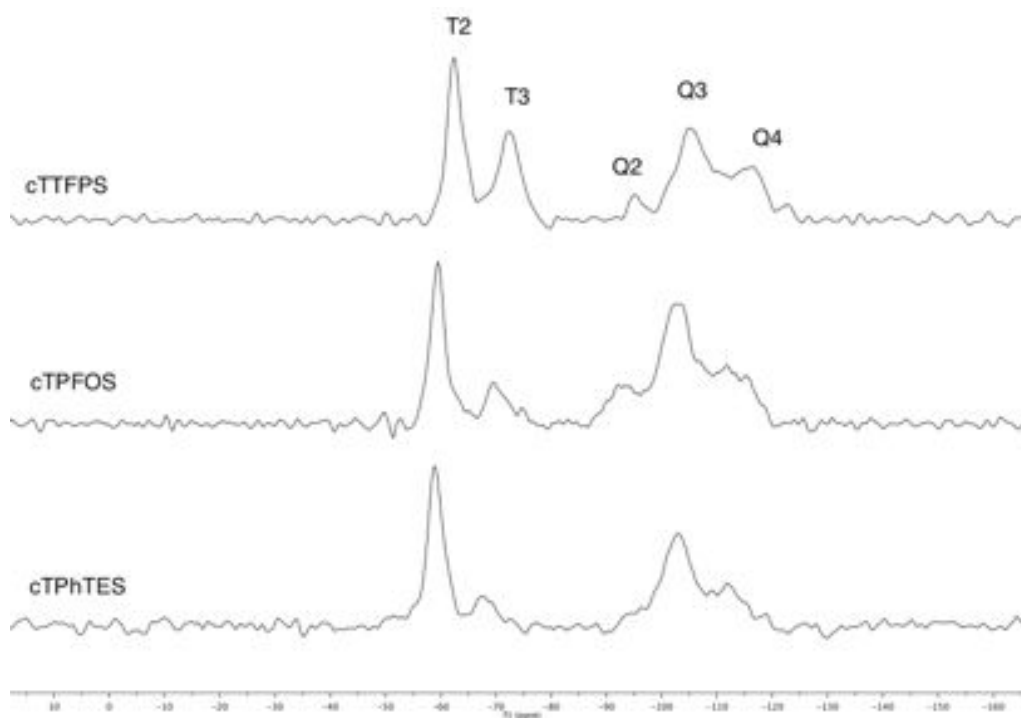
Figure 23. ²⁹Si NMR spectra of functionalized silane.

34

Silicon Solid State NMR spectra were recorded on treated paper; ^{13}C and ^{19}F SS-NMR were performed but did not add any relevant information. ^{29}Si NMR spectra (Figure 23) show the presence of Q^4 (-110 ppm),Q^3(-98 ppm),Q^2 (-91 ppm) units due to TEOS and T^3 (-65 ppm) and T^2(-57 ppm) units of functionalized silane. The areas under the peaks were obtained through deconvolution and the values were used to calculated the degree of condensation (DOC). These systems are characterized by quite high DOC: 84 (cTTFPS), 80 (cTPFOS), 79 (cTPhTES). It is means that the coating are stable.

We performed mechanical test in tensile mode and recorded Young modulus (E), fracture strength, strain at fracture and energy loss (Table 6). The surface treatments improve the paper mechanical properties and the effect of different hydrophobic groups is similar. The coating increase the tensile strength and so the necessary load to break the paper. The values of elastic modulus are higher respect to methylated films obtained in acidic condition but lower than basic catalyzed samples. High values of elastic modulus would have indicated a stiffening of the samples, in this case the treated papers are still quite flexible. In general, the values obtained with these chemical are comparable to those of methylated samples (acid condition).

Sample	E (Pa)	Fracture Strength (N/mm	Energy Loss Z (MJ/m	Strain at fracture εf (%)
cTTFPS	5,04E+09 ± 4,80E+08	37,22 ± 4,90	0,20±0,06	0,93±0,18
cTPFOS	4,51E+09 ± 6,20E+08	36,7±5,5	0,22±0,09	1,03±0,20
cTPhTES	4,67E+09±5,80E+08	38,68±4,79	0,21±0,06	1,08±0,22

Tab 6. Mechanical test results.

The real hydrophobic behavior of the treated surface was tested by VIECA method, Vibrational Induced Contact Angle. The results have been compared to those obtained with the previous treatments (Figure 24). Fluoralkyl and phenyl functionalized silanes have the highest equilibium contact angle values. The static contact angle are 115°, 132° and 126° for cTTFPS, cTTPFOS and cTPhTES respectively; these values are close to those of superhydrophobic surfaces. When a sonic vibration is applied on the surface causes the system to a lower energy. The equilibrium contact angle values are lower, the hydrophobic behavior of cTTFPS is the same of double layers samples obtained with methylated compounds. cTPFOS and cTPhtes are characterized by a wettability lower than the other treatments.
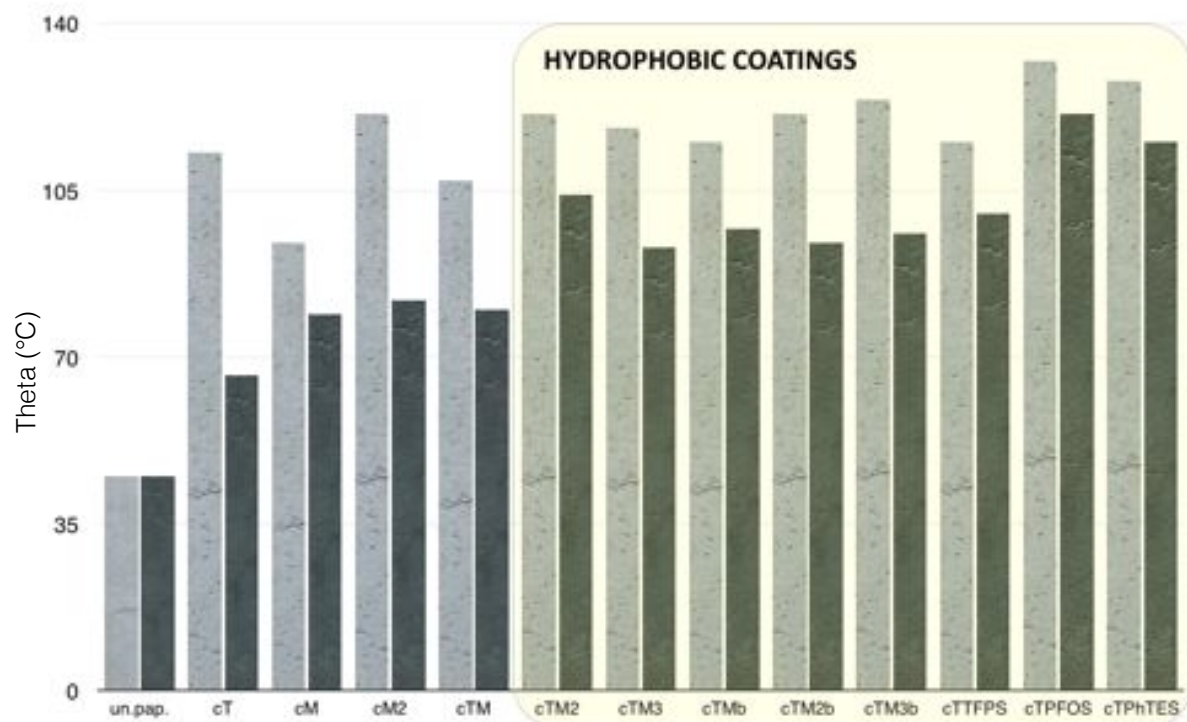
Figure 24. Wettability of the treated sample. Static (light gray) and equilibrium (dark grey) contact angle values.

Fluoralkyl and phenyl functionalized silanes have the highest equilibium contact angle values. The static contact angle are 115°, 132° and 126° for cTTFPS, cTTPFOS and cTPhTES respectively; these values are close to those of superhydrophobic surfaces. When a sonic vibration is applied on the surface causes the system to a lower energy. The equilibrium contact angle values are lower, the hydrophobic behavior of cTTFPS is the same of double layers samples obtained with methylated compounds. cTPFOS and cTPhtes are characterized by a wettability lower than the other treatments.

Optical properties of the treated surface were measured with a portable Konica Minolta CM 2600d spectrophotometer. The changes due to the treatments are reported in Figure; b* represents the blue/yellow component, ΔE* is the deviation from the original value as a cumulative effect of the different components of the light. The results were compared with those presented in the article (Figure 25). The fluorinated chemicals modify the blue / yellow component causing a yellowing of the treated surface. This effect is visible to the human eye, the delta is greater than the limit identified in the standard (1.5). cTPhTES does not involve substantial changes to the optical properties of the samples.
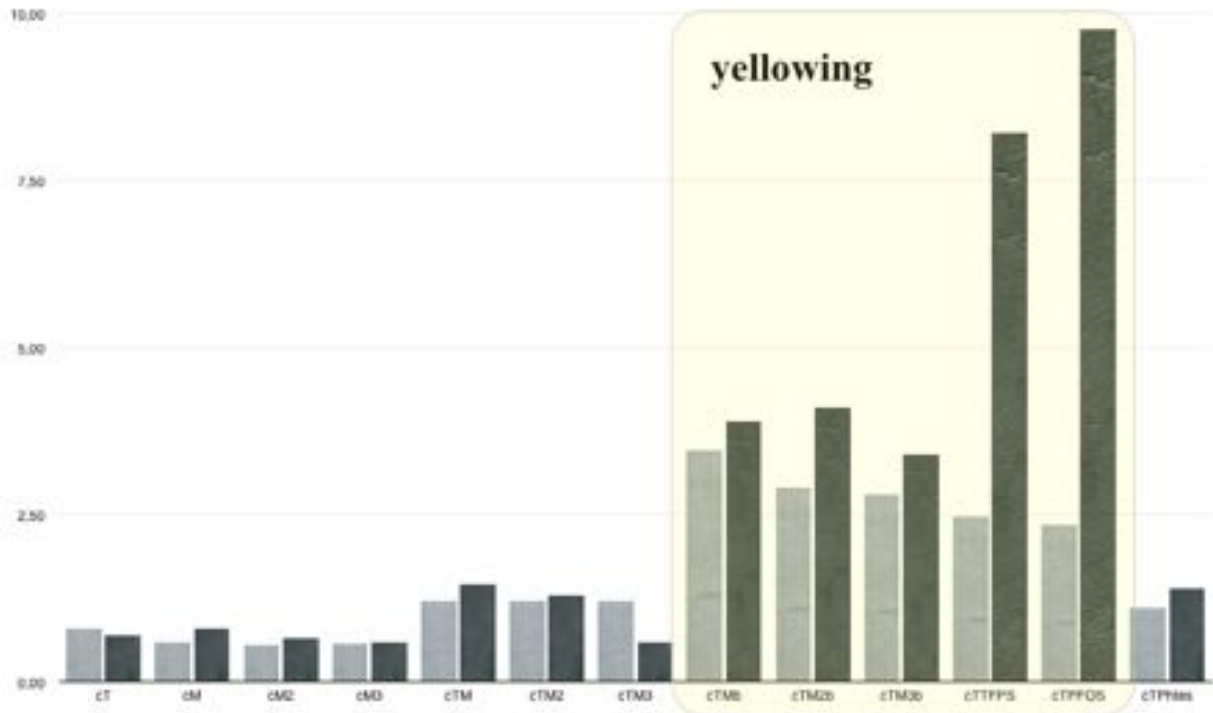
Figure 25. Optical properties of treated samples: Δb* (white bars) and ΔE* (black bars).

2.6.2 <u>Biological Test</u>

Taking into account the results, the best coatings were chosen and their efficacy against fungal attack was evaluated. Tests were performed at the Poznan University of Life Sciennces (Poland) in collaboration with CNR-IVALSA of S. Michele all'Adige (Trento). Mycological test was carried out according to methodology proposed by Cofta and others [2006]. Each treated samples (and untreated reference papers) was placed in sterilised petri dishes containing the selected fungi: Chaetomium and a mixture (1:1:1) of Aspergillus niger van, Penicillium funiculosum and Trichoderma viride. These fungi are able to degrade the cellulose in basic molecules of glucose through cellulase complex enzymes (cellulolytic fungi). The fungal attack can affect the mechanical resistance and the aesthetics properties of paper, pigmentation or discolouration are a consequence of endo- and exo-pigments produced by fungi. The petri dishes were placed in a thermo-static chamber (25°± 1 and 95% rH) for infestation. This test consists in a visual evaluation of the degree of fungal growth on the paper based on a scale of four points proposed by Terziev (): 3 means no growth and 0 means very abundant growth with surface coverage of more then 75%. Samples were observed on the 2nd, 4th, 7th, 14th and 21st days after infestation.

In general, the treated samples showed a slow initial fungal growth (Table 7), while uncoated paper was immediately covered by fungi that have infested the petri dish and the surface of the control sample. The fungal growth became exponential after seven days when the surfaces appeared entirely cover by fungi. cTPhtes has shown the best efficiency against the fungi, after 7 days the substrate surface is still partially visible. Monolayer sample (cM2) showed the worst performance; cTM2, cTM2b, cTPhTES had a similar behavior against the fungal attack. There were not significant differences between the fungal attack of Chaetomium and that of the mixture.

Sample	Fungi	Observation period (day)				
		2	4	7	14	21
unt.paper	Ch.	0	0	0	0	0
	Mix.	0	0	0	0	0
cM2	Ch.	3	3	0	0	0
	Mix.	3	3	0	0	0
cTM2	Ch.	3	3	0	0	0
	Mix.	3	3	0,33	0	0
cTM2b	Ch.	3	3	0	0	0
	Mix.	3	3	0,17	0	0
cTPFOS	Ch.	3	3	0	0	0
	Mix.	3	3	0	0	0
cTPhTES	Ch.	3	3	0	0	0
	Mix.	3	3	0,5	0	0

Table 7. Results of mycological test.

These treatments, exposed to extreme conditions, have shown the ability to slow down the fungal attack; in the future, such systems could be functionalized with biocides to improve their resistance to biological attack.

2.7 Wood surface protection with different alkoxysilanes: a hydrophobic barrier

Elisa Cappelletto, Simona Maggini, Fabrizio Girardi, Giovanna Bochicchio, Barbara Tessadri, Rosa Di Maggio

Abstract

This paper describes coatings on wood surfaces made by dipping the wood into solutions of different alkoxysilanes. The silanes used as precursors contain different organic groups [R'Si(OR'')]. These materials tend to deposit as inorganic–organic polymeric films, where the organic groups (aliphatic hydrocarbons, fluorinated hydrocarbons or aromatic substituents) show hydrophobic properties, which reduce the wettability of the surface. The effects of these treatments on the wood surface were extensively studied using various analytical techniques: scanning electron microscopy with energy dispersive X-ray spectrometry, Fourier transform infrared spectroscopy, nuclear magnetic resonance spectroscopy, water contact angle measurements, and flame resistance tests. The resulting data show that the chemical treatment changes the wood's surface energy, reducing its wettability and reaction to fire. The main innovative finding of this research is that the coatings obtained from a cheaper precursor have a similar performance to that of the more expensive precursors normally used.

Introduction

Wood is widely used in many applications, such as solid wood buildings and infrastructure, because of its many excellent material properties. Cellulose, hemicellulose and lignin are the main components of wood, which has a hydrophilic character due to the hydroxyl groups they contain [**Hill** (2007)]. The hydroxyl groups (OH) are responsible for dimensional changes with moisture content, and the high carbon (C) and hydrogen (H) content makes wood susceptible to biological attack and fire (the most important hazards for wood structures). Many studies have been conducted on how wood surfaces can be modified using chemical, biological or physical agents with a view to improving its properties [**Hill** (2007), **De Meijer** (2001), **Hill** (2001), **Trey** (2010) (2012), **Esteves** (2009), **Podgorski** (2000), **Maggini** (2012), **Mahltig** (2008)]. One of the most important methods involves a chemical modification induced by means of chemical reagents that form covalent bonds between the chemicals and the wood substrate (this excludes simple impregnation of chemicals, coatings, heat treatments, etc.) [**Ziegler** (2003), (2004), (2006), (2008)]. Different systems have been described for treating wood surfaces, such as acetylation with acetic anhydride, acidification with acid chloride or carboxylic acids, chemical reaction with isocyanates, alkyl chlorides and toxic compounds containing Cu, Cr, As, etc. [**Palanti** (2011), **Lu** (2000), **Graziola** (2012)]. Nowadays, one the most of the important goals is to develop a non-toxic treatment. In this regard, siloxane compounds obtained from sol–

gel processes have shown the ability to improve wood properties such as strength and dimensional stability without any toxic side effects [**Mai** (2004), **Donath** (2004)].

This paper explores the use of different alkoxysilanesdimethyldiethoxysilane, perfluorooctyltriethoxysilane and phenyltriethoxysilane all of which are able to make the hydrophilic wood's surface hydrophobic, so that moisture absorption from the environment (and its unwanted side effects) is reduced or prevented [**Donath** (2004), **Cappelletto** (2012)]. When the sols prepared with the precursors are applied to wood by impregnation, their low viscosity enables them to penetrate inside the cells, where the water bound to the walls favors the sol–gel process, involving the hydroxyl groups of the wood in condensation reactions and firmly binding them to the siloxane network. Previous works have studied similar systems, focusing on specific properties of the coatings such as their hydrophobic behavior [**Hozumi** (1996)]. In this paper, the treated wood samples were investigated at macroscopic and microscopic level for the purpose of identifying the best system. In addition the modified wood's hydrophobic behavior, which was studied by measuring static and equilibrium contact angles, its surface features and properties were studied using scanning electron microscopy (SEM) with elemental diffraction spectroscopy (EDS), Fourier transform infrared spectroscopy (FT-IR), solid-state nuclear magnetic resonance (NMR), and flame resistance tests. The resulting data were analyzed, also considering the cost of the raw materials and their ease of handling and environmental friendliness; the economic aspect becomes important for future industrial applications, in the building and civil engineering sectors, for instance.

Experimental

Materials

Larch (Larix decidua, a softwood from Trentino, Italy) was the wood mainly used for the tests, with the exception of the reaction to fire test, which was performed on large blocks of Scots pine (Pinus sylvestris L., a sapwood from Val di Susa, Turin, Italy). The wood blocks were cut from planks with their longitudinal faces parallel to the direction of the grain: the tangential direction of the wood grain intersected the long face of the sample at an angle of between 30° and 45°. All chemical reagents were purchased from Sigma-Aldrich (Italy) and used without further purification.

Synthesis

Sols with a nominal silicon dioxide concentration of 100 g/l were prepared by hydrolysis of the precursors (tetraethoxysilane TEOS, dimethyldiethoxysilane DM2TES, perfluorooctyltriethoxysilane PFOS, and phenyltriethoxysilane PHTES) in absolute ethanol at room temperature under stirring. Water was added to the sols to reach the ratio of OEt/H2O = 1. Then HCl 0.05 M was added dropwise as a catalytic agent in

stoichiometric amounts with respect to the ethoxy groups to ensure hydrolysis. The sols were used for wood impregnation after 4 h of aging.

Preparation of coated samples

The surface of the wood was sandblasted prior to any treatment. The mass of each sample was measured after conditioning in an oven (100 °C) for 12 h to ascertain the anhydrous mass. The samples were conditioned at room temperature and 65 % relative humidity (RH): under these conditions, the wood reaches an equilibrium moisture content at about 12 % (conditioned mass). In the case of the single layer sample (wM2), the wood was submerged for 5 min in the dimethyldiethoxysilane sol. For the double layer coatings, the tetraethoxysilane (TEOS) was used as a precursor for the first layer. The wood blocks were immersed in the TEOS sol for 5 min, then the samples were left at atmospheric pressure for 30 min to allow the solvent to evaporate, then they were submerged in a second sol when a double layer was to be prepared. The treated samples were placed in an oven at 60 °C for 1 h. The mass of each sample was measured after each preparation step. The samples prepared are listed in Table 1, which shows the precursors of the first and any second layer(s) and the average amount of coating per unit of surface (g/m2). The first letter of each label indicates the substrate (w = wood), and the second and the third stand for the precursors of the first and second layers, respectively (Table 8).

Sample ID	First Layer	Second Layer	Weight of coating per unit of surface area (g/m²)
wM2	Dimethyldiethoxysilane $(CH_3)_2Si(OC_2H_5)_2$		33
wTM2	Tetraethoxysilane $Si(OC_2H_5)_4$	Dimethyldiethoxysilane $(CH_3)_2Si(OC_2H_5)_2$	41
wTPFOS	Tetraethoxysilane $Si(OC_2H_5)_4$	Perfluorooctyltriethoxysilane $(C_8H_{13}F_{13}O_3Si)$	56
wTPHTES	Tetraethoxysilane $Si(OC_2H_5)_4$	Phenyltriethoxysilane $(C_6H_5)Si(OC_2H_5)_3$	37

Table 8. List of coated wood samples.

Instrumentation and methods

Scanning electron microscopy (SEM) scans were obtained using a JEOL JSM 5500 scanning electron microscope, and the microanalysis was conducted using an energy-dispersive X-ray spectrometer (EDS). Samples were covered by galvanic gold deposition with a current of 5 mA for 45 s. The analyses were performed with 20 kV acceleration voltages. For the EDS analysis on the inner cross-section of the coated wood samples, samples 30 mm longitudinal x 10 mm tangential x 5 mm radii were cut along their cross-section to obtain two parts of the same length, using a Struers Minitom equipped with a M1D13 diamond

cut-off wheel (size: 127 mm dia. x 0.4 mm x 12.7 mm dia.), at a speed of 350 rpm. Fourier transform infrared spectra (FTIR) were recorded in reflectance mode (ATR system with a zinc selenide crystal) in the range of 4,000–650 cm-1, using a Perkin Elmer Spectrum One instrument. The size of the samples was 30x10x5mm. The spectra were recorded with a resolution of 2 cm-1, with each spectrum averaged over 64 scans. All stack spectra were normalized and baseline corrected before plotting to facilitate their comparison. Solid-state NMR analyses (^{29}Si and ^{13}C) were conducted using a Bruker Avance 400 WB spectrometer with a carrier frequency of 400.13 MHz (1H). Samples were reduced to a powder and packed in 4 mm zirconia rotors and spun at 6.5 kHz under an air flow. ^{29}Si single pulse (SP) spectra were obtained with a 4.3 ls pulse length, a 15 s pulse delay, and 2 k scans with a proton decoupling power of 47 kHz. Q8M8 was used as the external secondary reference. Conventional chemical notation was used to identify the siloxane structure (Qn, Tn, Dn, Mn, where n is the number of bridging oxygen atoms per silicon atom); the relative amounts of silicon species were ascertained by integrating the peaks of the ^{29}Si NMR spectra. The degree of condensation was defined as: DOC=[($4*Q^4+3Q^3+2Q^2+Q$)/4+($3*T^3+2*T^2+T$)/3+($2*D^2+D$)/2+M]. ^{13}C NMR spectra were acquired with a 3.36 ls pulse length, a 7.5 s pulse delay, and 3 k scans with a proton decoupling power of 51 kHz. Adamantane was used as the external secondary reference. Water contact angle measurements were taken using the sessile drop method on wood blocks (30x10x5 mm). The volume of the water drop was 3 µL. The static contact angle was recorded with a camera immediately after the drop was deposited (10–15 s), processing the images with IMAGE j software and approximating the drop to an ellipse. The measurements were performed along the wood's grain. The sessile contact angle is not the most accurate measurement because it corresponds to the greatest possible contact angle when the surface is heterogeneous and/or rough, as in the present case [**Ziegler** (2004) (2006)], whereas the vibrationally induced equilibrium contact angle (VIECA) technique affords a value closer to the true thermodynamic contact angle (equilibrium contact angle). A sonic vibration of appropriate frequency, waveform and duration is applied to the surface, inducing a further relaxation of the drop to a configuration with a lower free energy [**Graziola** (2012)]. The water used for the tests was purified in a Millipore MilliQ device with UV control, showing a constant electrical resistivity of 18.2 MX cm and a surface tension of 72.7 mJ/m2 at 20 °C. All data were collected at a room temperature of 26 ± 2 °C. The mean of five measurements was calculated for each type of sample. The fire retardance of the coated wood samples was measured in accordance with the procedures specified in the ISO 5660-1 standards using a fire testing technology cone calorimeter. The wood panels were conditioned before the test. The wood blocks were 24x100x100 (mm) in size; all samples were measured in the horizontal position. The specimens were irradiated with a heat flux of 50 kw/m2 using an external igniter. The results reported in this paper include the following measurements: time to ignition (t.i., s), total heat released during the test (THR, MJ/ m2) obtained by measuring the oxygen consumption and the average mass loss rate (MLRav, g/sm2). Three tests were performed for each type of coating.

Results and discussion

Different coatings of amorphous silica were deposited on the surface of the wood. A single-layer sample, wM2, and a series of double-layer coatings using TEOS as the precursor of the first layer were produced. After its hydrolysis, the excess silanol ensures the reaction with both the OH groups of the substrate and those of the precursor in the second layer. Neither a double layer made with the same chemical, nor a single layer of tetraethoxysilane were taken into account because previous studies had demonstrated that they were ineffective (in the case of a single layer of TEOS, the OH groups give rise to a hydrophilic surface) or the coatings were excessively stiff [**Cappelletto** (2012)].

SEM–EDS

The morphology of the coated samples was investigated using SEM: their surfaces appeared smoother than the uncoated specimens, suggesting the presence of a coating on the wood's surface (Figure 26 a, b).
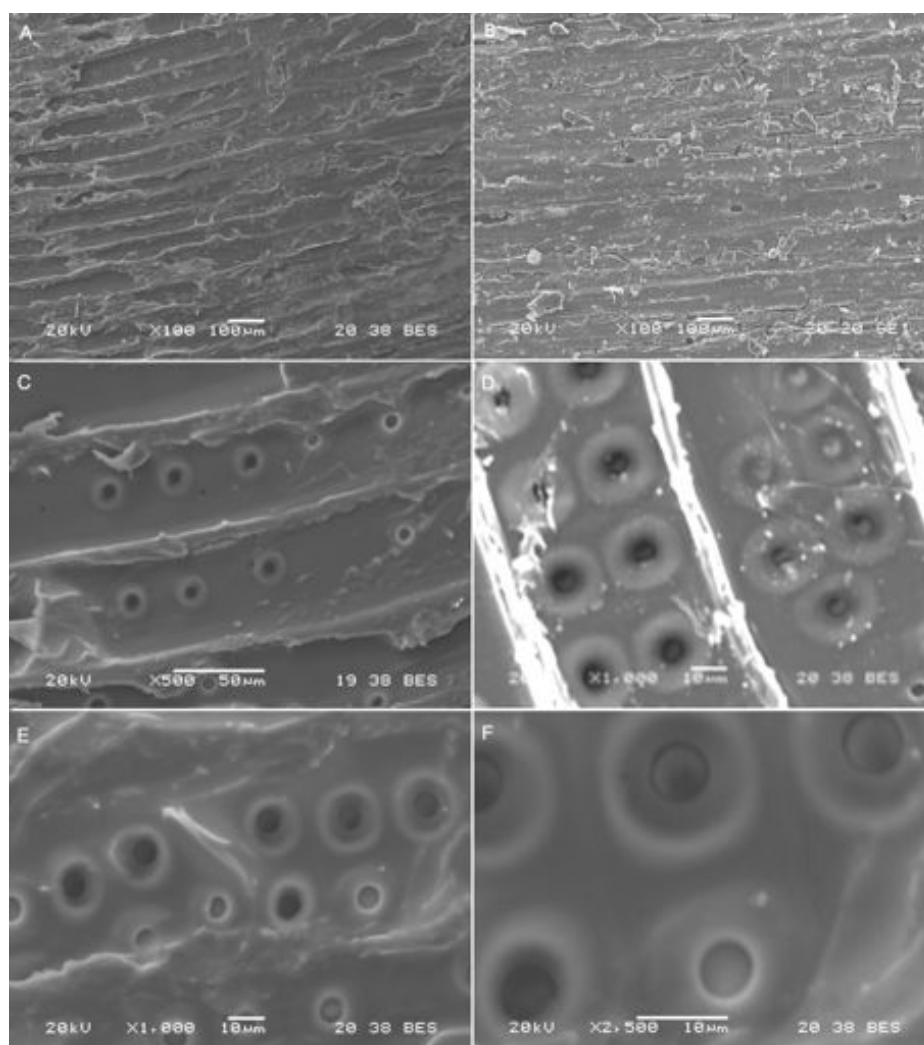
Figure 26. SEM micrographs collected at different magnifications: a surface of untreated wood x100; b wTM2 sample x220; c wM2 x500; d wTPFOS x1000; e wTPHTES x1000; and f detail of the pores at high magnification, wTM2 x2500.Figure 2 SEM micrographs and EDS map: silicon distribution at x400 (wM2).

The wood's natural porosity was not completely sealed by the siloxane, however. Figure 1c–f shows the surface profile of the cell walls, which gave the wood a partial permeability. Wood has a natural capacity for exchanging moisture with the outside by means of dimensional changes in response to changes in the relative humidity of the atmosphere. A good coating should not prevent this natural exchange with the outside. EDS confirmed that silicon was quite evenly distributed over the surface of the wood (Figure 27), and even on the cell wall (Figure 28).
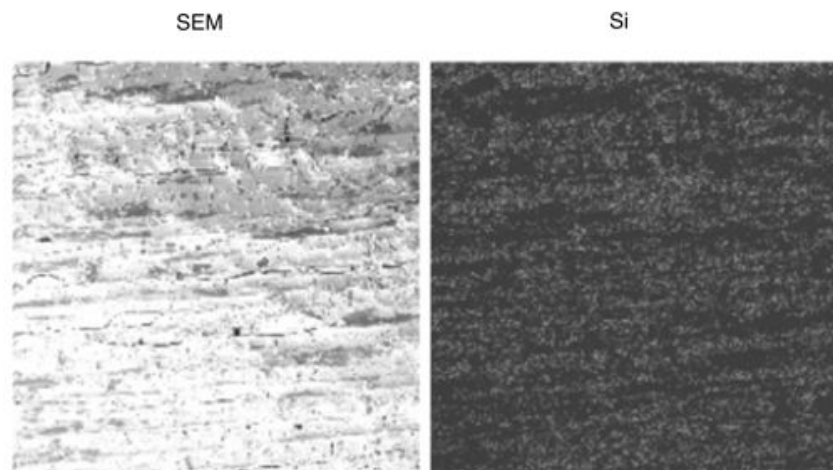
Figure 27. SEM micrographs and EDS map: silicon distribution at x400 (wM2)
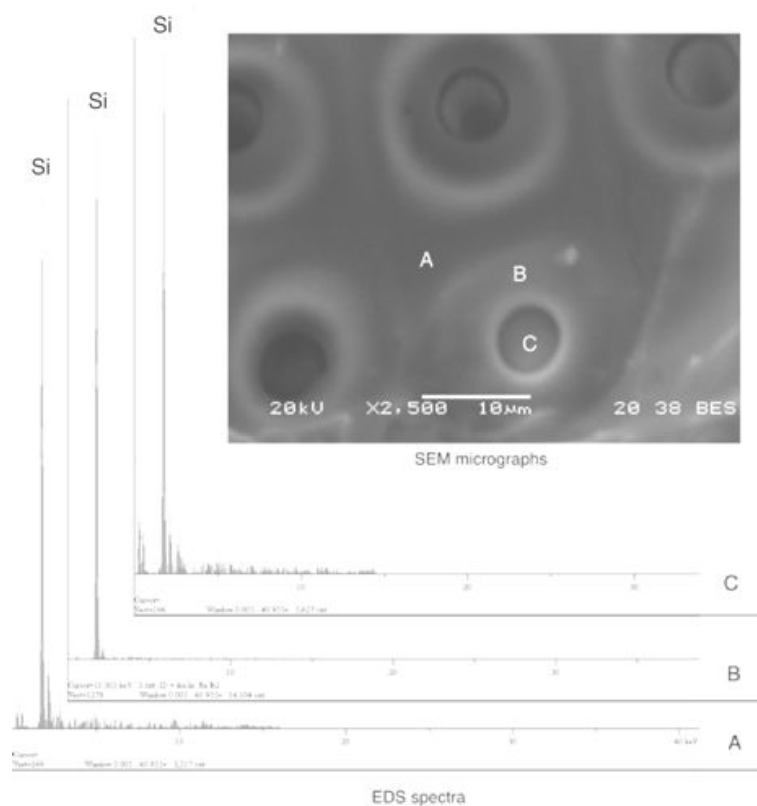
Figure 28. SEM micrograph of the natural porosity of the wood (wTM2) at x2500 (above) and EDS spectra at three different points (below).

44

FT-IR/ATR

FT-IR analysis enabled us to study the changes on the surface of the coated block, and any presence of OH groups in particular. The uncoated wood was used as a control, after conditioning in the same conditions. The treated samples showed a decrease in the intensity of the OH bands (symmetric and anti-symmetric stretching) between 3000 and 4000 cm^{-1} and that (scissoring) peaked at 1640 cm^{-1} (Figure 29). This was most evident on the sample coated with phenyltriethoxysilane (wTPhtes). IR spectra of all samples showed the Si–O–Si stretching band (1029 cm^{-1}). The peaks at 2920 and 2840 cm^{-1} were due to CH_3 (Cappelletto et al. 2012). There was a visible asymmetrical stretching vibration of the C–F bonds at 1240 cm^{-1} (Girardi et al. 2011) in the FT-IR spectrum of the wTPFOS sample. The carbon–carbon double bond vibration of the phenyl group at 1500 and 1600 cm-1 was apparent in the FT-IR spectrum of the wTPhtes sample. All FT-IR spectra also contained peaks due to cellulose and lignin, partially overlapping the following bands of siloxane: 3415, 2935, 2840, 1714, 1606, 1502, 1462, 1425, 1268, 1214, 1140, 1086, 1029, 866 cm^{-1} [**Girardi** (2011)].
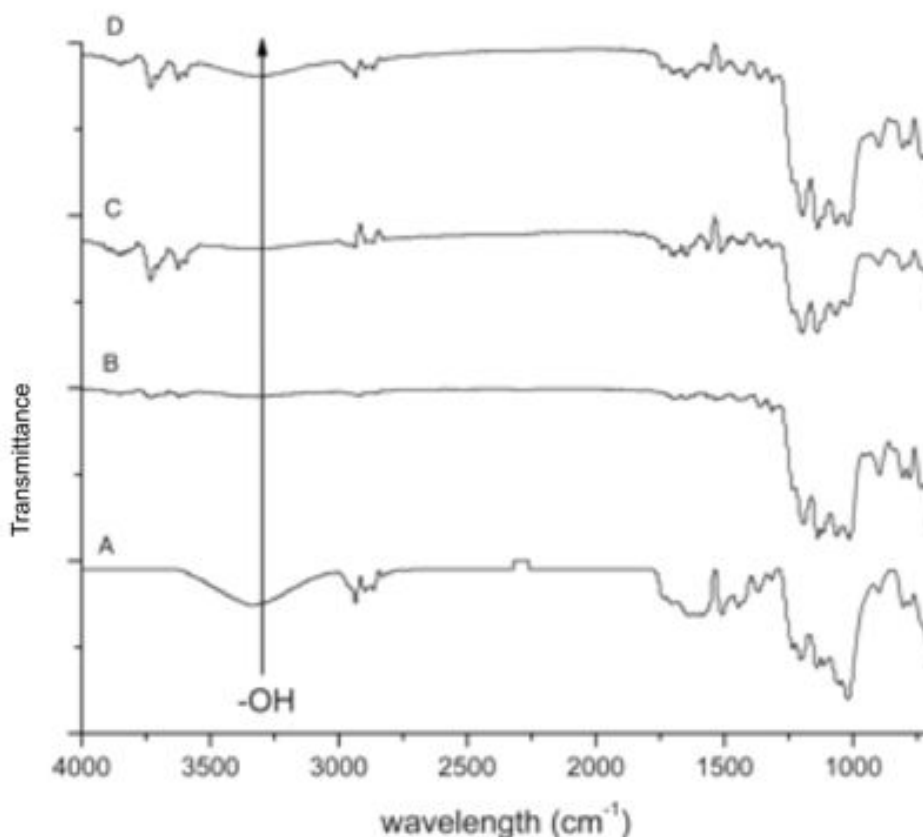
Figure 29. FT-IR spectra. a Uncoated wood, b wTPHTES, c wTPFOS, d wTM2 (spectra are offset for the sake of clarity).

^{29}Si MAS solid-state NMR

Sample	Structure unit	ppm	Real Area	DOC
wM2	D^2	-21	232609	100
wTM2	D^1	-10	92334	87
	D^2	-21	479466	
	Q^3	-100	860565	
	Q^4	-109	504057	
wTPFOS	T^2	-58	367585	89
	Q^3	-103	505840	
	Q^4	-111	226415	
wTPHTES	T3	-68	462473	80
	Q^3	-100	3543449	
	Q^4	-110	209850	

Table 9. ^{29}Si MAS NMR chemical shifts and assignments.

The ^{29}Si MAS NMR analyses enabled us to assess the structure and the degree of condensation (DOC) [Di Maggio (2012)] of the polysiloxane material. ^{29}Si units are labeled in the spectra (Figure 30) according to the chemical notation: {Q^4 [Si(OSi)$_4$], Q^3 [(OR)Si(OSi)$_3$], Q^2 [(OR)$_2$Si(OSi)$_2$], T^3 [RSi(OSi)$_3$], T^2 [RSi(OSi)$_2$(OR')], T^1 [RSi(OSi)2(OR')$_2$], D^2 [R2Si(OSi)$_2$], D^1 [R$_2$Si(OSi)(OR')]} [Bardet (2012)]. DOC values (Table 9) were calculated by integrating the area under the peaks of each ^{29}Si unit. It is worth noting that all the samples showed a high degree of condensation already after their preparation. This means that the coatings would change very little with aging. This is particularly true for the wM2 sample because only the signal of the D^2 unit is visible in the spectrum. This also suggests that the coating cannot bond chemically to the substrate. According to the DOC formula (see experimental part), the lower values of the samples wTM2, wTPHTES and wTPFOS are due to the contribution of the signal of the Q^3 unit given by the TEOS. The Q^3 units may indicate the presence of Si–O–C bonds between the siloxane network of the coatings and the substrate.
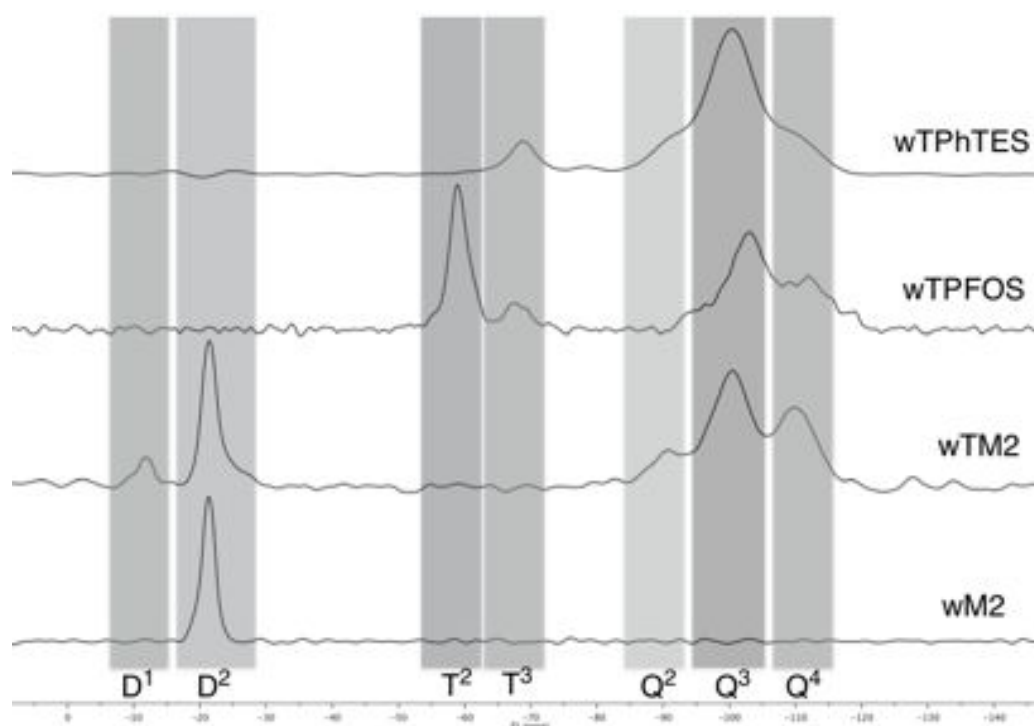
Figure 30. ^{29}Si SS-CPMAS spectra of coated wood blocks.

Contact angle test

The static and equilibrium contact angle values are shown in Table 10. Wood is a very hydrophilic material, so the contact angles are very low. Regardless of their value, the contact angles of untreated wood cannot be measured using the methods adopted for this study and described in the experimental section. Some authors [**Boehme** (1996)] have reported a Young' angle of about 20° for untreated wood. All the coatings make the contact angle exceed this value, due to their lower surface energy. It is only the equilibrium contact angle (which is the closest to Young's angle) that can really indicate a surface's hydrophobic or hydrophilic behavior. It is worth noting that, despite the high static angles recorded for all the samples, only the wTPFOS and wTPHTES samples are really hydrophobic, reaching a value of 90°. For all the other coatings, the large hysteresis between the static and equilibrium contact angles goes to show that the chemical characteristics of the surface are not homogeneous. The main explanation for this result could be that some areas of the surface remained uncoated (and therefore hydrophilic), while the surface tension was lower (and therefore hydrophobic) where the siloxane coated the wood. wTPFOS and wTPHTES warrant further comment. Although the wTPFOS samples proved more hydrophobic than the samples with methyl residuals, their hydrophobicity was not as high as expected, and it was similar to that of wTPHTES. The hydrophobicity of this latter sample is induced simply by the phenyl groups.

47

Sample	Stat.(°)	Equil.(°)
wM2	106±5	79±6
wTM2	109±4	87±3
wTPFOS	115±3	90±3
wTPHTES	112±3	91±2

Table 10. Static and equilibrium contact angles.

This study therefore demonstrates that there is little to gain from using fluorinated coatings for the purpose of making the wood more hydrophobic. When we compare the cost of the raw materials, we find that phenyltrimethoxysilane is ten times more expensive than dimethyldiethoxysilane, while it is fifty times cheaper than perfluorooctyl-triethoxysilane. Another advantage of using the sol–gel process using silanes as precursors lies in that they are easy to handle and require very few safety precautions. The degree of hydrophobicity achieved with the fluorinated compound is much the same as with wTPHTES and wTM2, and the difference does not justify a higher cost.

Cone calorimeter test

Time to ignition, THR and MLRav are important parameters for assessing the behavior of coated samples exposed to fire under specified conditions [**Harada** (2001), **Grexa** (2001), **Lee** (2011)]. The values recorded for these parameters are given in Table 11.

Sample	t.i. (s)	THR (MJ/m2)	MLRav (g/sm2)
Untreated wood	13.33	156.65	7.18
wM2	13.33	157.33	7.61
wTM2	15.33	145.22	7.00
wTPFOS	14.67	151.92	7.11
wTPHTES	18.00	148.46	6.88

Table 11. Fire test parameters: time of ignition (t.i), total heat release (THR) and average mass loss rate (MLRav).

All the treated samples except for wM2 performed better than the untreated wood samples or surprisingly those protected with a commercial product (sold as a fireproof paint for wood). Concerning this last sample, such an unexpected result might be explained by the fact that the product was used together with other treatments, not alone. The wTM2, wTPFOS and wTPHTES samples took longer to ignite than the uncoated wood, indicating that they burn less easily (Table 11). The THR of all the samples with double-layer coatings was significantly lower than for the uncoated wood, suggesting that these coatings improve fire resistance and thermal stability. The samples with double-layer coatings also performed better in terms of MLRav, with the exception of wTPFOS; a lower MLRav value means that a material burns out more slowly. The better performance of the samples coated with a double layer can be explained by the presence of siloxane materials, which behaved like a thermal barrier (albeit thin) and prevented heat transfer and the transportation of combustion products, thereby reducing the THR and MLRav. FT-IR, SEM and EDS analyses on the surface of the burned samples confirmed that the siloxane matrix remained even after the heat treatments, leaving the cellular structure of the wood still visible (Figure 31) underneath it. The untreated wood block burned completely. The FT-IR spectrum of a burnt coated sample still showed the typical bands of the siloxane matrix at around 1100 cm^{-1} (Figure 32).
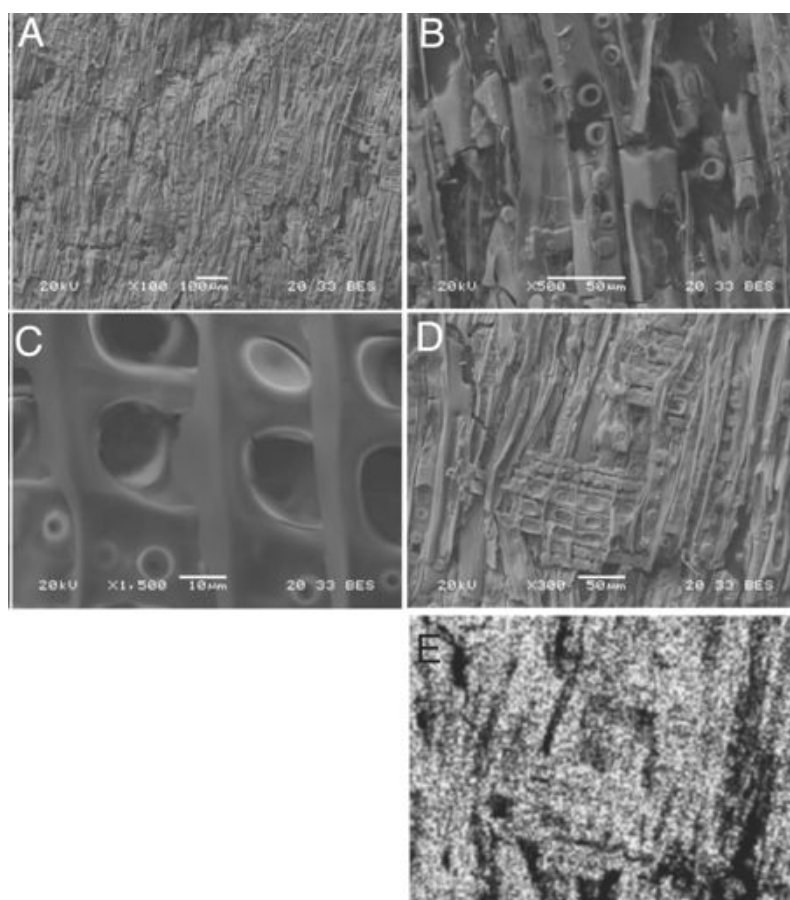
Figure 31. SEM micrographs of the samples after the reaction to fire test: a wTPHTES at x100; b wM2 at x500; c wTPFOS at x1500. d, e wTM2 SEM micrograph at 9300 and EDS map showing distribution of Si atoms.
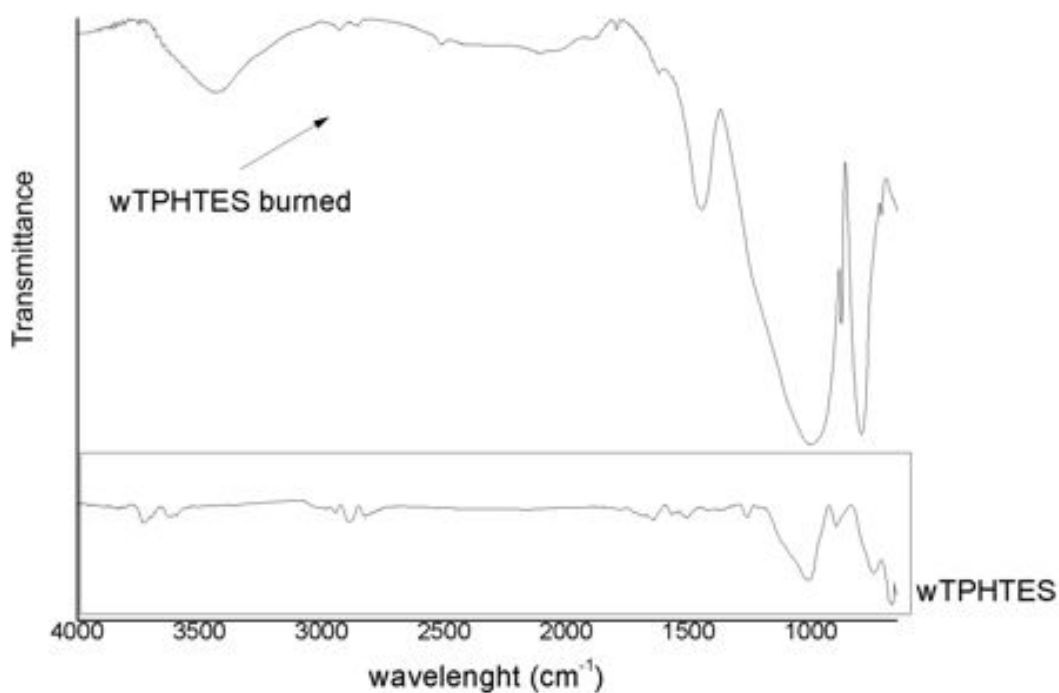
Figure 32. IR spectra of wTPhtes before and after the reaction to fire test (spectra are offset for the sake of clarity).

Conclusion

In this work, we studied different wood coatings by means of a series of experiments designed to identify the best system in terms of protecting against moisture and fire. Taking all the data collected into account, the samples coated with a double layer performed better than those with a single layer, the latter (wM2) proving unable to guarantee a uniform distribution of the coating on the wood's surface. This was confirmed under the electron microscope and by the contact angle results. The ^{29}Si NMR spectrum showed that the siloxane matrix of the single-layer coating was fully condensed, meaning there were no interactions with the substrate. The double-layer coatings were quite evenly distributed over the surface of the wood. The siloxane matrixes were able to penetrate inside the natural pores in the cellulosic material. A thin inorganic layer was deposited on the cell walls and did not fill the holes, thus ensuring the breathability of wood. SEM micrographs of the samples coated with a double layer showed little difference between the coatings. The

^{29}Si SSNMR spectra indicated that the coatings were quite stable (e.g. they had a high DOC). The wettability study demonstrated that the samples coated with a double layer achieved the best performance. All coatings reduced the surface energy of the wood, making its surface more hydrophobic (as confirmed by the lower hydroxyl signals in the FT-IR spectra. The equilibrium contact angle values only exceeded the hydrophobicity limit (90°) in the case of wTPFOS and wTPHTES, so these are the only samples that can be considered genuinely hydrophobic. The better performance of the double-layer than the single-layer coatings was also confirmed by the fire resistance test, which showed that the former reduce the material's flammability. Taking all the parameters considered into account, the double-layer coatings improve the wood's hydrophobicity and reaction to fire. The wTPHTES performed best of all, but it is important to emphasize that the results obtained with the wTM2 sample were comparable with those achieved using the more expensive chemicals (perfluorooctylsilane and phenyltrimethoxysilane). The performances of all the coatings could be improved by preparing the samples differently, e.g. by impregnating the wood under a vacuum, using ultrasonic treatments or increasing the amount of material applied.

2.7.1 Leaching and Biological tests

Biological tests were performed on selected treatments between the three different series studied in this thesis. The measures against biological attack were made in collaboration with CNR-IVALSA of Sesto Fiorentino (Florence, Italy). The wood samples were derived from Scots pine (Pinus sylvestries L.) sapwood. The results have not been published in none scientific communication. The resistance of decay fungi of the coated wood were performed on leached samples. Wood blocks (0.5x1x3 cm, conditioned at 103°) were subjected to leaching according to EN 84 (1997). Before the leaching, the sample were conditioned at 103° in a oven for 18 hours. Then wood specimens were placed in a glass beaker filled with deionized water, the beaker was put in a desiccator and vacuum was applied (residual pressure 4kPa). Wood blocks were maintained in distilled water (ratio of water to wood 5:1) for 14 days with 9 water changes, and then conditioned to constant mass. The samples were weighted before and then the leaching, data reported in Table 12 were the mean of eight replicates for treatment.

Sample	Wood blocks treated % mass loss (average)
wM2	$1,3 \pm 0,30$
wTM2	$1,1 \pm 0,31$
wTPFOS	$0,55 \pm 0,28$
wTPhTES	$0,82 \pm 0,20$

Table 12. Results of leaching test.

All coated samples are not susceptible to leaching by water, this means that the treatments are stable in agreement with the DOC values obtained by NMR investigation, at last, they can be used outdoor. Wood moisture content was calculated from the following formula:

$$\text{Humidity \%} = \frac{M_1 - M_o}{M_o} \times 100$$

where M_1 is sample mass at environmental conditions, M_o is sample dry mass at 103°.

A wood humidity between 9,5% and 10,1% was detected, i.e. near to the Equilibrium Moisture Content (EMC) of 11-12% reported for wood in equilibrium with the environmental conditions (20°C, 65% RH). After leaching test, the efficacy of treatments against fungi basiodiomycetes was evaluated throughout the

accelerated methodology proposed by Bravery (1979). The samples were sterilized (121°C) and exposed to the brown rot fungus *Coniophora puteana*. Groups of 4 treated samples were pleaced together with two untreated reference samples in a Kolle flask containing the brown rot fungus (Figure 33).

Figure 33. wTPhTES samples within Kolle flask.

The strain virulence was assessed by placing six pairs of untreated wood inoculated with the same fungus. The test lasted six weeks during which the wood blocks were incubated with the fungus at 22°C and 75% RH. The resistance of the treated samples was evaluated through the measurement of wood mass loss. The mass loss was calculated for each blocks as difference between dry mass before the treatment and after the fungal exposure (Table 13).

Sample	Sample mass, g (20°C, 65%)	Sample dry mass, g (103°C, 18 hours)	Humidiy %	Sample mass after leaching, g	Sample dry mass after leaching, g (103°C)	% Mass Loss
wM2	0,83 ± 0,08	0,76 ± 0,07	9,5 ± 0,2	1,88 ± 0,09	0,74 ± 0,07	21,9 ± 1,9
wTM2	0,84 ± 0,04	0,75 ± 0,04	10,1 ± 0,2	1,88 ± 0,07	0,73 ± 0,04	15,5 ± 1,4
wTPFOS	0,85 ± 0,09	0,77 ± 0,08	10,1± 0,1	1,87 ± 0,08	0,77 ± 0,08	19,3 ± 3,3
wTPHTES	0,90 ± 0,10	0,82 ± 0,09	10,0± 0,2	1,93 ± 0,07	0,81 ± 0,09	10,7 ± 2,2

Table 13. Decay test results.

The test was considered valid since untreated sample were attacked, wood blocks used to control the fungal virulence gave an average mass loss of 26,1% confirming the vitality of the fungal strain. All the samples are characterized by mass loss values enough high. Among them, wM2 showed the worst efficacy against the fungal attack, its mass loss is comparable to that of untreated reference. This data confirms that a monolayer is not sufficient to protect the wood surface. The best performance was obtained by wTPhtes, its mass loss value is halved respect to that of its reference as happened in the biological test on cellulose samples. In general, those results indicates that the increase of hydrophobic behavior of surface can help against fungal attack, their efficacy could be improved with the addition of biocidal compounds.

2.8 NMR Study of Polyamidoamines PAAs (patent)

The synthesis of a new material has been investigated through SS-NMR.

This part of the research has been done in collaboration with the group of the Prof. Predieri (University of Parma). Synthesis and applications of this material are going to be patented.

Hybrid organic-inorganic polymers, poly(amidoamine)s (PAAs), were obtained from N,N'-methylenebisacrilamide (MBA) and ethanolamine (EtA) under different experimental conditions (Table 14).

Sample	Solvent	Mixing Condition	Curing treatment
PAAb1	Ethanol	EtA fast added into MBA	
PAAb2	Ethanol	EtA added dropwise into MBA	
PAAb3	Ethanol	MBA added dropwise into EtA	
PAAd1	Methanol	EtA fast added into MBA	
PAAd2	Methanol	EtA added dropwise into MBA	
PAAd3	Methanol	MBA added dropwise into EtA	
PAA	without		
PAAr	without		under laser radiation

Table 14. List of PAAs samples.

PAAs are polymers containing amido and amino groups regularly arranged along their polymer chains, which can can be obtained by addition of primary amines or secondary diamines to bis-acrylamides (Figure 34).
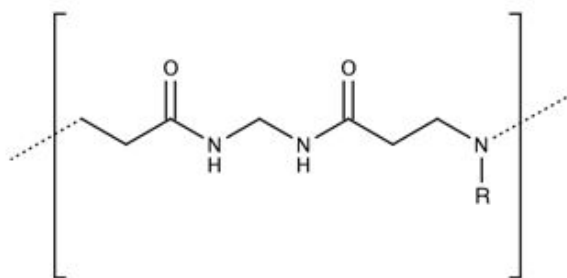
Figure 34. Polyaminoamide polymer.

These polymers have been studied as preservative formulations for wood; synthesis, application and characterization of treated wood have been done at the University of Parma.

SS-NMR spectroscopy has been used to find the optimum conditions for the synthesis of the resulting polymer through NMR spectroscopy. The influence of solvent (water, ethanol, methanol or no solvent), the way in which the reagents were reacted (whether EtA was quickly or slowly added to MBA or MBA dropped into the ethanolamine and vice versa) and the use of curing treatment have been investigated.

ppm	Assignment	
174	-C=O	MBA, PAA
168		
132	-CH=CH$_2$	MBA
128		
60	-CH$_2$-CH$_2$-	PAA, EtA
55		
45	-CH$_2$-NH-	MBA, PAA, EtA
35		
18	-CH$_3$	EtOH

Table 15. ^{13}C NMR chemical shifts and related assignments.

Solid State NMR spectroscopy

^{13}C spectra were recorded with a Bruker 300 spectrometer equipped with a double band probe. The NMR spectra were analyzed using Bruker and MestReNova software. Samples were packed in 4 mm zirconia rotors and spun at 9 kHz. ^{13}C SS-NMR spectra were obtained at a frequency 75.47 MHz. ^{13}C proton decoupling spectra were acquired with 90° pulse length, 2.2 μs, decoupling pulse length 6 μs, delay 10 s. Adamantane was used a external secondary reference (38.56 and 29.6 ppm).

Results

^{13}C NMR spectra allowed us to follow the reaction through the observation of methylene, vinyl and carbonyl signals. Chemical shift and assignments reported in the Table 15. Solvents and the operational mode affected the polymerization (Figures 35-37). Specifically, the slow addition of reagents promoted the polymerization reaction and the chain growth. Accordingly, the spectra have showed the disappearance of the signals due to the vinyl groups of the MBA.

When MBA, previously dissolved in ethanol is added dropwise to EtA, PAAb3, the vinyl signals (of MBA) intensity is very low, this means that the reaction of polymerization is complete (Figure 35). A similar result obtained by inverting the two chemicals, PAAb2, solvent traces are visible in the spectrum. The reaction is not promoted by the fast addition of MBA in EtA.
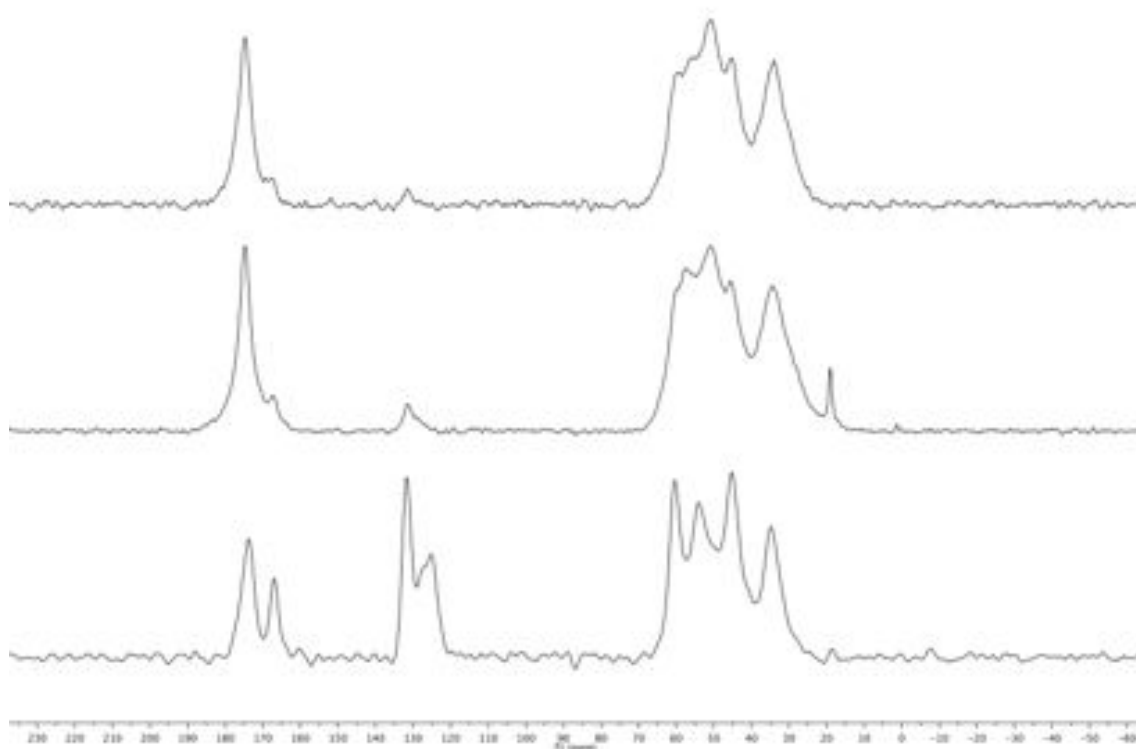
Figure 35. ^{13}C NMR spectra. Effects of mixing condition (ethanol as solvent).

The same effects have been found for the synthesis with methanol as solvent. The polymerization of PAA is favor when MBA, completely dissolved in methanol, is added dropwise at EtA, in the spectrum the signals of vinyl group are completely absent, PAAd3 (Figure 36).

56
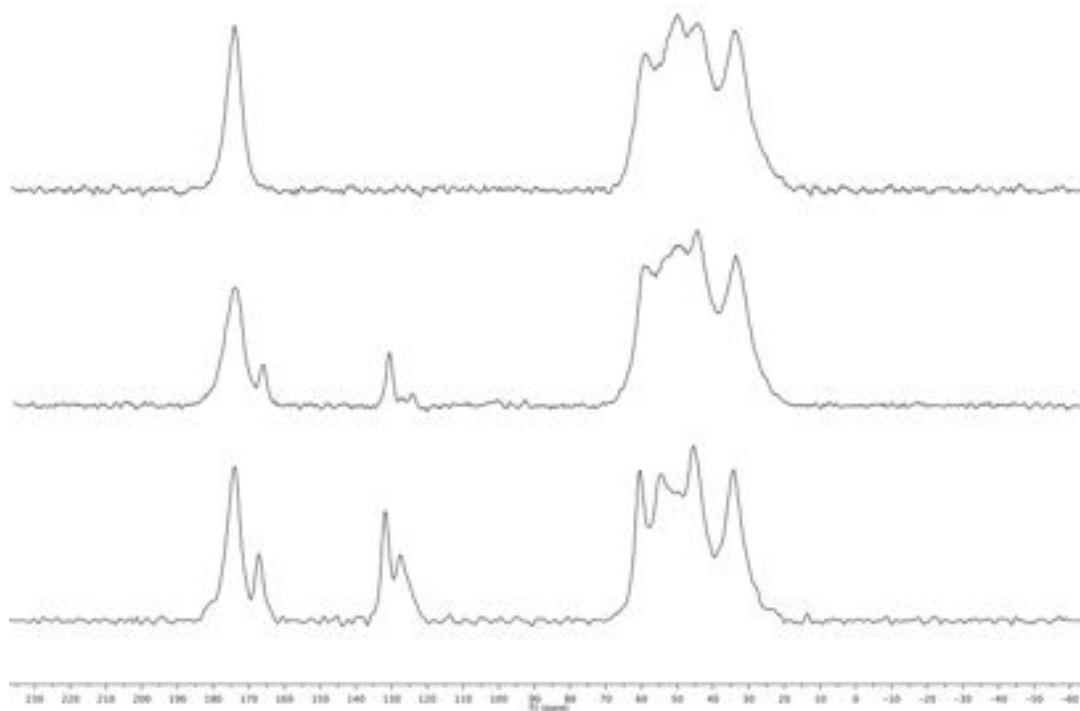
Figure 36. ^{13}C NMR spectra. Effects of mixing condition (methanol as solvent).

Finally the influence of the curing treatment with laser radiation (632.8 nm), in this case the vinyl signals significantly decrease and a single peak appears in the region of carbonyl signals (Figure 37).
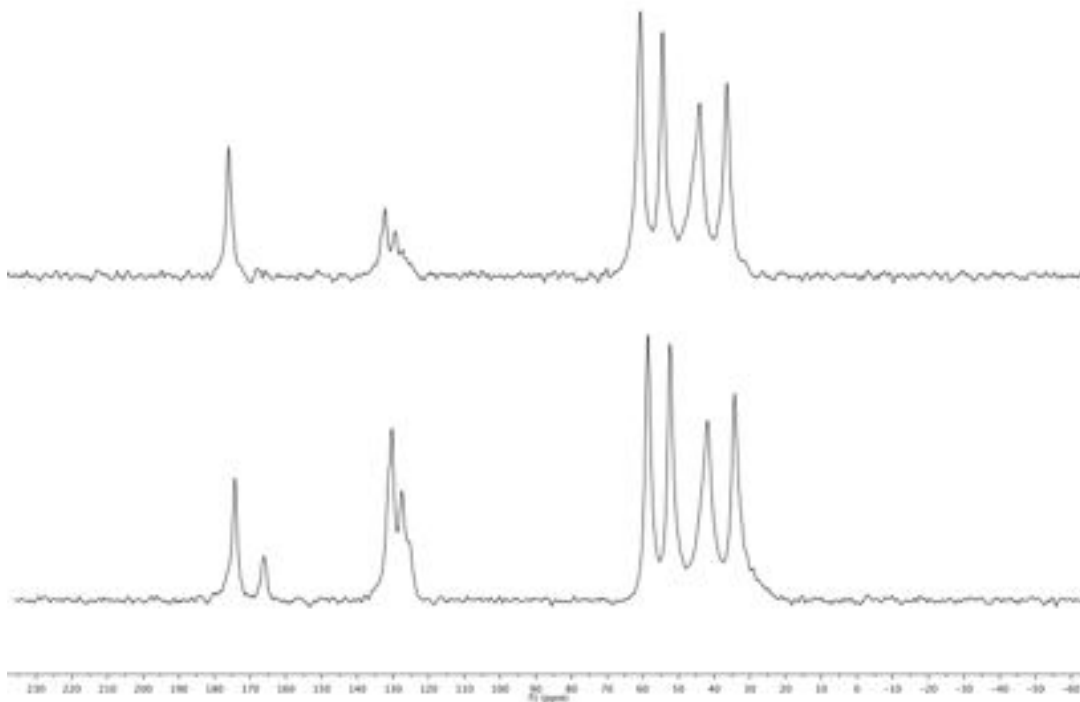
Figure 37. ^{13}C NMR spectra. Effects of laser radiation.

Conclusions

NMR spectroscopy is a useful technique to monitor the progress of reaction. The dropping of reagents and methanol as solvent are the main factors, which favoured polymerization of PAA. The analysis of the 13C spectra showed that the decrease of the vinyl signals is always followed by the disappearance of one of the two carbonyl peaks (168 ppm). The chemical shift of the carbonyl carbons is displaced depending on the conformations of the polymer [**Ando** (1984)]. The conformation-dependent 13C chemical shifts are mainly interpreted in terms of the change of the electronic structure. 13C NMR chemical shift of the carbonyl carbon is sensitive to the spatial arrangement of the nuclei comprising the hydrogen bond, since the electronic structure of the carbonyl carbon is greatly affected by the intermolecular hydrogen bond which is formed with N-H. The chemical shifts of CO depends on hydrogen bond length [**Ando** (1988)], and the downfield shift is associated to a decrease of the hydrogen bond length.

2.9 Genearal conclusions

This part of the thesis dealt with the investigation of treated cellulosic substrate with different chemicals, chosen to increase the hydrophobic behavior of the surfaces and improve their resistance against some external agents.

The present work has reached the following goals:

A wide characterization of protective systems on cellulose and wood substrates was performed. At microscopic level, several analyses provided information on morphology and stability of the treatments. SEM micrographs showed that, on the contrary of the double layer coatings, those monolayers are not uniform. Moreover, microscopic observation showed that the coatings prepared with basic conditions or with double layer of TEOS are too thick and useless due to cracks formation. These systems had not been considered for further coatings. The SEM micrographs showed that treatments useful for coatings penetrated inside the cavities without seal them completely, following the natural roughness of wood and ensuring the natural breathability of wood.

Infrared spectroscopy confirmed the presence of siloxane network on surfaces and the decrease of hydroxyl groups due to the coatings. High degree of condensation was calculated through the analysis of ^{29}Si NMR spectra for all coatings both on cellulose and wood samples. These data are in agreement with the results obtained by leaching test on treated wood blocks. At macroscopic level, the behaviour of the treated samples in contact with water, fire and fungal attacks were investigated. Double layer samples showed the best performances.

The investigation regarded also wettability, because to increase the hydrophobicity of paper and wood surface is the main goal of these treatments. VIECA method, able to measure the value much closer to the true thermodynamic contact angle, was used. In general, the treatments produce a decrease of surface energy, more evident in the cellulose samples than in wood ones.

The tests of both fire resistance and the efficacy against fungal attack showed an improvement of the resistance.

Finally the most interesting results is that coatings achieved by using methylalkoxysilane precursors have properties comparable to those prepared with more expensive chemicals, e.g. fluorinated silanes and phenyl functionalized siloxanes.

CHAPTER III

Solid State NMR characterization of Cement base material

3.1 Introduction

This chapter deals with the characterization of two cementitious mix by ^{29}Si NMR spectroscopy. Cement is the most important constituent of concrete, which formulation is modified in order to enhance performance. Polymers, fibers and chemical admixtures are becoming more popular in recent decades. Moreover new and "greener" cements have been developed and among these geopolymer cements are promising materials, which can replace ordinary Portland cement by giving environmental and technical benefits (reduction in CO_2 emission, improvement of the resistance to fire and aggressive environment).

3.2 Concrete and cement

Concrete is the most extensively used man-made material in the building construction, but the comprehension of the relation between microstructure and mechanism of setting received poor attention and only in the recent years sufficient data were collected in order to improve strength and resistance to chemical attack.

The word concrete comes from the Latin word "concretus" (meaning compact or condensed); a mix of quicklime, pozzolana and pumice as aggregate, was in fact extensively used by Roman engineers. The terms "cement" and "concrete" are often treated as synonymous in the everyday language, however, technically they are synonyms. Cement is a fine powder that, when mixed with water, gives a paste (the cement paste). It, after molded by casting, hardens via hydration and curing. The mix of cement, water and aggregates is called concrete and, during hardening, Portland cement and water fast react forming a gel of interlocking nano-crystals, which over time join into a rigid structure fixing the aggregates in place. The type of cement, aggregates nature, water content, additives and environment determine the physical chemical behaviour and durability of concrete. Cement is the key ingredient of concrete.

Portland cement contains four main compounds: tricalcium silicate (C_3S), bicalcium silicate (C_2S), tricalcium aluminate (C_3A) and tetracalcium alumino-ferrite (C_4AF). It is worth noting that in the cement chemistry symbols have different meaning from classical chemistry: C is for CaO, S is for SiO_2, A is for Al_2O_3, F is for Fe_2O_3 and H for H_2O. The most important mineralogical constituents are silicates, which react with the water leading to the formation of calcium silicate hydrate (CSH). CSH is responsible for the mechanical properties of hardened cement.

The hydration reactions of C_3S (1) and C_2S (2) are the following:

$$C_3S \ + \ H_x \longrightarrow CySH_{(x+y-3)}+CH_{(3-y)} \qquad (1)$$

$$2C_2S \ + \ H_5 \longrightarrow C_3S_2H_4 + CH \qquad (2)$$
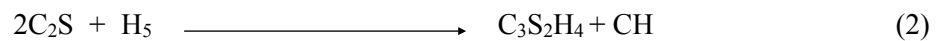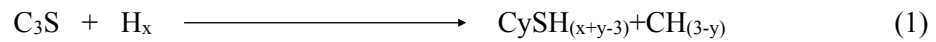
Hydration is accompanied by a considerable heat release. The stoichiometry of the final product is approximate because it depends on temperature and additives.

Generally high concentrations of C_3S are preferred because it reacts faster than C_2S, providing early strength. Small amount of tricalcium aluminate can strongly affect the hydration kinetic. C_3S has a fast hydration that causes an increase of the temperature mix and flash set. In order to avoid this drawback, a certain amount of chalk is added to the cement. The occurring reaction is below:

$$C_3A \ + \ 3(CaSO_4 \cdot 2H) \ + \ 26H \longrightarrow C_3A \cdot 3CaSO_4 + 32H \qquad (3)$$
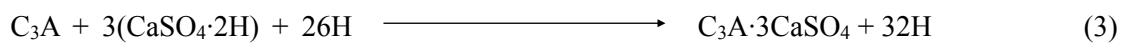
The formed *ettringite* ($C_3A \cdot 3CaSO4$) covers cement particles surface, avoiding the hydration reactions go further, until all the casting and vibration step are complete.

3.3 Modern cement pastes formulations

Cement and concrete are materials available everywhere and the last improvements let to obtain greater amount of "high performance concrete", decreasing costs and carbon dioxide (CO_2) emissions.

The first two features were achieved mainly by adding additives. They are often organic polymers able to change the properties of the fresh concrete.

Regarding the reduction of CO_2 emissions during the production of cement at very high temperature (>1400°C), new formulations have been studied, among these geopolymer cements seem to be particularly promising

3.4 Modified cement: the additives

Several research [**Miyake** (1985), **Yosuf** (1995), **Aitcin** (2000), **Ferraris** (2001), **Sobolev** (2003-2005), **Ran** (2006), **Heikal** (2006)] have been carried out in order to improve cements and concretes behavior and in the recent years, the composition of the concrete mixes have radically changed with the introduction of additives.

- *plasticizers*: they increase the workability of fresh concrete with less consolidating effort andcan be used to reduce water content and usually called *water-reducers*;
- *setting accelerators*: they hasten the initial and final setting time;
- *setting retarders*: they delay the initial reaction between water and cement;
- *hardening accelerators*: they improve the hydration rate of the concrete, favouring a faster development of compression resistance;
- *air-entraining admixtures*: they are foam agents improving the workability and reducing the fatigue due to the cycles of freezing-thawing on the concrete;
- *water retention additives*: they prevent a rapid evaporation of water;
- *rheology modifiers*: they modify rheology of slurry.

Each additive shows secondary effects, e.g. water reducers are also able to delay hydration, acting like a setting retardant. These chemicals are generally added to concrete mix in very low percentage (0.1% ÷ 3%).

3.3.1 Superplasticizer: composition and mechanism of action.

In the present work the effect of *superplasticizer* (or high water-reducer) on CSH nanostructure was investigated. Superplasticizers have greatly contributed to make possible high performance concretes. These admixtures are able to disperse cement particles, preventing the flocculation of cement and causing an increase in the fluidity of the mix.

There are several types of superplasticizers: SPS (polystyrene sulphonate), SMF (melamminesulphonate), SNF (naphthalene sulphonate), LSG (ligninsulphonate) and polycarboxyl copolymers. In the 70's the main superplasticizers were water soluble synthetic polymers such as sulfonated melamin formaldehyde condensates, sulfonated naphthalene formaldehyde condensates, additives based on a single repeating unit (naphthalene or melamine sulfonate) (Figure 38). In the last decade polymers has been investigated as additives, e.g. polycarboxylate, based on two or more structural oups that provide greater diversity in molecular structures (Figure 38).
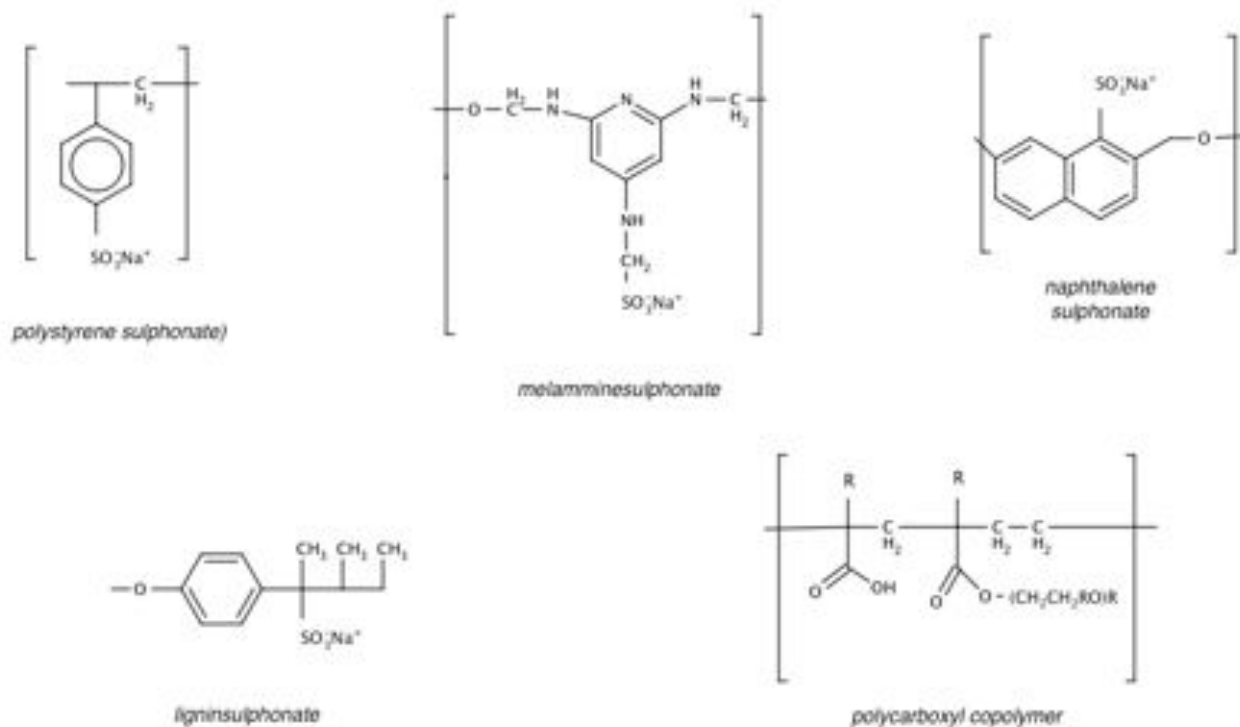
Figure 38. Type of super plasticizer additives.

There are three manners to use superplasticizer:

- to increase the workability;
- to reduce the amount of water and w/c ratio, so that strength and durability increase (w/c ratios higher than 0.36 lead to porosity, which is detrimental to strength and resistance to chemical attack);
- to reduce both water and cement in order to reduce costs, but also creep, shrinkage and thermal strains caused by heat release of cement hydration.

The attractive forces among cement particles, which cause agglomeration, stem from the opposite charges on their surface. Superplasticizers have been proposed to cause dispersion of fine cement particles, because they develop the same electrostatic charges on the particles, which repel each other. This mechanism has been confirmed through zeta potential measurements for several admixtures, e.g. polystyrene sulphonate [**Yoshiola** (1997), **Ferrari** (2010)]. The new class of additives, such as acrylic polymers and polycarboxylic esters (PCEs), do not exhibit high zeta potential and repulsive effect [**Yoshiola** (1997), **Collepardi** (1999), **Sakai** (2003), **Zhang** (2007)]. Accordingly the dispersion mechanism is related more to steric hindrance caused by the surface adsorption itself and the presence of side long graft chains, rather than to the negatively charged anionic groups COO^-.(Figure 39).
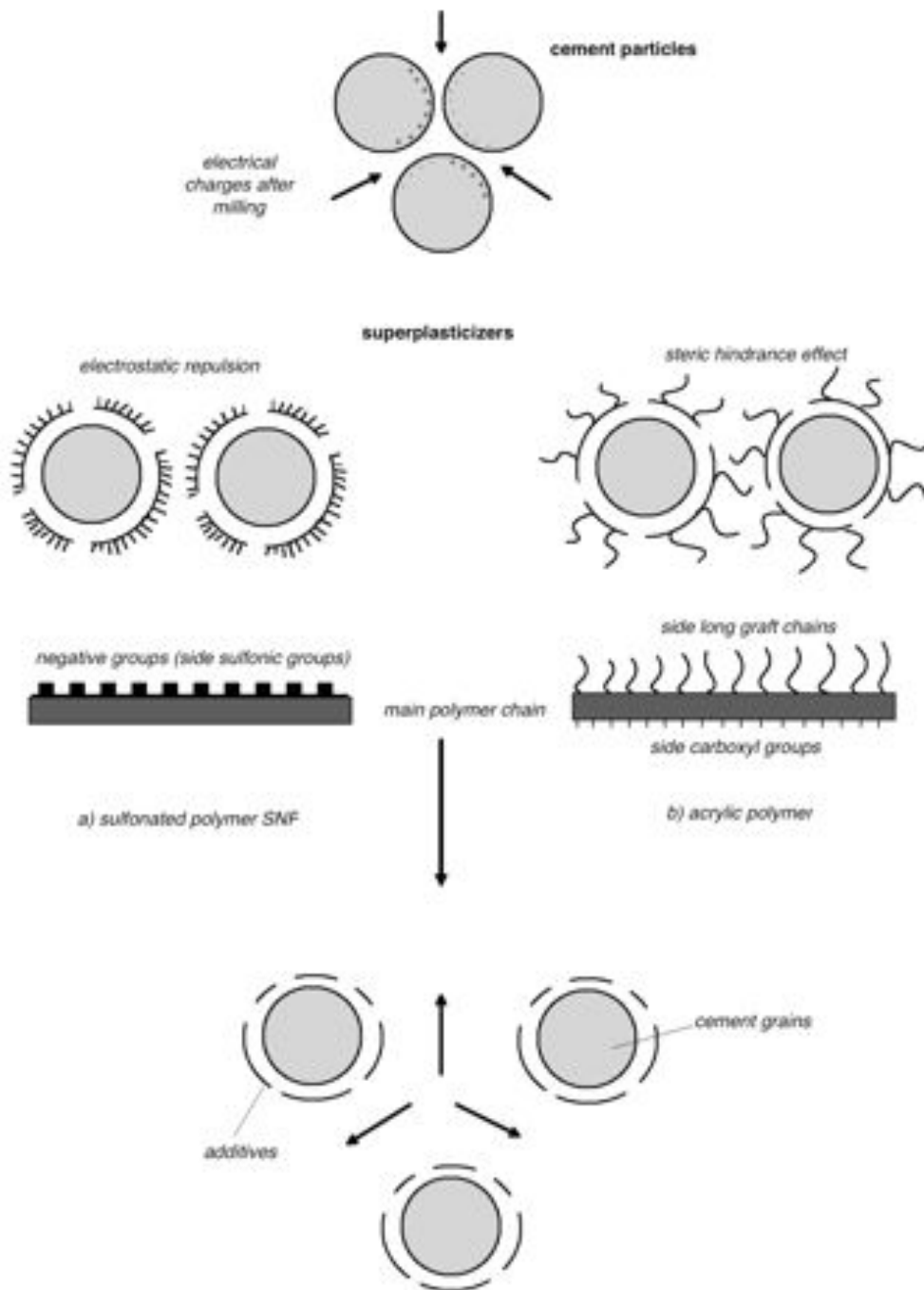
Figure 39. Mechanisms of action of superplasticizers.

3.3.1.2 Comb-Shaped Polymers as Nanostructure Modifiers of Calcium Silicate Hydrate: A ^{29}Si Solid-State NMR Investigation

Elisa Cappelletto, Silvia Borsacchi, Marco Geppi, Francesca Ridi, Emiliano Fratini,and Piero Baglioni

Abstract

Calcium silicate hydrate gel (C−S−H) is the complex phase mostly responsible for the binding properties and the mechanical resistance of Portland cement. The clarification of the C−S−H nanostructure and how the presence of organic additives affects it is still an intriguing and not trivial task, especially due to C−S−H scarce crystallinity and intrinsic complexity. In this work, we exploited ^{29}Si solid-state nuclear magnetic resonance (NMR) to investigate the effects of different comb-shaped superplasticizers on the silicate structure. The analysis of ^{29}Si solid-state NMR spectra shows that the additives increase the degree of polymerization and hence the average length of the silicate chains in C−S−H. This finding correlates well with the increase of the globule dimensions estimated by means of small angle scattering techniques showing that the comb-shaped polymers are able to tune the overall dimension of the C−S−H globule. This effect is dependent on the molecular architecture of the superplasticizer and allows a molecular imprinting to the globular structure of the C−S−H gel.

Introduction

The hydrated phase mostly responsible for the binding properties and for the final mechanical resistance of Portland cement is calcium silicate hydrate (shortly, C−S−H). This colloidal phase [**Ridi** (2011)] is formed as a consequence of the hydration of tricalcium and dicalcium silicate, through complex dissolution and reprecipitation processes. Its structural properties have been studied since long time by means of both experimental and theoretical approaches, in the attempt to provide a clear picture of this material. Anyway, because of the intrinsic complexity of the system being mainly amorphous, this effort has been only partially fulfilled.

In the last decades solid-state nuclear magnetic resonance (SS-NMR) spectroscopy has been widely used in the studies of cement-based materials [**Richardson** (2000), **Skibsted** (2008), **Brunet** (2010),]. High-resolution magic angle spinning (MAS) SS-NMR can investigate the local electronic structure, providing detailed structural information on the chemical environments of the nuclei. This is particularly useful in the investigations of cement pastes since ^{29}Si isotropic chemical shifts reflect the structural surroundings of a silicon atom, and they can be associated to the different types of SiO_4 tetrahedra, whose relative amounts can also be determined [**Rawal** (2010), **Porteneuve** (2001), **Cong** (1996), **Beaudoin** (2009)]. The different Q^n sites, where Q represents the SiO_4 tetrahedron and n refers to the number of Si−O−Si bonds, have different ^{29}Si isotropic chemical shifts in solid silicates [**Hansen** (2003), **Johansoson** (1999), **Chen** (2004)]. Previous

^{29}Si MAS NMR studies suggested that CSH has a disordered layered structure made of dreierketten linear silicate chains similar to that of tobermorite (Figure 40), the ^{29}Si MAS NMR spectrum being characterized by the presence of end-group Q^1 and middle-group Q^2 resonances [**Pardal** (2012), **Brunet** (2004)].

Nowadays, almost all the cement formulations contain organic polymers, whose role is to confer specific characteristics to the paste. In particular, superplasticizers are essential components of every formulation, as they confer high workability to the pastes keeping low the water content. Last generation superplasticizers are comb-like polymers, made of polycarboxylic chains partially esterified with polyethylene oxide lateral chains. One of the most interesting issues in the cement research is the assessment of the effect of these organic polymers on the C−S−H nanostructure. Indeed, understanding the organic/inorganic interactions on a molecular level could enable tailoring the bulk properties by controlling the nanoscale structure, through a bottom-up process. Although SS-NMR has been extensively applied for studying organic−inorganic composite materials [**Geppi** (2008)], only a limited number of papers reported on this topic [**Beaudoin** (2009), **Matsuyama** (1999), **Wang** (2006), **Alizadeh** (2011), **Ding** (2012), **Le Saout** (2012), **Comotti** (1996), **Puertas** (2005), **Rottstegge** (2006), **Tritt** (2000)], showing that ^{29}Si SS-NMR can be successfully exploited to investigate the effects of polymers on the silicate network. In particular, the relative intensities of Q^2 and Q^1 signals are an indicator of the silicate polymerization degree, which can change in the presence of additives.
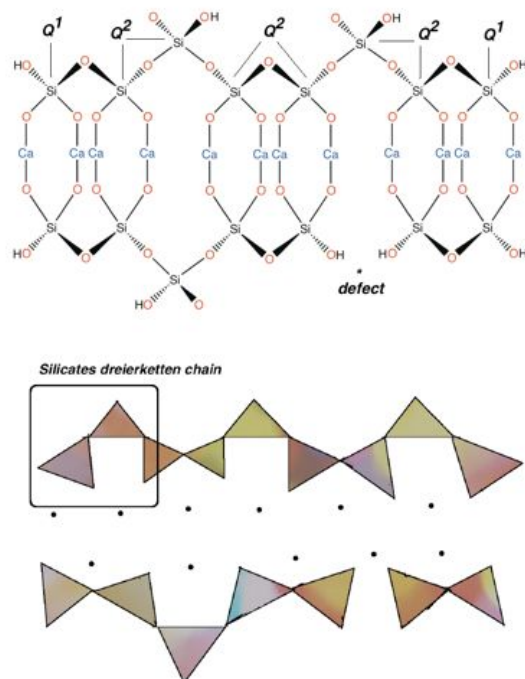
Figure 40. Two schematic representations of the tobermorite structure. (top) Qn sites are explicitly highlighted (bottom). Triangles represent silicate tetrahedrons arranged in the well-known silicate dreierketten chains. The calcium atoms (circles) are located at the center of Ca−O octahedra.

This article aims to investigate the effect of comb-shaped superplasticizers on the nanostructure of C−S−H through ^{29}Si SS-NMR measurements. Infrared spectroscopy has been used to further inspect organic/inorganic interactions.

Experimental section

The chemically pure batch of synthetic C_3S (CTG-Italcementi, Bergamo) had a specific surface area of 0.65 m^2/g (BET). Polycarboxylic esters (PCEs) were obtained from BASF. They are polymethacrylic chains partially esterified with polyethylene oxide lateral chains. The molecular structure is sketched in Figure 41. Each polymer is identified by the acronym PCEp−n, where p is the number of repeating PEO units in the lateral chains and n identifies the number of free carboxylic groups per esterified group.
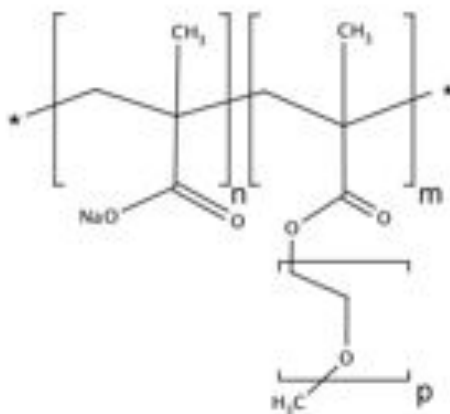
Figure 41. Sketch of the PCEs molecular formula.

Shortly resuming the PCE characteristics: PCE23−2 and PCE23−6 have PEO side chains, which are five times shorter than PCE102−2 and PCE102−6, while PCE23−6 and PCE102−6 have more free carboxylic groups on the backbone. Previous studies [**Winnefeld** (2007), **Zingg** (2008)] have shown that the adsorption of PCEs on cementitious phases is higher for molecules with shorter side chains and a lower side chain density.

Synthetic C−S−H was prepared by hydrating 4 g of pure tricalcium silicate (C_3S) in 1150 g of pure water or of polymer solution. Two sets of modified C−S−H were synthetized, respectively, with low concentration and high concentration of PCE. The low concentration set (L series) contained 0.4 g of polymer per 100 g of dry C_3S; the high concentration set (H series) was obtained hydrating the powder with 40 g of polymer per 100 g of dry C_3S. The water and the solutions were degassed to avoid carbonation. The hydration reaction was conducted at 25 °C for 40 days in sealed polyethylene bottles. The dispersions were filtered, and the

final water content was standardized by dehydrating the samples at 60 °C in a N_2 atmosphere. This synthetic route is known to minimize the $Ca(OH)_2$ content while forming quite polydisperse C−S−H phase, which is usually refereed to as C−S−H (I) [**Taylor** (1950)]. Further specific details on the synthesis can be found elsewhere [**Chiang** (2012), (2013)]. Table 16 summarizes the characteristics of the polymers and of the pastes synthetized for the investigation.

Sample acronym	number of monomeric units of PCE side chain (p)	density of PCE side chains (n:m)	PCE concentration in water (mg/mL)
C-S-H			
L_PCE102-2	102	2:1	$1,4 \times 10^{-2}$
L_PCE102-6	102	6:1	$1,4 \times 10^{-2}$
L_PCE23-2	23	2:1	$1,4 \times 10^{-2}$
L_PCE23-6	23	6:1	$1,4 \times 10^{-2}$
H_PCE102-2	102	2:1	1,4
H_PCE102-6	102	6:1	1,4
H_PCE23-2	23	2:1	1,4
H_PCE23-6	23	6:1	1,4

Table 16. Characteristics of the Polycarboxylate Superplasticizers and Concentration of Polymers in the Pastes.

The ^{29}Si NMR spectra were collected on a dual channel Varian Infinity Plus 400 spectrometer operating at Larmor frequencies of 400.03 and 79.44 MHz for ^{1}H and ^{29}Si nuclei, respectively, using a 7.5 mm CP-MAS probe-head. All the experiments were performed at room temperature, using air as spinning gas. Spectra were obtained using a Direct Excitation (DE) pulse sequence with high power proton decoupling and a MAS frequency of 4 kHz, accumulating 660 transients. Spectra were recorded with different recycle delays (from 5 to 300 s, see Figure 42) to find suitable conditions to obtain quantitative spectra. A recycle delay of 300 s is necessary to achieve a complete relaxation. This value is much larger than that commonly used to obtain quantitative ^{29}Si NMR spectra of cements, possibly due to the fact that the formulations here investigated do not contain Fe^{3+} ions, able to reduce the longitudinal relaxation time (T_1) of ^{29}Si. However, in order to reduce the experimental times, all the spectra were recorded with a recycle delay of 60 s, and the peak areas, obtained through spectral fittings and also taking into account spinning sidebands (Figure 43), were rescaled to the quantitative areas through suitable scaling factors. These were calculated as the ratios between the areas of the peaks at the two different pulse delays determined for one sample, under the reasonable assumption that the ^{29}Si T_1 relaxation times were the same for all the cement pastes.

Infrared spectra were acquired in the range 4000−400 cm^{-1}, with a Nexus 870-FTIR (Thermo-Nicolet), using a 4 cm^{-1} resolution and 64 scans, with a DTGS-TEC detector. To register the spectra, the samples were mixed with KBr with a sample/KBr weight ratio of ~1/100 and compressed to obtain pellets.

The effective amount of polymer in each sample has been determined by thermal gravimetric analysis (see Supporting Information, Figure SI1). In particular, the mass losses (in the range 200−500 °C) due to the presence of adsorbed polymers are about 7.0% (and 0.4%) for PCE102−6, 7.5% (and 0.4%) for PCE23−6, 7.8% (and 0.2%) for PCE102−2, and 9.4% (and 0.2%) for PCE23−2 in the case of the H (and L) series, respectively. The errors in the determination were about 0.9% in the case of H series and 0.1% for the L series. These results show that C−S−H formed in the presence of low amounts of PCE almost completely incorporates the polymer, while in the samples prepared with high concentration of PCE, it only retains a portion of the available polymer approximately ranging f rom 15 to 25%.
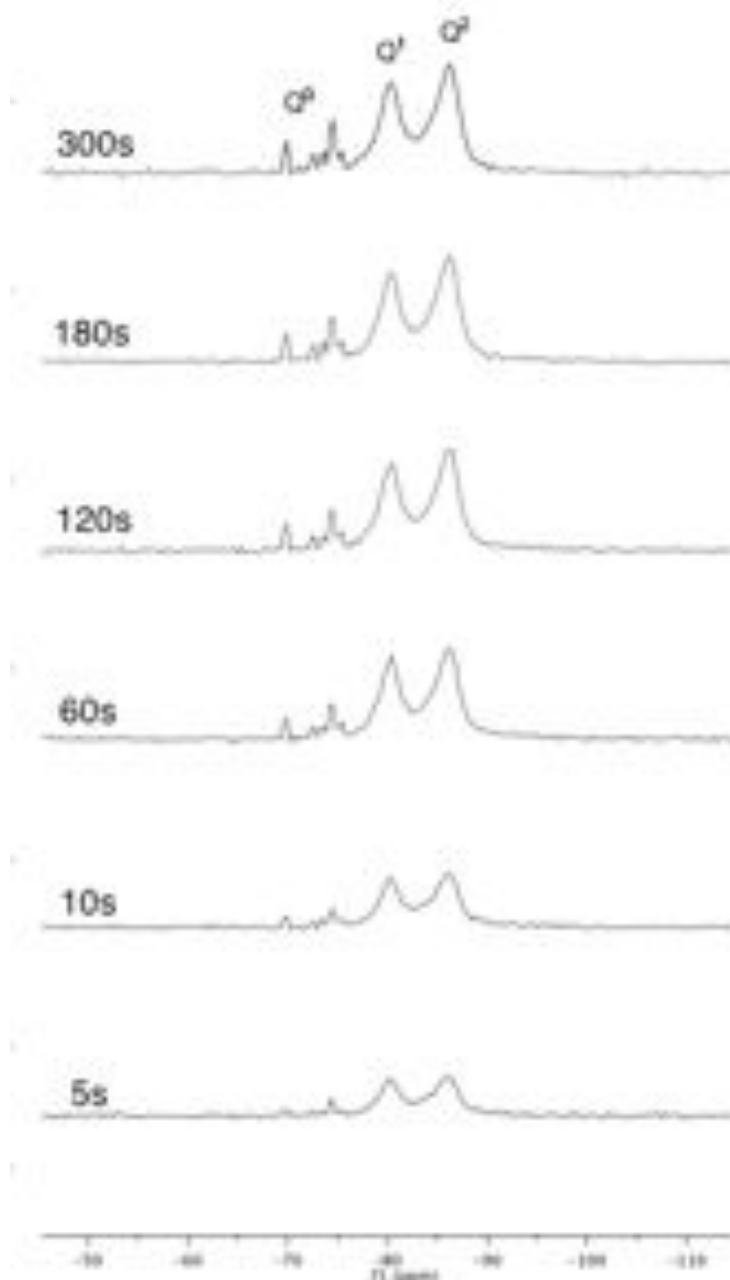
Figure 42. ^{29}Si DE-MAS NMR spectra obtained with the recycle delays indicated.
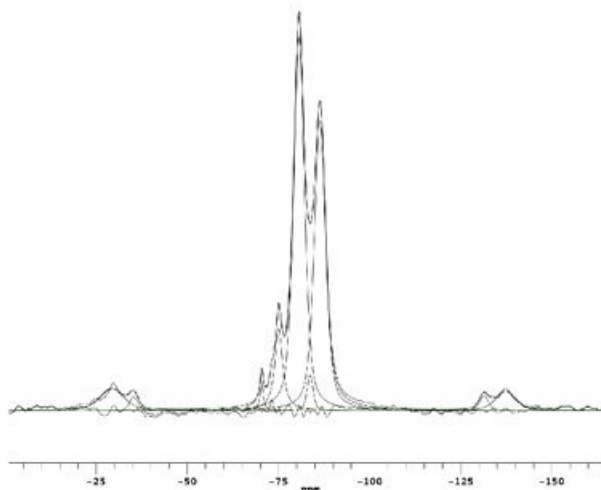
Figure 43. Example of fitting of ^{29}Si DE-MAS NMR spectrum.

Results and Discussion

The ^{29}Si DE-MAS NMR spectra of all samples are shown in Figure 44. The spectrum of C_3S presents typical Q^0 signals (−70/−76 ppm) attributed in the literature to the monoclinic form [**Johansson** (1999), **Moudrakovski** (2010)]. These resonances disappear with the hydration: the spectrum of pure C−S−H is characterized by the presence of very intense Q^2 and Q^1 signals only (−80/−86 ppm), in agreement with the literature [Chen (2004), Brunet (2004)]. The presence of very weak Q^0 signals indicates that C_3S has almost completely reacted. However, Q^0 signals are clearly observed in the spectra of modified C−S−Hs, indicating that part of C_3S remains unreacted in the presence of the organic additives. The set of samples investigated allowed the modifications of the silicate structure to be studied at different (i) concentrations of additive, (ii) side chain lengths of the additive, and (iii) side chain densities of the additive. A selection of representative ^{29}Si DE-MAS spectra showing the effects of these three variables is reported in Figure 45. The experimental and data analysis procedures described in the Experimental section allowed quantitative peak areas (in the following indicated as Q^i for the sake of simplicity) to be extracted from ^{29}Si spectra and used to calculate useful structural parameters, such as the degree of silicate polymerization, DP, $(Q^2/Q1)$ and the reactivity $100(Q^1 + Q^2)/(Q^0 + Q^1 + Q^2)$.

Moreover, it is straightforward to show that in the case of missing Q^3 signals the mean silicate chain length (MCL) can be easily calculated from DP as it is given by $2(DP + 1)$ [**Beaudoin** (2009)]. The values obtained for these three parameters for each sample are reported in Table 17 and Figure 46. DP increases in the presence of the organic additives from 0.61 (C−S−H) to 1.55 (H_PCE23−6). This means that C−S−H is characterized by very short silicate chains that become longer in the presence of the additives. In H_PCE23−6, where DP assumes its highest value, silicate chains are formed on average by three Q^2 and two

70

Q^1. DP increases by increasing the concentration of additive, as a result of the higher amount of adsorbed polymer. Regarding the effects of the chemical structure of the polycarboxylate, it is possible to observe that shorter side chains favor the silicate polymerization ("PCE23" series samples always show higher DP values than the corresponding samples of "PCE102" series). The side chain density of the polymer also affects DP.
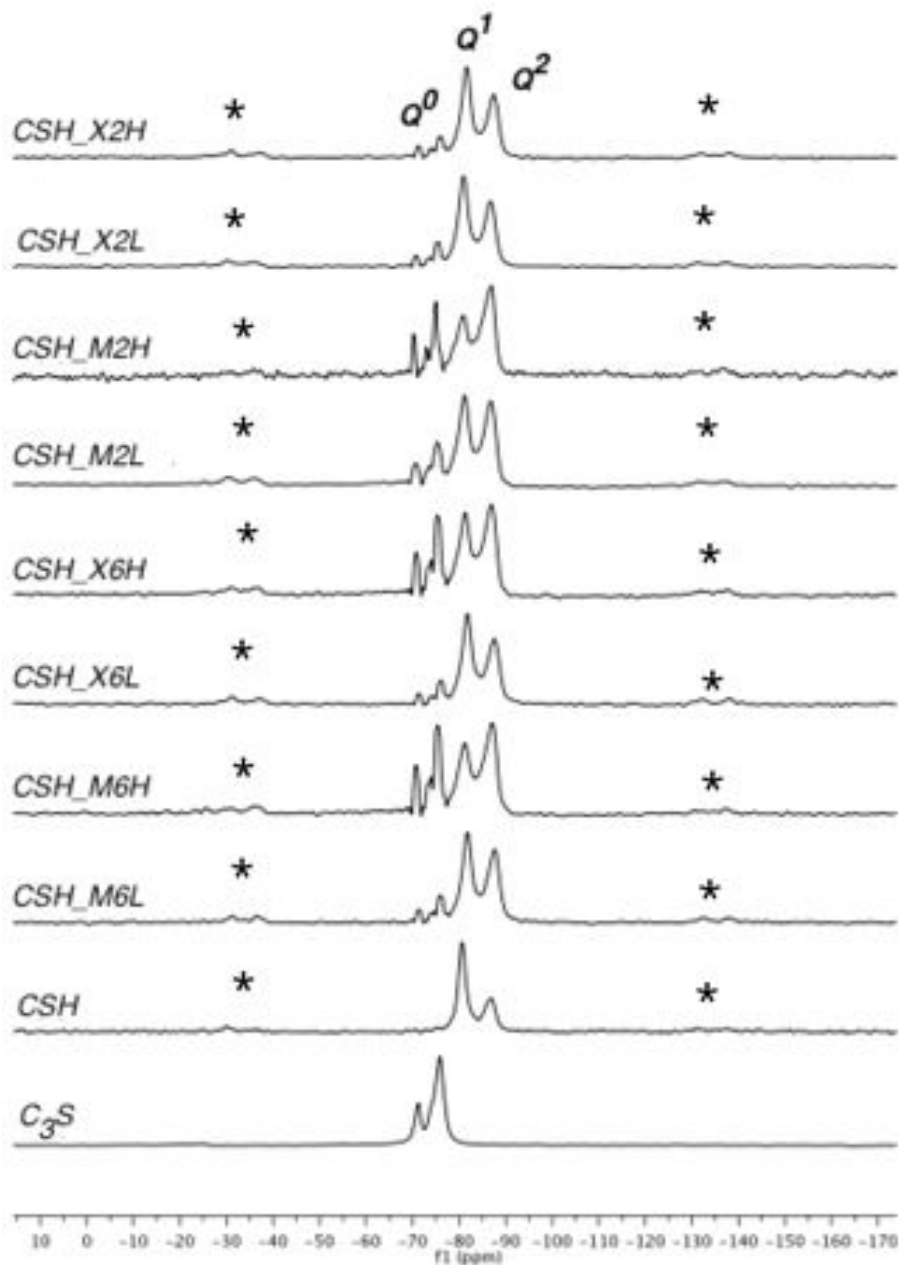
Figure 44. ^{29}Si DE-MAS NMR spectra of C3S (bottom) and C-S-H samples, acquired at a MAS frequency of 4 kHz and a recycle delay of 60 s. Spinning sidebands are marked with asterisks.
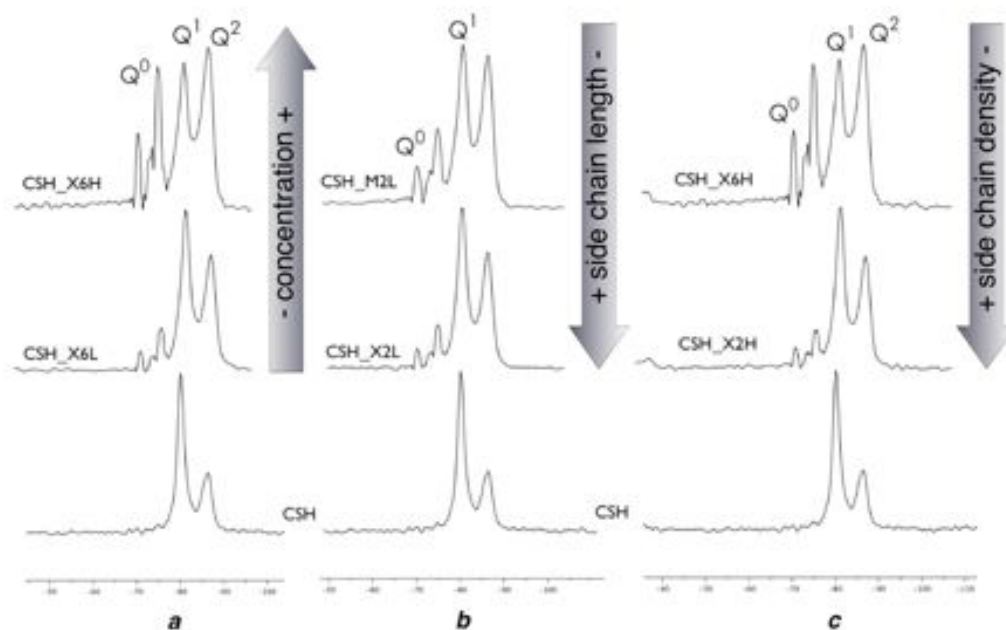
Figure 45. ^{29}Si DE-MAS spectra of some representative samples. The effects of: a) concentration; b) side chain length; c) side chain density can be clearly observed.

Sample	DP (Q2/Q1)	Reactivity (100(Q2+Q1)/ (Q0+Q1+Q2))	MCL ((Q2/ Q1)+1)x2	estimated chain length (Å)	globule diameter (nm) [29]
C-S-H	0.61	94	3.22	8.4	6.2
L_PCE102-2	0.96	86	3.92	10.2	7.3
L_PCE102-6	1.55	69	5.10	13.3	
L_PCE23-2	0.89	87	3.78	9.8	7.9
L_PCE23-6	1.33	72	4.66	12.1	
H_PCE102-2	1.25	81	4.50	11.7	12.4
H_PCE102-6	1.42	72	4.84	12.6	
H_PCE23-2	0.80	87	3.60	9.4	6.4
H_PCE23-6	1.08	77	4.16	10.8	

Table 17. Degree of Polymerization (DP) , Reactivity, and Mean Silicate Chain Length (MCL) of the Different Samples[a]. ([a]The values were obtained from the fitting of 29Si DE-MAS NMR spectra. The uncertainties on the values of the degree of polymerization, reactivity and mean silicate chain length are ±0.04, ±3, and ±0.08, respectively. Estimated chain lengths are calculated as MCL·2.6 Å, as described later in the text. The C−S−H globule equivalent diameters obtained by a SANS/SAXS investigation[29] are also reported).

In the case of the longest side chains ("PCE102" series), at low concentration, the effect of this parameter is negligible, while at high concentration DP is higher when the density is lower (i.e., in the sample H_PCE102−6). The two polymers belonging to the "PCE23" series show similar DP values when mixed with C_3S at high concentration. At low concentration, the L_PCE23−2 sample presents a higher DP value than L_PCE23−6.
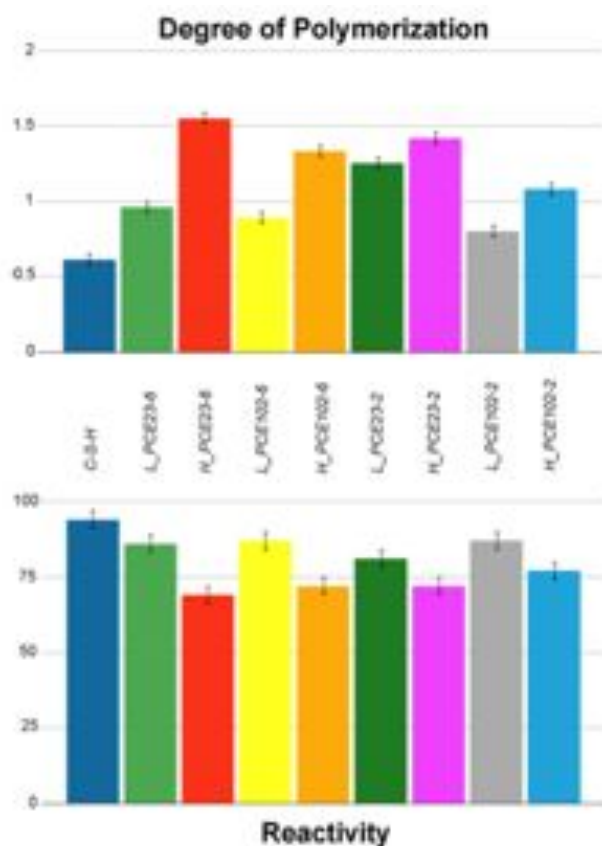
Figure 46. Degree of polymerization (above) and reactivity (below) of the different samples. The values were obtained from the fitting of ^{29}Si DE-MAS NMR spectra.

In all cases, the presence of the organic polymers decreases the reactivity of C_3S. The drop in the reactivity is higher increasing the concentration of additive. The "PCE23 series" is slightly more effective than "PCE102 series" in reducing the reactivity: this is consistent with the higher retarding power of PCE23−2 and PCE23−6 with respect to PCE102−2 and PCE102−6 [**Zingg** (2009)]. The influence of side chain density is very small.

In previous papers it has been reported that FTIR in the near-infrared region can be used both to investigate the reaction of a hydrating cement pastes [**Ridi** (2006)] and the state of water inside the pores of the developing C−S−H gel [**Ridi** (2009)]. Moreover, some bands in the mid-infrared region of the FTIR spectrum are indicative of the polymerization degree of calcium silicate hydrate [**Yu** (1999)] Figure 47

shows the FTIR spectra registered on all the samples. The band centered at 813 cm^{-1} can be assigned to the Si−O stretching of Q^1 tetrahedra: this band is reported to increase in intensity with increasing C/S ratio, i.e., with low polymerized samples. In our case, this band is well-defined in the C−S−H sample, while it appears less prominent in the samples containing PCEs. Additionally, the band at 660 cm^{-1}, due to Si−O−Si bending, is reported to have low intensity and large width in poorly polymerized phases. This is the case for the pure C−S−H samples, while the above-mentioned band is more defined in C−S−H/PCE samples (see Figure 47). All these findings strengthen the evidence provided by SS-NMR that the organic additives increase the polymerization of the silicate in the C−S−H nanostructures.
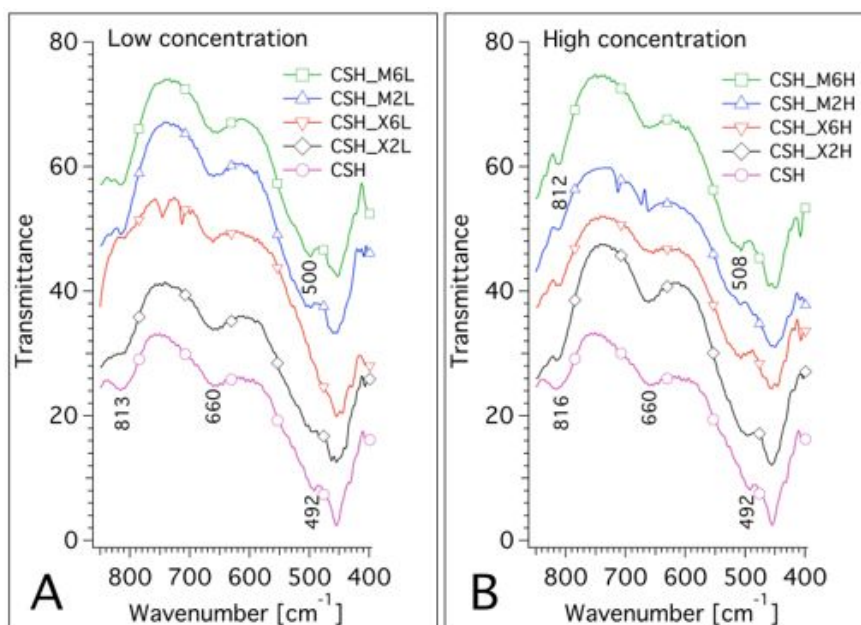
Figure 47. FTIR spectra for the investigated samples: A) at low concentration; B) at high concentration.

In a previous paper [**Chiang** (2013)] some of the authors of the present study have investigated the very same gels synthetized with 0.4% of PCE (L series) by a SAXS/SANS combined experiment highlighting the effect of the polymer on the C− S−H base unit. The model applied to analyze the small angle curves [**Chiang** (2012)]) was based on the Colloidal Model-II by Jennings [**Jennings** (2008], that describe the C−S−H gel as a hierarchical system, where the arrangement of disk-like units of C−S−H (sometimes referred to as globules or "bricks") generates a superstructure being mass-fractal in nature [**Ambrosi** (2012)]. The main outcome from the SANS/SAXS analysis is the estimation of the equivalent dimension of the globule as a function of the added polymer. Since the MCL refers to the average number of tetrahedral SiO$_4$ units constituting a single silicate chain, it is possible to convert this value to a real dimension by multiplying it by the length of the edge of the tetrahedron. Using geometrical relations, this value can be estimated to be about 2.6 Å if the Si−O bond length is around 1.6 Å. This is also in agreement with the literature on C−S−H phases [**Pelleq** (2009)] where the distance between the Si and the second shell of O is about 4.2 Å, and hence, the tetrahedron edge is 4.2−1.6 = 2.6 Å. Following the above mentioned conversion, the chain length estimated for the entire series of investigated samples is reported in Table 2 along with the equivalent dimension of the

basic unit (globule equivalent diameter). The comparison between these two quantities shows that there is a strong correlation between the MCL and the average dimension of the globule (see Figure 48), where, as the silicate chain increases in length, also the globule size becomes greater. In particular, the smallest dimension is found in the case of pure and L_PCE102−2 added C−S−H (6.2−6.4 nm) where the silicate chain length is minimum (8−9 Å), while the maximum dimension is encountered with L_PCE23−2, which is also characterized by the longest silicate chain found in this series of samples Gels with L_PCE23−6 and L_PCE102−6 lie in the middle having a silicate chain of about 10 Å and a corresponding globule dimension of 7−8 nm. This result highlights the hierarchical nature of C−S−H gel where the building block (the silicate chain) influences the size of the globule and eventually the fractal dimension of the overall globular arrangement. Roughly 7−8 silicate chains are needed to span the entire globule diameter. At the moment the globule dimensions have not been measured for the series H, and no comparison can be done in this specific case. However considering the good correlation present in the series L, globules greater than or similar to L_PCE23−2 are expected to be present in the C−S−H gels synthesized with a higher concentration of PCE polymers. The only exception is encountered in the case of H_PCE102−2 where the silicate chain length is only 10.8 Å and a globule with a dimension similar to sample L_PCE23−6 is expected. As already shown in the L series, even at high concentration the polymer PCE102− 2 has the smallest propensity in changing the molecular structure of the C−S−H phase. This result is strictly related to the fact that PCE102−2 has the lowest adsorption ability in the series of superplasticizers used in the present investigation.
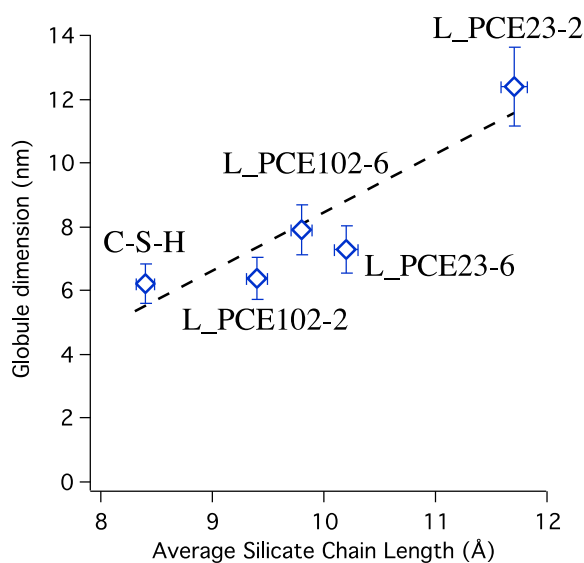
Figure 48. Equivalent C-S-H globule diameter as a function of the average silicate chain length in the case of the L series. The pure C-S-H case is reported for comparison (first point on the left).

Conclusions

This ^{29}Si SS-NMR study coupled with FTIR findings showed that the organic additives delay the hydration of tricalcium silicate and affect the nanostructure of the calcium silicate hydrate. The retardation effect in the hydration process is evident from the persistence of the Q^0 signals in the ^{29}Si spectra of C−S−H produced in the presence of PCE and is in agreement with the previous literature. Our study shows for the first time, that the C−S−H formed in the presence of PCEs has a degree of polymerization higher than the one obtained in pure water, meaning that PCEs induce the formation of silicate chains longer than those of the plain sample. Both the retardation and the increment of DP are dependent on the molecular architecture of the PCEs: in general, they increase with the increasing of the charge density of PCE, which corresponds to the increase of the adsorption propensity: abundant and long side chains hinder the interaction of the additive with the inorganic particles; however, PCEs with short and scarce side chains easily adsorb the inorganic particles, slowing down the hydration and consequently lowering the reactivity. For these reasons, the effects are maximal in the presence of the PCE23−6 additive, which is characterized by a small density of short side chains. However, the scarcest organic−inorganic interactions occur with PCE102−2 (characterized by long side chains and high side chains density), which shows DP and reactivity values very close to those of unmodified C−S−H. PCE concentration also plays an important role, as we observe that the effects on reactivity and DP increase with increasing the amount of PCE. These results show that a combined ^{29}Si SS-NMR, FT-IR, SANS/SAXS investigation can provide a very detailed picture of the nanostructure formed in the presence of additives, allowing the understanding at the supramolecular level of the C−S−H/polymer interaction that is fundamental in the design of novel performing additives for cement-based building materials.

3.3.2 Geopolymer concretes

Geopolymers represent a replacement for ordinary Portland cement (OPC).

Geopolymer is produced by the reaction of alkali with minerals containing silica and alumina. The term geopolymer was used for the first time by Davidovits for describing a new family of mineral binder, whose matrix is based on a poly(sialate) Si-O-Al-O 3D framework, with alternating SiO_4 and AlO_4 tetrahedra, joined together by sharing oxygen atoms. Geopolymer has a chemical composition similar to natural zeolites; the basic structural model of a geopolymer [**Barbosa** (2000)] is illustrated in Figure 49.
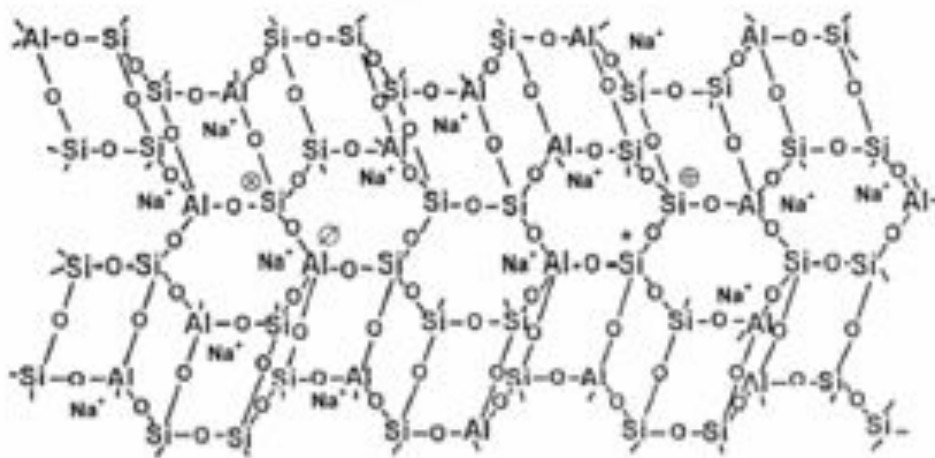
Figure 49. Model of a short range order of a geopolymer.

Due to the growing concerns related to global climate change, Portland cement manufacture is becoming less acceptable for the large carbon dioxide (CO_2) emissions, estimated to be responsible for 5 to 7% of the global production of CO_2. In terms of CO_2 emission per unit volume of concrete, geopolymers manufacture has an impact 10 times lower than Portland cement [**Gartner** (2004)]. Moreover experimental studies demonstrated that geopolymer mortar has excellent resistance chemical attack and fire [**Davidovits** (1991)], superior than ordinary mortars. Accordingly, geopolymer could be used in preparing concrete resistant in aggressive environments, where the durability of Portland cement concrete is low, e.g. life service of concrete structures in urban and off-shore environment is reduced to 20 to 30 years, though their design life was of at least 50 years. Furthermore, extensive investigations demonstrated also that geopolymer concrete showed good mechanical properties as compared to conventional concrete. [**Hardito** (2005)].

3.3.2.1 ^{29}Si SS-NMR characterization of geopolymers

Solid state nuclear magnetic resonance (SS-NMR) is an important tool to understand the short-range structure of geopolymers. ^{29}Si, ^{27}Al, ^{17}O MAS NMR were largely employed to investigate the formation of these aluminosilicate, synthesized with different alkali solutions and raw materials. In particular ^{29}Si MAS NMR provides information about the silica structure. In order to indicate the connection of SiO_4^{4-}tetrahedra, the abbreviated notation Q^n is used [Engelhardt (1987)]. *Q* represents a silicon atom bonded to four oxygen atoms forming a tetrahedron and *n* indicates the connectivity, i.e. the number of other Q units attached to the SiO_4 tetrahedron under study. Thus, Q^0 denotes the monomeric orthosilicate anion, Q^1 the endgroup of chains, Q^2 the middle groups in chains or cycles, Q^3 the chain bridging sites and Q^4 the fully cross-linked groups. Chemical shifts and the assignment of the different Q^n units is reported in the Table 18.

Q^n unit	Q^0	Q^1	Q^2	Q^3	Q^4
ppm	-67 ∿ -73	-74 ∿ -78	-83 ∿ -88	-95 ∿ -100	-103 ∿ -118

Table 18. Assignement of silicon tetrahedron [Puertos (2003)].

For aluminosilicate the number of AlO_4 tetrahedra bound to the central silicon of a Q^n unit is given in parentheses, e.g. $Q^n(mAl)$ indicates an SiO_4 group connected via oxygen bridges to m Al and n-m other Si atoms, where n=0-4 and m≤n. The substitution of silicon by aluminium shifts signals 3 or 5 ppm towards more positive values. The presence of non-bridging oxygens sites in geopolymeric systems is considered negligible with all tetrahedra sites present observed by NMR to have cross-link density n=4 [**Barbosa** (2000)]. Davidovits was the first, who published NMR spectra of geopolymers showing a very broad resonance around -94.5 ppm in the 1980s. He speculated that the peak was the overlap of all five silicon $Q^4(mAl)$ species. This original observation was then confirmed, even when geopolymers had been prepared using different raw materials.

Five different structural units can be found in the ^{29}Si NMR spectra of aluminosilicate: $Q^4(4Al)$, $Q^4(3Al)$, $Q^4(2Al)$, $Q^4(1Al)$, and $Q^4(0Al)$ resonating at approximately -84, -89, -93, -99, and -108 ppm, respectively. Obviously, $Q^4(0Al)$ represents aluminium-free silicon of silica. A large number of previous studies described preparation and characterization of geopolymeric products [**Xu** (2002), **Barbosa** (2003)], also for applications as "green" cementitious binder [**Duxson** (2007)]. The objective of this study is to investigate the use of clay sediment as main precursor and understand also how secondary phases (illite, quartz) affect the synthesis of geopolymer.

3.3.2.2 Thermally treated clay sediments as geopolymer precursors

B. Liguori, C. Ferone, I. Capasso, F. Colangelo, R. Cioffi, E. Cappelletto, R. di Maggio

in Applied Clay Science

Abstract

The management of reservoir is a great environmental problem, since regular de-silting operations produce huge quantities of sediments. Among the recycling possibilities, the use of clay sediments for the manufacture of geopolymer-based materials seems to be an interesting alternative to disposal, due to their low cost and easy availability. In particular two sediments, coming from reservoirs located in Southern Italy, have been firstly characterized by X-ray diffraction, differential thermogravimetry and Fourier transformed infrared (FTIR) spectroscopy. Reactivity of raw and thermally treated clay sediments in alkaline media has been also investigated. Finally geopolymeric samples have been produced and chemically, physically and mechanically characterized. The results show that the calcined clay sediments can be suitable precursors in polycondensation reactions.

Introduction

The term "geopolymer" was coined by Davidovits in the 1970s, originally referring to the investigations on the reaction of metakaolin in alkaline media forming aluminosilicate polymers [**Davidovits** (1976) (1999)]. The prefix "geo" was selected to symbolize the constitutive relationship of the binders to geological materials, natural stone and/or minerals. Their synthesis takes place by a process of polycondensation and can start from metakaolinite or many natural and artificial silicoaluminates by reaction with alkali metal (Na or K) hydroxide and/or silicate [**Davidovits** (1991), **Van Jaarsveld** (1999), **Cioffi** (2003), **Andini** (2008), **Ferone** (2011)]. Amorphous geopolymers are obtained at temperatures from 20 to 90°C, while crystalline ones are formed in the autoclave at higher temperatures, up to 200°C [**Davidovits** (1991)]. Geopolymeric materials are attractive because of their excellent mechanical properties; durability and thermal stability can be also achieved [**Palomo** (1992), **Schmücker** (2005)]. Owing to their lower calcium content, they are more resistant to acid attack than materials based on Portland cement [**Bakharev** (2005). In addition, they are of great interest because of the reduced energy requirement for their manufacture and the higher sustainability. In fact, the geopolymer technology has the potential to reduce emissions by 80% [**Davidovits** (1993b)] compared to that of Portland cement. Nowadays, the utilization of natural raw materials (beside metakaolinite) is out of focus. The use of secondary resources such as fly ash and slags as aluminosilicate source material to form geopolymers has been widely proven [**Buchwald** (2006), Duxson (2007), Palm (1999). In particular the use of fly ash promised high ecological benefit and lower cost, but this kind of secondary raw materials may enclose difficulties in availability, handling or product quality [**Ferone** (2011).

Recently the search for alternative low cost and easily available materials lead among others to "normal clays". Clay generally consists of a mixture of different clay minerals and associated minerals, which are strongly affected by the nature of the parent rocks [**Chen** (2009)]. These materials are widely available all over the world and may show certain reactivity after a thermal activation process [**He** (1995a). In fact the thermal activation of clay minerals in the temperature range between 500 and 800 °C results generally in the dehydroxylation of the clay mineral [**Heller-Kallai** (2006), the octahedral sheets lose water and decompose into a disordered metastable state [**Evans** (1959), **Mendelovici** (1997)]. This meta-state is widely addressed as being reactive as pozzolana [**Baronio** (1997), **He** (1995a,b) (2000), **Kakali** (2001), **Sabir** (2001)]. Firing to higher temperatures results in the formation of new phases such as spinel and mullite [**Mendelovici** (1997)]. Moreover the calcination activates the material leading to an increase of its geopolymeric reactivity [**Xu** (2002)] that causes an increase in terms of compression strength of the final product obtained [**Sumajouw** (2004)]. Among the silicoaluminate wastes, reservoir sediments are worthy of consideration. Most of these contain different types of clay minerals, mostly illites, smectites, chlorites and kaolinites, and must be periodically removed to avoid the progressive reduction in reservoir capacity. The management of reservoir sediments is a great problem, since regular de-silting operations can make huge quantities of sediments available. Among the recycling possibilities, applications as raw materials in the manufacture of artificial aggregate, bricks and cement clinker have been recently studied [**Chiang** (2008), **Tang** (2011), **Liao** (2011a,b)]. The use of clay sediments for the manufacture of geopolymer-based materials can be an interesting alternative to disposal [**Chen** (2009), **Ferone** (2013)].

The samples of clay sediments used in this paper were collected from two different reservoirs, located in the south of Italy, Occhito (Carlantino, Foggia) and Sabetta (Morigerati, Salerno). Afterwards they were thermally activated and then widely characterized determining their chemical and physical properties in order to provide the behavior as precursor for the preparation of geopolymer binders. Geopolymeric samples have been also produced and have been chemically, physically and mechanically characterized.

Experimental

Selection and characterization of materials

Clay sediments were collected from two different reservoirs in the south of Italy: Occhito reservoir [Carlantino, Foggia], named throughout the text as OC, and Sabetta [Morigerati, Salerno), indicated as SA. They were sampled by three cores for each lake. The cores were 10 cm in diameter and 1 m in height. The three cores coming from the same site were crushed in a jaw crusher, milled in a ring mill and carefully mixed to get a unique, homogeneous sample for each lake. After drying at 105°C in oven, the characterization of each sample was performed by means of chemical, mineralogical, thermal and spectroscopic analyses. The chemical composition of the sediments was determined by X-ray fluorescence, using a Bruker Explorer S4 apparatus. The mineralogical analysis was performed by means of a Philips PW 1730 diffractometer [Cu Kα radiation, 5–60° 2θ range, step width 0,02° 2θ and 1 s data collection per step).

Thermal analysis was performed using a Netzsch STA409PC Luxx apparatus [weight of the sample, 10 mg; heating rate, 10°C min-1; atmosphere, nitrogen and air).

The FTIR absorption spectra were recorded in the 4000–400 cm^{-1} range using a Nicolet system, Nexus model, equipped with a DTGS KBr [deuterated triglycine sulphate with potassium bromide windows) detector. A spectral resolution of 2 cm^{-1} was chosen. Each test sample (2.0 mg) was mixed with 200 mg of KBr in an agate mortar and then pressed into 200 mg pellets of 13 mm diameter. The spectrum of each sample represents an average of 32 scans.

Since the thermal activation can be useful for enhancing the sediment reactivity in polycondensation processes [**Mendelovici** (1997), **Buchwald** (2009)], weighted amount of sediments were thermally treated at two different temperatures (400°C and 750°C). The calcination was performed using a Nabertherm furnace with a heating rate of 10°C/min.

Geopolymeric samples were characterized by FT-IR, mechanical test and ^{29}Si MAS NMR analysis in order to investigate the modification of the structures after the treatments. The ^{29}Si NMR spectra were collected on a Bruker Avance 300 spectrometer operating at Larmor frequencies of 59.6 MHz. All the experiments were performed at room temperature and pressure, using air as spinning gas. The grinded samples were loaded in 7 mm zirconia rotors and spun at 4 KHz. The spectra were obtained using a pulse width of 5.5 μs and 5 s recycle delay to ensure quantitatively reliable spectra.

In the supporting informations, reactivity test was reported in order to verify the leaching in alkaline media of each raw material, before and after the thermal treatments. The leaching of the raw materials was conducted by mixing 0.5 g of solid with 20 ml of alkaline solution for certain hours under continuous stirring. The variables studied were the concentration of the alkaline solution (3 and 7 M) and the time of dissolution (5, 10, 24 and 72 h). After filtering, the liquid part was diluted to 250 ml, the pH adjusted to pH < 1 by adding concentrated HCl acid [**Panagiotopoulou** (2007)] and plasma optical emission spectroscopy (ICP) was used in order to determine the Al and Si concentration. The process parameters of this reactivity test are summarized in Table 22. The solid part was examined by means of XRD and FTIR in order to evaluate the effect of Al and Si leaching on the structure of the starting material.

Binder preparation

The geopolymeric precursors and alkaline activator were mixed by hand for about 5 minutes before being cast into polyethylene cylindrical molds (diameter, 2.1 cm; height, 5 cm). The alkaline activator solutions were prepared using sodium silicate solution (Na2O 8.15%, SiO2 27.40%, provided by Prochin Italia S.r.L. from Marcianise (CE)), NaOH in pellets (NaOH 98%, J.T. Baker, "Baker analyzed"), bidistilled water and ground granulated blast furnace slag. The composition of each activator solution, and the list of geopolymeric samples has been reported in Table 18.

	Sediment		ACTIVATOR SOLUTION		
Sample	SA	OC	NaOH	Sodium Silicate Solution (SS)	GBS
SA/N	105		v		
SA/N/SS	105		v	30	
SA/N/GBS	105		v		45
SA/N/SS/GBS	105		v	60	45
OC/N		105	v		
OC/N/SS		105	v	45	
OC/N/GBS		105	v		45
OC/N/SS/GBS		105	v	45	45

Table 19. List of samples and geopolymer mixtures composition (g).

Three samples were prepared for each mixture. These samples were cured for 3 days at 60°C in oven, at 100% relative humidity conditions. At the end of the curing, all the specimens were removed from the molds and stored at room temperature. Finally the specimens were tested for compressive strength after 28 days using a Controls multipurpose testing machine (mod. MCC8) with a load cell of 100 kN. The compressive strength (N/mm2) was calculated dividing the maximum load applied to the specimens for the area (A) of their cross-section. The ends of each specimen were polished with sandpaper before the mechanical test, in order to have flat surfaces in contact with the testing machine. Moreover a thin layer of lubricant coating has been spread at the ends of specimens to minimize friction between the surfaces of samples and the steel plates of the machine reducing the shear stresses. All the samples (Table 19) were characterized by XRD, FT-IR and ^{29}Si MAS-NMR.

Results and discussions

Sediments characterization

The chemical composition of the sediments used as geopolymer precursor is presented in Table 20.

sediment	SiO	Al	Fe	CaO	MgO	K	Na
Occhito	46,31	15,57	6,58	9,92	2,34	1,87	0,30
Sabetta	52,54	16,75	5,97	7,29	2,03	1,79	0,99

Table 20. Chemical compositions of the sediments (wt%).

82
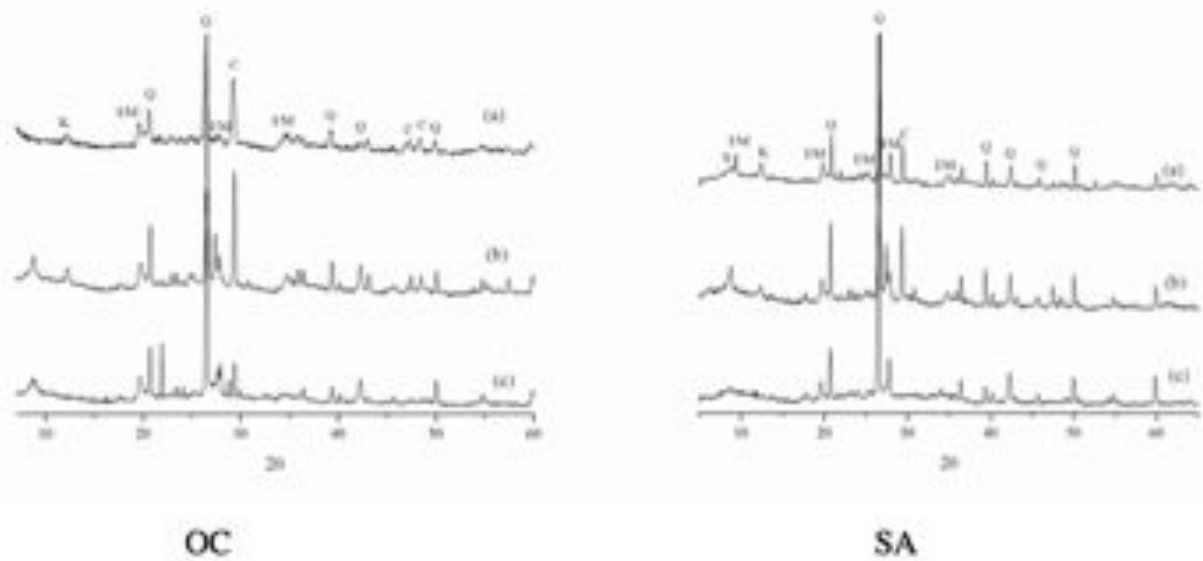
Figure 50. XRD spectra of Occhito and Sabetta not treated (a), calcined at 400°C (b) and 750°C (c). K=Kaolinite, Q=Quartz, C=Calcite, I/M=Illite/Muscovite, S=Smectite.

No marked differences exist between the two samples. In fact for both sediments SiO_2 and Al_2O_3 are the main components, while CaO and Fe_2O_3 are present in lower concentrations; K_2O, MgO and Na_2O are present in such small percentages that can be considered not much significant in order to alter the structure of final geopolymer. Theoretically any aluminosilicate material can undergo geopolymerization under specific conditions so, due to their chemical composition, both Occhito and Sabetta sediments can be considered as potential geopolymer precursors.

In figure 49 the XRD spectra of the raw and calcined sediments are reported. X-ray diffraction patterns show the presence of quartz, calcite and clay minerals, in particular kaolinite and illite/muscovite, as principal mineralogical phases for non-calcined sediments.

Following the thermal evolution of the crystalline structures of the Occhito sediment in the left side of Figure 50, it is possible to see that the peak of kaolinite is still present at 400°C (Figure 49b), but disappears increasing the temperature up to 750° C (Figure 49c), when an amorphous phase appears. The changes in the spectrum for the illite/muscovite peaks are less significant because of the thermal stability of these phases. Beside the higher amount of quartz (Table 21), determined by the analysis of XRD data, similar considerations can be made for the XRD spectra of the Sabetta sediment reported in the right side of Figure 50.

The results of the thermal analysis are reported in Figure 51. In the range from room temperature to 180°C is visible a weight loss related to the loss of adsorbed or weakly bound water for both sediments; the range from 200 to 400°C corresponds to the oxidation of algae and other organic residues, in this case the weight loss for the Sabetta sediment is more pronounced than the Occhito one.

83

Materials	Mineralogical phases
Occhito	Quartz (18%), Calcite (17%), feldspars (3%), clay phase (62%)
Sabetta	Quartz (23%), Calcite (8%), feldspars (2%), clay phase (67%)

Table 21. Mineralogical compositions of raw sediments (wt%) determined by quantitative analysis of XRD data of Figure 49.
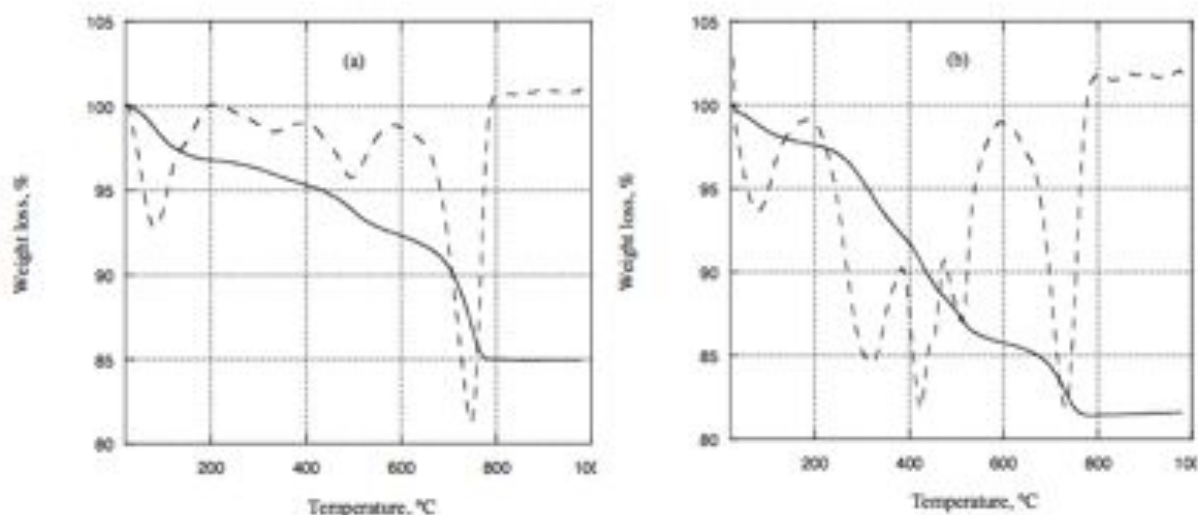
Figure 51. Differential thermogravimetry analysis of sediments not calcined, Occhito (a), Sabetta (b).

The range from 400 to 600°C can be related to clay structure collapse and also in this case Sabetta sediment presents a higher weight loss due to its higher content of clay minerals than Occhito one. Finally between 700 and 800°C the carbonate decomposition with CO_2 loss is present in both thermograms.

The range from 400 to 600°C can be related to clay structure collapse and also in this case Sabetta sediment presents a higher weight loss due to its higher content of clay minerals than Occhito one. Finally between 700 and 800°C the carbonate decomposition with CO_2 loss is present in both thermograms.

In order to improve the chemical characterization of the sediments, FTIR spectroscopy has been performed. The FTIR spectrum shown in Figure 52, related to the OC sediment before calcination, is typical of a smectite based material, even if non-smectite phases are also present in the sample.

84
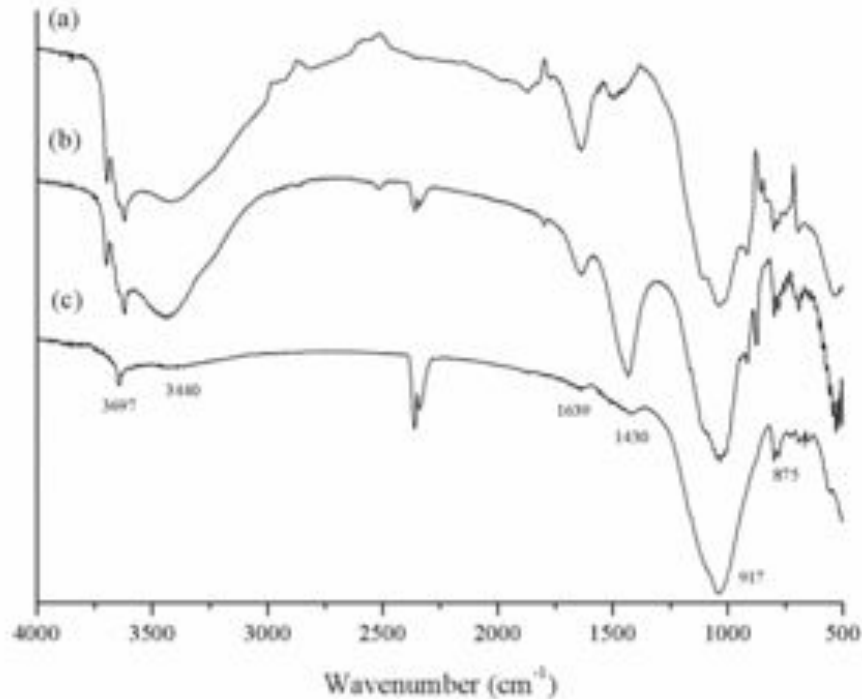
Figure 52. FTIR spectra of Occhito sediment a) before and after thermal treatment at b) 400°C for 2 h c) 750°C for 2 h.

The well-resolved, sharp and intense band at 3697 cm^{-1} in the –OH stretching region along with the band at 917 cm^{-1} in the –OH bending region indicates the presence of crystalline kaolinite in the sample. Furthermore, bands at 793 and 692 cm^{-1} show the presence of quartz [**Tyagi** (2006)]. The FTIR spectrum indicates also the presence of $CaCO_3$, mainly in the form of calcite, as identified by its main absorption bands at 1430 and 875 cm^{-1} [**Shahraki** (2011)]. The FTIR spectra of the calcined Occhito sediment show that the kaolinite structure is completely collapsed after a 2h treatment at 750°C (the bands at 3697 and 917 cm^{-1} disappeared), while the smectite structure is only partially damaged. The latter result is supported by the disappearance of the band at 3623 cm^{-1} (assigned to hydroxyl groups coordinated to Al^{3+} cations) and the persistence of the bands at 3440 and 1639 cm^{-1}, which are the stretching and bending vibrations for the hydroxyl groups of water molecules present in the clay [**Tyagi** (2006)]. Calcite is still present at 400°C, while at 750°C, it is absent (the bands at 1430 and 875 cm^{-1} disappeared due to decarboxylation). This fact is further confirmed by the appearance of the –OH stretching band of $Ca(OH)_2$, easily formed by the reaction of CaO with atmospheric water vapor, at 3644 cm^{-1} [**Ferone** (2013)]. The modification of the shape of the Si–O stretching band at 1000 cm^{-1}1 indicates a change in Si environment after calcination [**Tyagi** (2006)]. FTIR spectra of Sabetta sediment are not reported because they resulted to be similar to the Occhito ones.

Geopolymeric binder characterization

Mechanical Test

Compressive strengths of geopolymeric specimens produced are reported in Figure 53, which shows that the thermal treatment of sediments significantly affects the mechanical properties of samples.
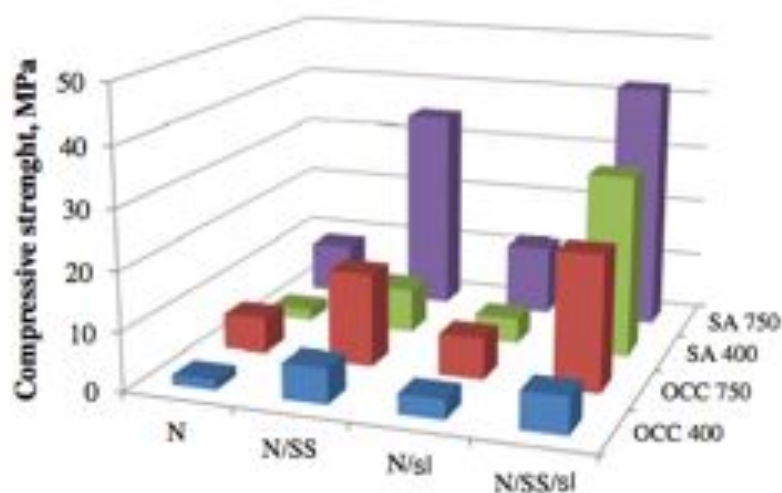
Figure 53. Compressive strengths of different mixtures produced.

In fact, for both sediments, the increase of the calcination temperature from 400°C to 750°C results in a significant increase of compressive strength values. The use of more alkaline solutions (5, 7 and 10M) and/or of sodium silicate leads to a more efficient activation of Si and Al present in the sediments and allows a more compact final geopolymeric product. In particular after the addition of higher concentrations of sodium silicate (SS), that causes an increase of the SS/NaOH ratio, stronger ion-pair formation is expected, which will result in longer chain silicate oligomers as well as Al–O–Si complexes, that promote polycondensation [**Xu** (2000)], **Ferone** (2013b)]. In order to further increase the mechanical properties of specimens, blast furnace slag has been added to the starting mixture. In fact, blast furnace slag can significantly contribute to the mechanical properties of the geopolymer, since its content of calcium, present as CaO, can promote the hydraulic consolidation of specimens and the removal of free water. In Figure 53 it is possible to see that, as expected, the addition of slag leads to higher compressive strength values. Finally the highest value of compressive strength was obtained with sediment Sabetta treated at 750°C mixed with NaOH, sodium silicate and slag.

The solids resulting from the mechanical tests, after drying in oven at 105°C, were characterized by means of FTIR and ^{29}Si MAS-NMR.

FT-IR

The results of FTIR analyses relative to the Occhito sediment are reported in Figure 54. The spectra of the Sabetta sediment are not shown, since the characterization results are very similar to the Occhito ones.
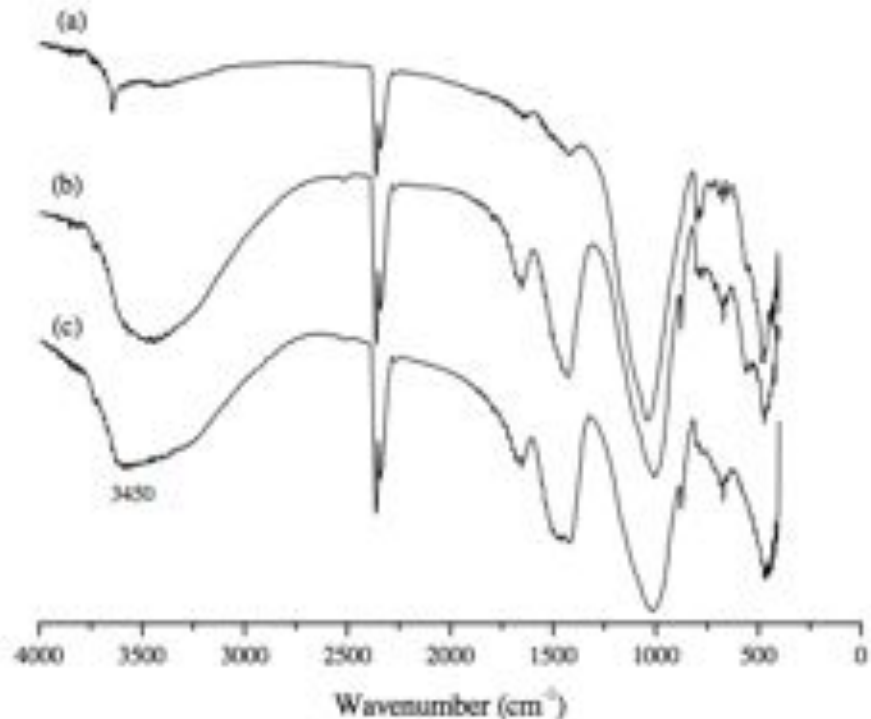
Figure 54. FTIR spectra of Occhito sediment (a) calcined at 750°C, (b) geopolymer mixture with Occhito sediment and NaOH and (c) geopolymer mixture obtained with Occhito sediment, NaOH, sodium silicate and slag.

It is well known that geopolymers produced starting from aluminosilicate powders are amorphous aluminosilicates themselves, so that they present FTIR spectra characterized by the typical absorption bands of Si-O-Si and Si-O-Al bonds (absorption range 600-800 cm^{-1}). One of the FTIR signals that give information about the degree of geopolymerization, is the band at 3450 cm^{-1} of the band correlated to the "chemically bonded water" (Leonelli and Romagnoli, 2011). As it can be seen in Figure 54, the band is absent in the spectrum of sediment calcined at 750°C, whereas it appears in those of both the two other samples, confirming the formation of the geopolymer. Furthermore, the geopolymerization induces a shift of the band of T-O-Si (T = Si o Al) stretching towards lower wavenumbers because of the formation of hydrogen bonds with hydroxyl groups present in the system [**Verdolotti** (2008)] with respect the same bonds in the spectrum of just calcined Occhito sediment. In all the spectra in Figure 53, an absorption peak is visible at about 1450cm^{-1}, due to sodium carbonate formed on the geopolymer surface by the carbonation of unreacted hydroxide during the drying process. Similar considerations can be obtained comparing the FTIR spectra of geopolymer samples produced starting from sediments calcined at different temperatures. The

spectra in Figure 55 make clear that an increase in the temperature of calcination leads to a more reactive geopolymer precursor and consequently to a better geopolymerization.
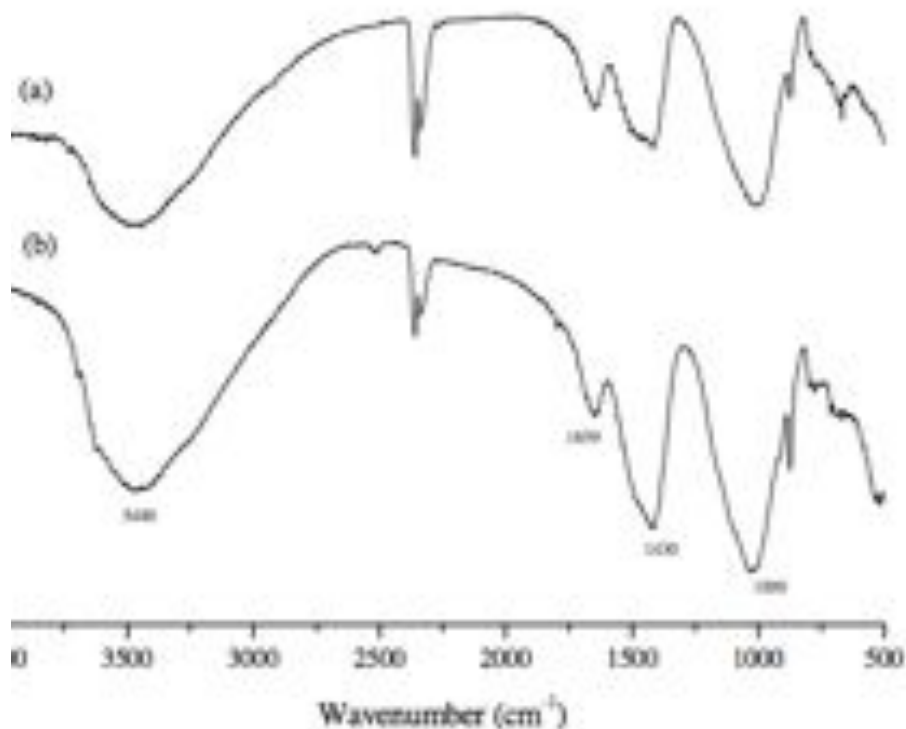
Figure 55. FTIR spectra of (a) geopolymer mixture with Occhito sediment calcined at 750°C, NaOH, sodium silicate and slag and (b) geopolymer mixture with Occhito sediment calcined at 400°C, NaOH, sodium silicate and slag.

^{29}Si NMR

NMR analysis was performed on the sediments in order to follow their geopolymerization with different solutions. The ^{29}Si MAS-NMR analyses provide information on the structural surroundings of silicon atom, so that the different Q^n sites, where Q represents the SiO_4 tetrahedron and n refers to the number of Si-O-Si bridging oxygen atoms, have different ^{29}Si isotropic chemical shifts. For aluminosilicate the number of AlO_4 tetrahedra bound to the central silicon of a Q^n unit is given in parentheses, e.g. $Q^n(mAl)$. ^{29}Si chemical shifts (ppm) are reported in Table 22 [**Zibouche** (2009)].

Qⁿ(mAl)	Q⁴(4Al)	Q⁴(3Al)	Q⁴(2Al)	Q⁴(1Al)	Q⁴(0Al)
position (+/- 2 ppm)*	-83	-88	-92	-97	-107

*Table 22. ^{29}Si NMR chemical shifts of the $Q^n(mAl)$ units (in ppm). * Position depends on Si/Al ratio.*

The ^{29}Si spectrum of the Occhito sediment (Figure 56) indicates a wide range of Si environment with overlapped resonances. Accordingly, the structure of the sediment is characterized by Q^3 and Q^4 units. The major peak (Q^3 region) is located at -93 ppm with two shoulders at -89 and -98 ppm associated respectively to kaolinite, illite and smectite [**Carrolla** (2005)]. The resonance at -108 ppm corresponds to Q^4 (amorphous silica), even if according to **Oudadesse** et al. (2007), surrounded and mixed with Q^3 and Q^4 groups.
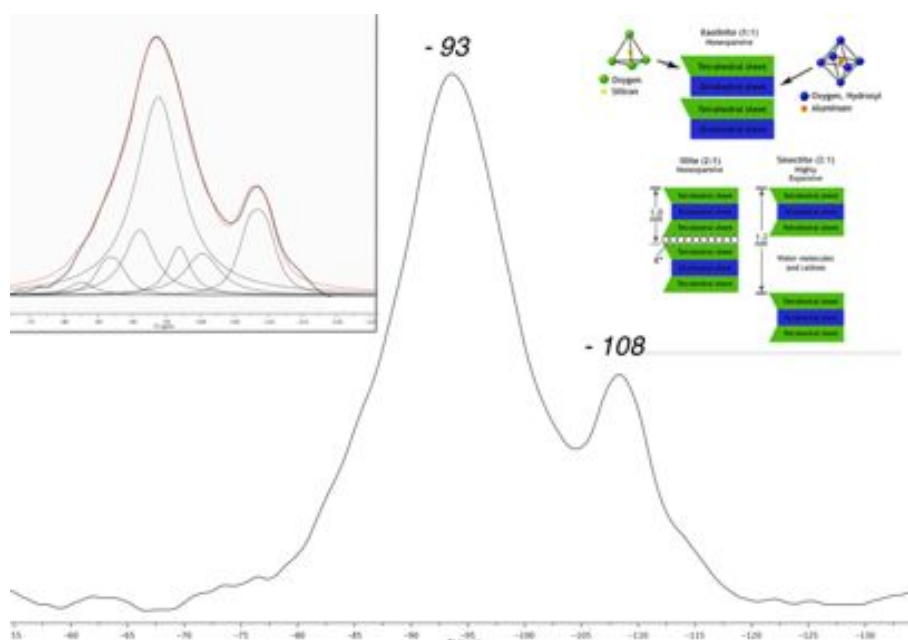
Figure 56. ^{29}Si spectrum OC. In the box above the deconvoluted spectra.

The ^{29}Si MAS NMR spectrum of sediment after thermal treatment is shown in Figure 57. This spectrum is characterized by a broad resonance around -100 ppm assigned to Q^3 "sheet-like" layers. The center of gravity of the resonance is shifted significantly downfield and this is typical of the metakaolin formation. The heat treatment produces distortions in the silica layer, in fact dehydroxylation of kaolin to metakaolin is associated to a change of bond angles and lengths of the silica layer. The resonance at − 108 ppm is assigned to the residual quartz.
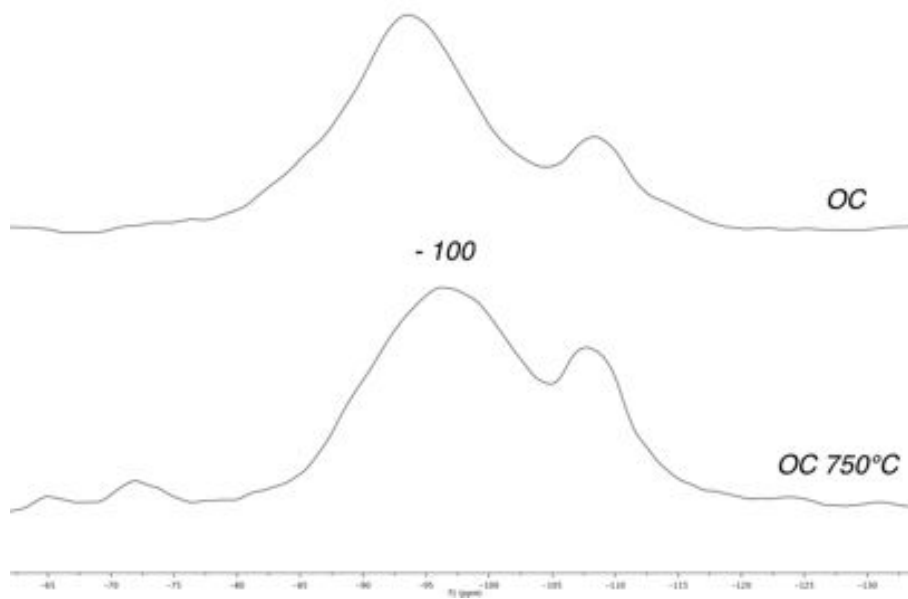
Figure 57. ^{29}Si spectrum of clay treated at 750°C. Above the comparison of untreated sample.

First geopolymerization was attempted by reaction of the thermally treated sample with NaOH, ^{29}Si NMR spectrum of the product is reported in Figure 58. The main resonance around -100 ppm indicates a non complete dissolution of metakaolin, this phenomenon was just observed in high-Si systems which generally react more slowly [**Provis** (2007)]. Deconvolution of spectrum has allowed to identify the following Q^4(mAl) species: -89 ppm (Q^4(3Al)), -94 ppm (Q^4(2Al)), -98 ppm (Q^4(1Al)), -110 and -120 ppm (Q^4(0Al)). The presence of the two last bands are yet related to quartz impurities in the geopolymer samples [**Fletcher** (2005)].
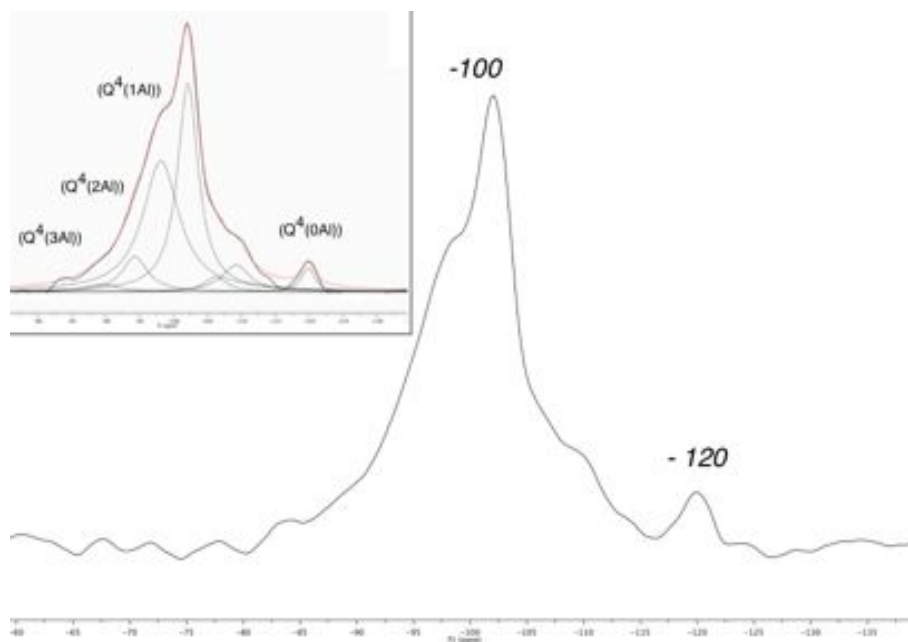
Figure 58. ^{29}Si spectrum OC/N. In the box above the deconvoluted spectra.

90

The adding of sodium silicate solution to the activator solution involves a very broad band centered at -97 ppm. Decomposing the observed spectrum into its components indicates the presence of Q^4(4Al) (-82 ppm), Q^4(3Al) (-89 ppm), Q^4(2Al) (-92 ppm), Q^4(1Al) (-97 ppm), Q^4(0Al) (-107 ppm). The broadening of the resonance is related to very disordered lattice (Figure 59).
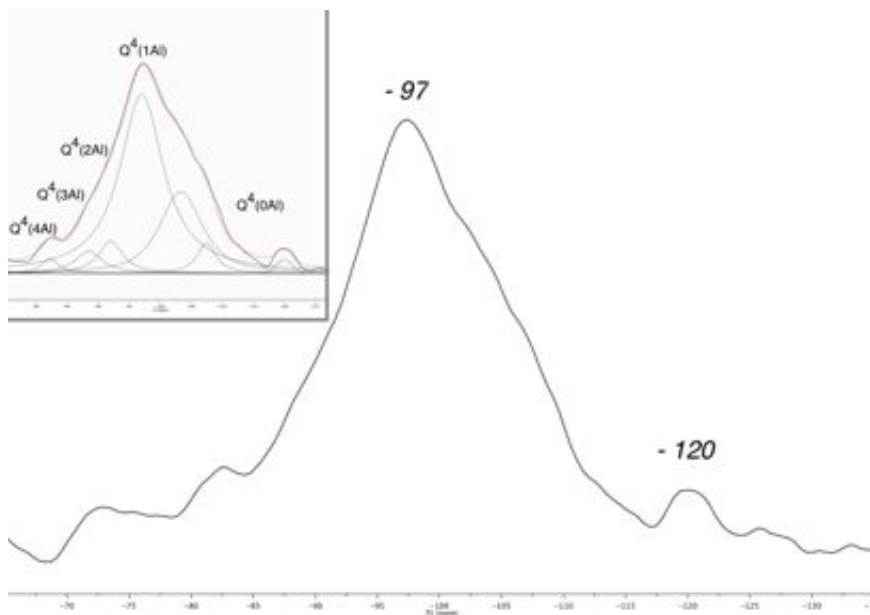
Figure 59. ^{29}Si spectrum OC/N/SS. In the box above the deconvoluted spectra.

The spectra in Figure 60-61 illustrate the influence of furnace slag in geopolymerization process. ^{29}Si NMR spectrum of OC/N/GBS shows the presence a more narrow resonance centered at -99 ppm, it can be deconvoluted in seven different ^{29}Si environments: Q^4(3Al) (-86 ppm), Q^4(2Al) (-92 ppm), Q^4(1Al) (-95 ppm and -99 ppm), -103 ppm, Q^4(0Al) (-108, -120 ppm).
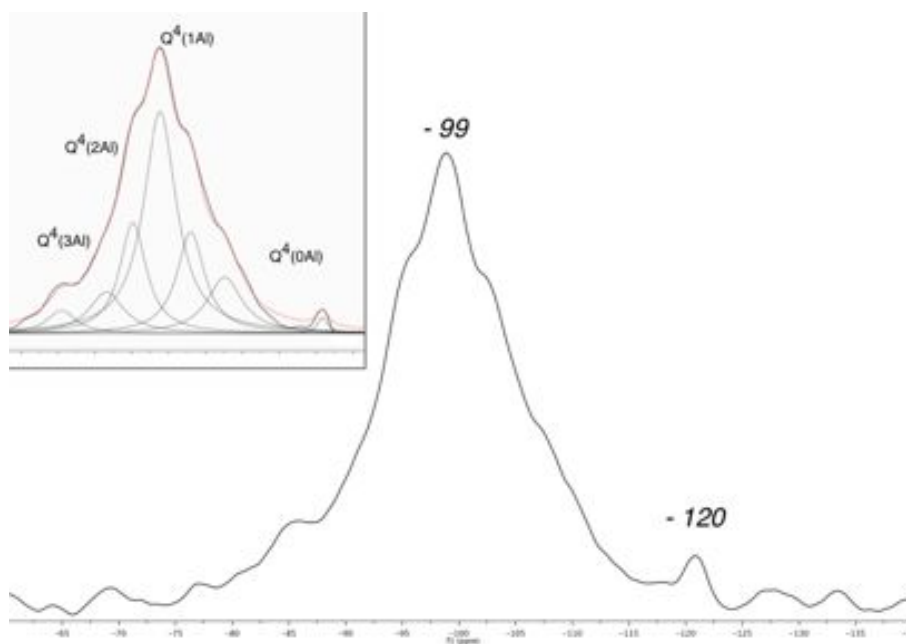
Figure 60. ^{29}Si spectrum OC/N/GBS. In the box above the deconvoluted spectra.

91
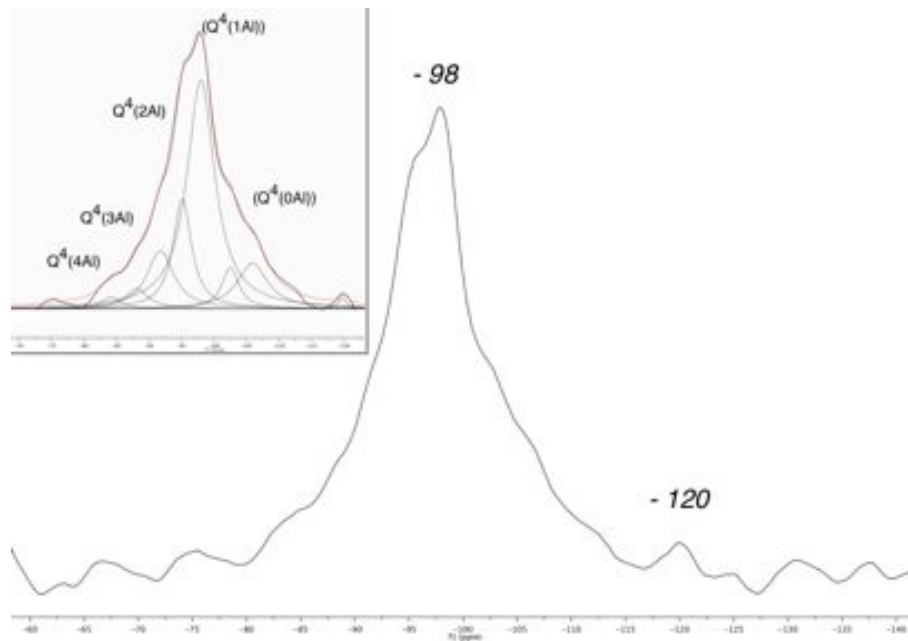
Figure 61. ^{29}Si spectrum OC/N/GBS. In the box above the deconvoluted spectra.

Finally, the simultaneous use of sodium hydroxide, sodium silicate solution and slag (OC/N/SS/GBS) implies a very low content of unreacted quartz impurities in the geopolymer product. The deconvolution procedure allows to identify this following $Q^4(mAl)$ species: $Q^4(4Al)$ (-84 ppm), $Q^4(3Al)$ -88 ppm, $Q^4(2Al)$ (-92 ppm), $Q^4(1Al)$ (-95 ppm, -98 ppm), -103 ppm, $Q^4(1Al)$ (-106 ppm, -120 ppm).

The fact that the this ^{29}Si signal of this last geopolymer sample is narrower suggests that a three-dimensional ordered phase was formed in which the Si occurs in a variety of environments but with a predominance of $Q^4(1Al)$ and $Q^4(2Al)$ units [**Barbosa** (2000), **Brew** (2007), **Tsai** (2010)].This result is also in good agreement with the obtained strength values discussed in the previous paragraph and could be extended to samples prepared from Sabetta sediment too.

Supporting information

Reactivity in alkaline media

The formation of geopolymers involves a chemical reaction between an aluminosilicate material and sodium silicate solution in a highly alkaline environment. The exact mechanism of geopolymerization is not yet fully understood, but it is believed to consist of three main stages: (1) the surface dissolution of Al and Si in a highly alkaline solution and diffusion of the dissolved species through the solution, (2) the polycondensation

of the Al and Si complexes with the solution and the formation of a gel and (3) the hardening of the gel that results to the final geopolymeric product [**Panagiotopoulou** (2007)].

Alcalinity NaOH	3-7M
Liquid/solid ratio	40
Time of dissolution	5-10-24-72 (hours)
Temperature	25°C
Stirring	✓

Table 23. Process parameters of reactivity test.

The dissolution stage is the only one that can be quantitatively studied. For this reason the leaching behavior of the calcined sediments in alkaline solution has been investigated. A lot of papers have been published on the dissolution of aluminosilicate compounds, especially in the geochemical literature [**Wolff-Boenisch** (2004), **Köhler** (2003), **Ganor** (1998), **Criscenti** (2005)]. There are different solubility tests in alkaline solution that allow the direct determination of the amount of reactive silicate and aluminate species [Fraay (1990), **He** (1994,1995a), **Xu** (2000)]. Two of the main aspects of the test regime are the solution/solid ratio and the alkalinity of the solution used. In fact too low values of the former (not enough dissolution) will result in condensation of the aluminosilicate. If this happens, the real amount of dissolved silicate and aluminate species cannot be measured in the solution. In table 5 and 6 the extent of Al and Si dissolution in relation to time, alkalinity of the solution and temperature of calcination of the sediments are reported. These values represent the amount of Al and Si in mg released for each gram of sample analyzed.

The data of Tables 23 and 24 show that the release is strongly affected by: (a) temperature of calcination of the sediments (b) molarity of the alkaline solution and (c) time.

		OC		SA	
		400	750	400	750
	hours				
3 M	5	1.02	6.40	2.52	14.89
	10	0.89	13.44	1.80	15.10
	24	1.09	21.84	2.96	14.69
	72	1.54	26,54	5.51	34.88
7 M	5	1.68	13.06	6.62	16.95
	10	2.13	18.45	5.38	10.59
	24	2.60	26.07	8.02	20.53
	72	4.03	35.88	12.26	33.72

Table 24. Extent of Al dissolution (mg/g) in relation to time and alkalinity of the solution.

	OC		SA	
	400	750	400	750
hours				
3 M				
5	7.04	20.80	10.26	27.93
10	7.02	30.98	9.15	25.93
24	7.78	43.17	9.45	21.27
72	5.59	50.40	10.53	43.30
7 M				
5	7.36	36.31	11.86	29.59
10	9,26	42.58	10.16	17.01
24	14.14	53.00	13.32	34.88
72	15.69	74.05	24.55	60.20

Table 25. Extent of Si dissolution (mg/g) in relation to time and alkalinity of the solution.
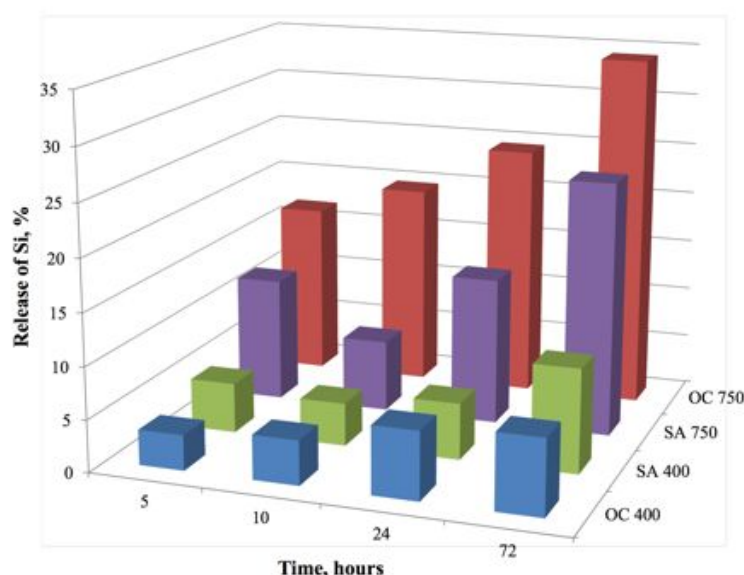
Figure 62. Release of Si in relation to calcination temperature and time of contact of sediments with NaOH 7M solution.

The increase of the calcination temperature of sediments from 400 to 750°C results in an increased extent of dissolution both for Al and Si. It's worth noting in Figure 60 that, after three days of contact with a 7M NaOH alkaline solution, the Occhito sediment releases the 7% of Si if treated at 400°C and the 33% when treated al 750°C.

This result is supported by the FTIR spectra in Figure 61 of Occhito sediments before and after reactivity test. The band at 1000 cm^{-1}, is associated to the stretching of Al-O and Si-O in amorphous alluminosilicate structure.
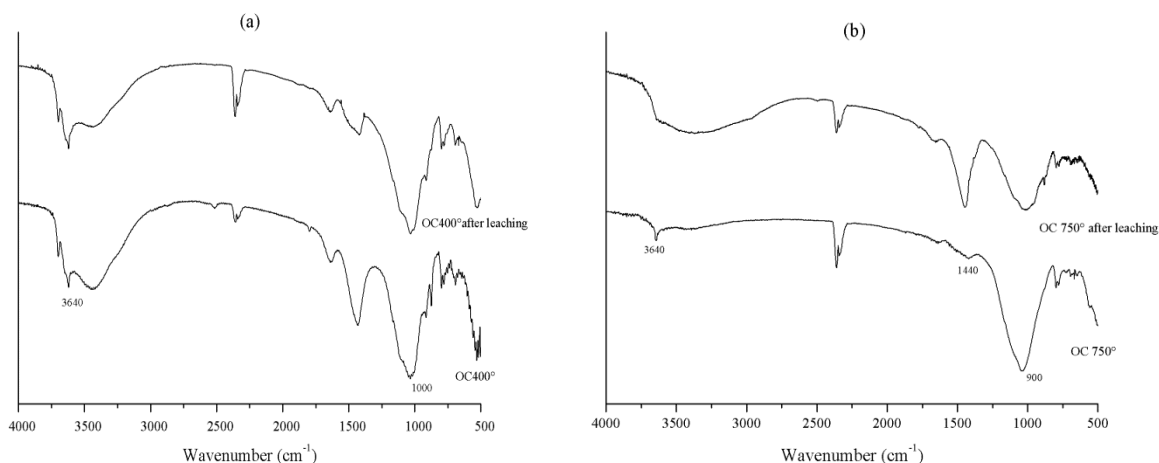
Figure 63. FTIR spectra of Occhito sediment calcined at 400°C before and after reactivity test (a) and Occhito sediment calcined at 750°C before and after reactivity test (b).

This band decreases and broadens significantly in the spectrum of the residual solid, confirming a considerable release of Si and Al in the alkaline solution, particularly in the sample treated at 750°C. The band at 3640 cm^{-1} in the residual solid from the test is associated to the –OH band of $Ca(OH)_2$.

A further confirmation of the disappearance of the clay phase of the sediment in the solid residual from the reactivity test comes from the XRD spectra in Figure 62. In the same figure it is observed that the siliceous part of the crystalline phases remains unchanged. Finally in Figure 63 is shown that the use of more concentrated NaOH solutions (from 3 to 7M) facilitates the processes of dissolution of the aluminosilicate phases present in both sediments. This effect is even clearer for the shorter times and for the sediments calcined at 400°C (data not reported). For both sediments the percentage of aluminum released is higher than the one of Si. This result is due to the chemical composition of the sediments: in both the cases aluminum is in the phases, soluble in alkaline media, whereas silicon is also present as quartz, which is less reactive than clay in alkaline environment.
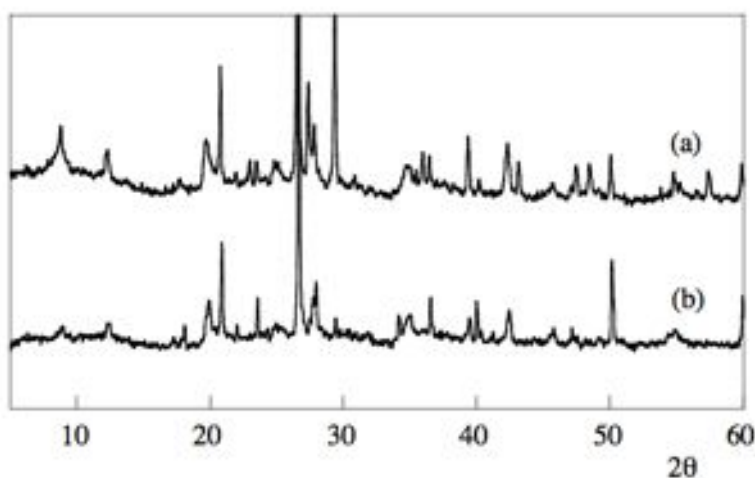
Figure 64. XRD of Occhito sediment calcined at 400 °C before (a) and after reactivity test (b).
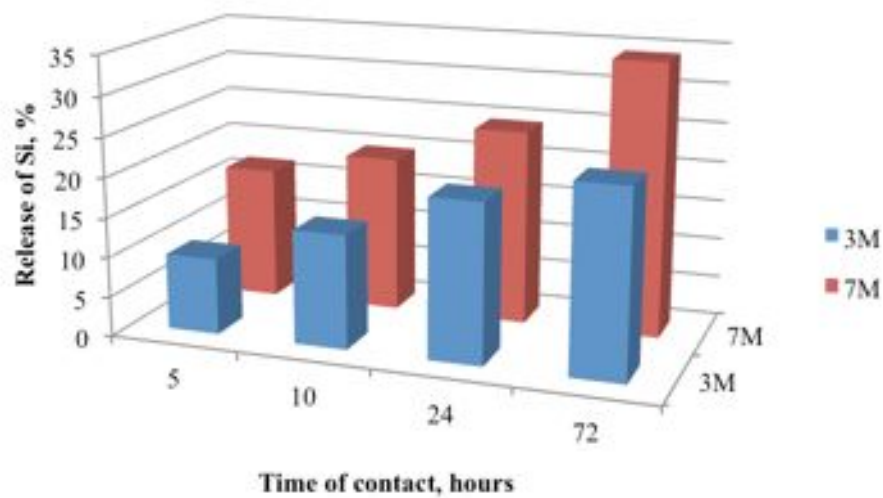
Figure 65. Release of Si in relation to time of contact of Occhito sediment calcined at 750°C with 3M and 7M NaOH solutions.

Conclusions

Reported data have demonstrated that each of clay sediment, coming from two different reservoirs located in Southern Italy, can be employed as precursor for the synthesis of geopolymers after suitable heat treatment. In particular, the increase of the calcination temperature of sediments from 400 to 750°C results in an increased extent of dissolution both for Al and Si, also confirmed by FTIR and NMR. This leads to a more reactive geopolymer precursor and consequently to a better geopolymerization. Accordingly, the mechanical properties obtained by the geopolymers specimens seem to be acceptable for all the samples prepared with heat-treated sediments. However, both the used characterization techniques (NMR and FTIR) and the measured mechanical strengths lead to the conclusion that the addition of a sodium silicate solution and ground granulated blast furnace slag allows to obtain a better degree of geopolymerization and consequently better mechanical performances.

3.4 General Conclusions

Solid state nuclear magnetic resonance (SS-NMR) spectroscopy is an important tool in studying the chemistry of cement based materials. In this thesis, ^{29}Si SS-NMR spectroscopy was used to study two different systems:

- ^{29}Si MAS NMR has allowed to obtain informations on the microstructure of calcium silicate hydrate in presence of additives. In particular ^{29}Si NMR spectra has shown the effects of superplasticizer on hydration and polymerization of silicate chains. This study shows for the first time, that the C−S−H formed in the presence of organic additives has a degree of polymerization higher than the one obtained in pure water.

- ^{29}Si MAS NMR spectroscopy has been employed to investigated the effect of alkali activator chemical composition on the structure of geopolymeric gels. The main result of the work presented in this paper is that a clay sediment (containing kaolin and secondary minerals) is suitable, after heat treatment, for synthesis of geopolymer solids by alkaline activation. Considering the large deposits of impure kaolins in many parts of the world, this opens the way to the large scale utilization of these mineral resources for the production of green construction materials.

- SS-NMR analysis has proven to be a valuable tool to complement other methods, e.g. the X-ray diffraction and FT-IR, in the study of building materials.

CHAPTER IV

REFERENCES

-A-

- **Abdelmouleh** M.; Boufi S.; Belgacem M.N.; Duarte A.P.; Ben Salah A.; Gandini A., M*odification of cellulosic fibers with functionalized silanes: development of surface*, International Journal of Adhesion and Adhesive, Vol.24, pp 43-54, **2004**

- **Aitcin**, P.C.; *Cements of yesterday and today. Concrete of tomorrow. Review*, Cement and Concrete research, vol. 30, pp 1349-1359, **2000**

- **Alizadeh**, R.; Beaudoin, J. J.; Raki, L.; Terskikh, V.; *C-S-H/ Polyaniline Nanocomposites Prepared by in Situ Polymerization*, Journal of Material Scienc, vol. 46, pp. 460−467, **2011**

- **Ambrosi**, M.; Fratini, E.; Canton, P.; Dankesreiter, S.; Baglioni, P.; *Bottom-up/Top-down Synthesis of Stable Zirconium Hydroxide Nanophases,* Journal of Mater. Chem., vol. 22, pp. 23497−23505, **2012**

- **Andini** S.; Cioffi R.; Colangelo F.; Montagnaro F.; Santoro L., *Coal fly ash as raw material for the manufacture of geopolymerbased products*, Waste Manage, vol. 28, pp. 416-423, **2008**

- **Ando** I.; Saito H.; Tabeta R.; Shoji A.; Ozaki T., *Conformation-Dependent 13C NMR Chemical Shifts of Poly(L-alanine) in the Solid State: FPT INDO Calculation of N-Acetyl-N'-methyl-L-alanine Amide as a Model Compound of Poly(L-alanine)*, vol. 17, pp. 457-461, **1984**

- **Ando** S.; Ando I.; Shoji A.; Ozaki T., *Intermolecular Hydrogen-Bonding Effect on 3CNMR Chemical Shifts of Glycine Residue Carbonyl Carbons of Peptides in the Solid State*, Journal of American Chemical Society, vol. 110, pp-3380-3386, **1988**

- **Atalla** R.H.; VanderHart D.L.; *The role of solid state 13C NMR spectroscopy in studies of the nature of native celluloses*, Solid State Nuclear Magnetic Resonance, vol.15, pp. 1–19, **1999**

-B-

- **Bae** E.; Park H.J.; Lee J.; *Bacterial cytotoxicity of the silver nano particle related to physicochemical metrics and agglomeration properties*, Environmental Toxicology and Chemistry, vol. 29, pp. 2154-2160, **2010**

- **Bakharev** T., *Resistance of geopolymer materials to acid attack,* Cement and Concrete Research, vol. 35, pp. 658–670, **2005**

- **Barbosa,**

- **Barbosa** V.F.F.; Mackenzie K.J.D., Thermal behaviour of inorganic geopolymers and composites derived from sodium polysialate, Material Research Bulletin, vol. 38, pp. 319–331, **2003**

- **Bardet** M.; Gerbaud G.; Doan C.; Giffard M.; Hediger S.; De Paepe G.; Tran Q.K., *Dynamics property recovery of archaeological-wood fibers treated with polyethylene glycol demonstrated by high-resolution solid-state NMR*, Cellulose, vol. 19, pp. 1537–1545, **2012.**

- **Baronio** G.,; Binda L., *Study of the pozzolanity of some bricks and clays*, Construction and Building Materials, vol. 11, pp. 41–46, **1997**

- **Beaudoin** J.J.; Raki L.; Alizadeh R., *A ^{29}Si MAS NMR Study of Modified $C−S−H$ Nanostructures,* Cement and Concrete Composite, vol. 31, pp. 85−590, **2009**

- **Belleville** P.; *Functional coatings: The sol-gel approach*, Comptes Rendus Chimie, vol. 13, pp 97–105, **2010**

- **Bhat** N.V.; Seshadri D.T.; Nate M.M.; Gore A.V., *Development of conduttive cotton fabric heating devices*, Journal of Applied Polymer Science, vol. 102, pp. 4690-4695, **2006**

- **Bodart** M.; De Peñaranda R.; Deneyer A.; Flamant G., *Photometry and colorimetry characterisation of materials in daylighting evaluation tools*, Building and Environment, vol. 43, pp. 2046–2058, **2008**

- **Boehme** C.; Hora G., *Water absorption and contact angle measurement of native European, North American and tropical wood species to predict gluing properties,* Holzf-orschung, vol. 50, pp. 269–276, **1996.**

- **Brew** D.R.M.; MacKenzie K.J.D., *Geopolymer synthesis using silica fume and sodium aluminate*, Journal of Material Science, vol. 42, pp. 3990–3993, **2007**

- **Brinker** C.J., *Hydrolysis and condensation of silicates: effects on structure*, Journal of Non-Crystalline Solids, vol. 100, pp. 31-50, **1988**

- **Brugnara** M.; Della Volpe C.; Maniglio D.; Siboni S.; Negri M., Gaeti N., *Wettability of Porous Materials. I. The Use of Wilhelmy Experiment: the Cases of Stone, Wood and Non-Woven Fabric,* in Contact Angle, Wettability and Adhesion, Utrecht ; Boston, Mass.: VSP An imprint of Brill, pp. 115-142, **2006**

- **Brugnara** M.; Degasperi E.; Della Volpe C.; Maniglio D.; Penati A.; Siboni S.; Toniolo L.; Poli T.; Invernizzi S.; Castelvetro V., *The application of the contact angle in monument protection: new materials and methods*, Colloids and surfaces. A, Physicochemical and engineering aspects, vol. 241, pp. 299-312, **2004**

- **Brunet** F.; Bertani, P.; Charpentier, T.; Nonat, A.; Virlet, J., *Application of Si-29 Homonuclear and ^1H-^{29}Si Heteronuclear NMR Correlation to Structural Studies of Calcium Silicate Hydrates,* Journal of Physical Chemistry B, vol.108, pp. 15494−15502, **2004**

- **Brunet** F.; Charpentier T.; Chao C.N.; Peycelon H.; Nonat *A., Characterization by Solid-State NMR and Selective Dissolution Techniques of Anhydrous and Hydrated CEM V Cement Pastes,* Cement and Concrete Research, vol. 40, pp. 208−219, **2010**

- **Buchwald** A., *What are geopolymers? Current state of research and technology, the opportunities they offer, and their significance for the precast industry*, Concrete Precasting Plant and Technology, vol. 72, pp. 42–49, 2**006**

- **Buchwald** A.; Hohmann M.; Posern K.; Brendler E.; *The suitability of thermal activated illite/smectite clay as raw material for geopolymer binders*, Applied Clay Science, vol. 46, pp. 300–304, **2009**

-C-

- **Campanella** L.; Casoli A.; Colombini M.P., Marini Bettolo R.; Matteini M.; Migneco M.; Montenero A.; Nodari L.; Piccioli C.; Plossi Zappalà M.; Portalone G.; Russo U.; Sammartino M., *Chimica per l'arte*, Zannichelli, **2007**

- **Cappelletto** E.; Callone E.; Campostrini R.; Girardi F.; Maggini S.; Della Volpe C.; Siboni S.; Di Maggio R., *Hydrophobic siloxane paper coatings: the effect of increasing methyl substitution*, Journal of Sol-Gel Science Technology, vol. 62, pp. 441–452, **2012**

- **Carrolla** D.L.; Kempa T.F.; Bastowab T.J.; Smitha M.E, Solid-state NMR characterisation of the thermal transformation of a Hungarian white illite, Solid State Nuclear Magnetic Resonance, vol. 28, pp. 31–43, **2005**

- **Chen** J.J.; Thomas J.J.; Taylor H.F. W.; Jennings H.M., *Solubility and Structure of Calcium Silicate Hydrate*, Cement and Concrete Research, vol. 34, pp. 1499−1519, **2004**

- **Chen** J.S.; Huang; Chang Y.W., *A preliminary study of reservoir sludge as a raw material of inorganic polymer*, Construction Building Materials, vol. 23, pp. 3264–3269, **2009**

- **Chiang** K.J.; Chien K.L.; Hwang S.J., *Study on the characteristics of building bricks produced from reservoir sediment*, J. Hazard Materials, vol. 159, pp. 499–504, **2008**

- **Chiang** W.-S.; Fratini E.; Baglioni P.; Liu D.; Chen S.-H, *Microstructure Determination of Calcium-Silicate-Hydrate Globules by Small-Angle Neutron Scattering,* Journal of Physical Chemistry C 2012, vol. 116, pp. 5055−5061, **2012**

- **Chiang** W.C.; Fratini E.; Ridi F.; Lim S. H.; Yeh Y. Q.; Baglioni P.; Choi S.M.; Jeng, U.S.; Chen S. H., *Microstructural Changes of Globules in Calcium-Silicate-Hydrate Gels with and Without Additives Determined by Small-Angle Neutron and X-Ray Scattering*, Journal of Colloid and Interface Science, vol. 398, pp. 67−73, **2013**

- **Cioffi** R.; Maffucci L.; Santoro L., *Optimization of geopolymer synthesis by calcination and polycondensation of a kaolinitic residue*, Resources, Conservation and Recycling, vol. 40, pp. 27-38, **2003**

- **Collepardi** S.; Coppola L.; Troli R.; Collepardi M., *Mechanism of Actions of Different Superplasticizers for High-Performance Concrete*, Proceedings of the Second CANMET/ACI Conference on "High-Performance Concrete. Performance and Quality of Concrete Structures", Gramado (Brazil), pp. 503-523, **1999**

- **Coltrain** B.K.; S.M. Melpolder S.M.; Salva J.M., *Effect of hydrogen ion concentration on gelation of tetra-functional silicate sol-gel systems*, in D.R. Uhlmann and D.R. Ulrich (Eds.), Ultrastructure Processing of Advanced Materials, Wiley, New York, pp. 69- 76, **1992**

-

- **Comotti** A.; Simonutti R.; Sozzani P., *Hydrated Calcium Silicate and Poly(vinyl Alcohol): Nuclear Spin Propagation Across Heterogeneous Interfaces*, Chemistry of Materials, vol. 8, pp. 2341−2348, **1996**

- **Cong** X.; Kirkpatrick R., ^{29}Si *MAS NMR Study of the Structure of Calcium Silicate Hydrate, Advanced Cement based Materials*, vol. 3, 144−156, **1996**

-D-

- **Davidovits** J., *Solid phase synthesis of a mineral blockpolymer by low temperature polycondensation of aluminosilicate polymers*, I.U.P.A.C. International Symposium on Macromolecules. Topic III, New Polymers of high stability, Stockholm, **1976**

- **Davidovits** J., *Geopolymers: inorganic polymeric new materials*, Journal of Thermal Analysis, vol.37, pp. 1633–1656, **1991**

- **Davidovits** J., *Geopolymer cement to minimize carbon-dioxide greenhouse warming*, Ceramic Transactions, vol. 37, pp. 165-182, **1993a**

- **Davidovits** J., *Global warming impact on the cement and aggregates industries*, World Resource Review, vol.6, pp. 263–78, **1993b**

- **Davidovits** J., Chemistry of geopolymeric systems, terminology. In: Davidovits, J. (Ed.), Second International Conference Geopolymere '99. St. Quentin, France, pp. 9–40**, 1999**

- **De Meijer** M., *Review on the durability of exterior wood coatings with reduced VOC-content*, Progress of Organic Coating, vol. 43, pp. 217–225, **2001**

- **De Vetter** L.; Van den Bulke J.; Van Acker J., *Impact of organosilicon treatments on the wood-water relationship of solid wood*, Holzforschung, vol. 64, pp. 463-468, **2010**

- **Della Volpe** C.; Dirè S.; Pagani E., *A Comparative Analysis of Surface Structure and Surface Tension of Hybrid Silica Films*, Journal of Non-Crystalline Solids, vol. 209, pp. 51-60, **1997**

- **Della Volpe** C.; Penati A.; Peruzzi R.; Siboni S.; Toniolo L.; Colombo C., *The combined effect of roughness and heterogeneity on contact angles: the case of polymer coating for stone protection*, Journal of Adhesion Science and Technology, vol. 14, pp. 273–299, **2000**

- **Della Volpe** C.; Maniglio D.; Morra M.; Siboni S., *The determination of a 'stable-equilibrium' contact angle on heterogeneous and rough surfaces*, Colloids and Surfaces A, Physicochemical and Engineering Aspects, vol. 206, pp. 47-67, **2002**

- **Della Volpe** C.; Brugnara M.; Maniglio D.; Siboni S.; Wangdu T., *About the possibility of experimentally measuring an equilibrium contact angle and its theoretical and practical consequences*, in Contact Angle, Wettability and Adhesion, Utrecht ; Boston, Mass.: VSP- An imprint of Brill, pp 79–99, **2006**

- **Di Maggio** R.; Callone E.; Girardi F.; Dire` S., *Structure-related behavior of hybrid organic-inorganic materials prepared in different synthesis conditions from Zr-based NBBs and 3-methacryloxypropyl trimethoxysilane*, Journal Applied Polymer Science, vol. 25, pp. 1713–1723, **2012**

- **Ding** Q.; Zhu Y.; Wnag Y.; Huang X.; Gong Z., *Effects of Molecular Structure of Polycarboxylate-Type Superplasticizer on the Hydration Properties of C_3S*, Journal of Wuhan University of Technology Material Science Ed., vol. 27, pp. 768−772, **2012**

- **Donath** S.; Militz H.; Mai C., *Wood modification with alkoxysilanes*, Wood Science Technology, vol. 38, pp.555–566, **2004**

- **Donath** S.; Militz H.; Mai C., *Wheathering of silane treated wood*, Hoz Roh Werkst, vol. 65, pp. 35-42, **2007**

- **Duxson** P.; Fernández-Jiménez A.; Provis J.; Lukey G.; Palomo A.; van Deventer J., *Geopolymer technology: the current state of the art,* Journal of Materials Science, vol 42, pp. 2917–2933, **2007**

-E-

- **Esteves** B.; Pereira H., *Wood modification by heat treatment: a review*, BioResources, vol. 4, pp. 370–404, **2009**

- **Evans** P.D., *Emerging technologies in wood protection*, Forest Products Journal, vol. 53, pp. 14-22, **2003**

- **Evans** P.D.; Wingate-Hill R.; Cunningham R.B., Studies of degradation and protection of wood surfaces, Wood Science and Tecnology, vol. 26, pp. 151-163, **1992**

- **Evans** J.L.; White J., *The thermal decomposition (dehydroxylation) of clays,* in: Kingery,W.D. (Ed.),Kinetics ofHigh Temperature Processes.MIT Press, pp. 301–312, **1959**

-F-

- **Ferone** C.; Colangelo F.; Cioffi R.; Montagnaro F.; Santoro L., *Mechanical performances of weathered coal fly ash based geopolymer bricks*, Procedia Eng., vol. 21, pp. 745–752, **2011**

- **Ferone** F.; Montagnaro, *Use of reservoir clay sediments as raw materials for geopolymer binders*, Advances Applied Ceramics, vol. 112, pp. 184 – 189, **2013**

- **Ferrari** L.; Kaufmann J.; Winnefeld F.; Plank J, *Interaction of cement model systems with superplasticizers investigated by atomic force microscopy, zeta potential, and adsorption measurements*, Journal of Colloid and Interface, vol. 347, pp. 15-24, **2010**

- **Fir** M.; Vince J.; Vuk A.S.; Vilcnik A.; Jovanovski V.; Mali G.; Orel B.; Simoncic B., *Functionalisation of Cotton with Hydrophobic Urea/Polydimethylsiloxane Sol-Gel Hybrid*, Acta Chimica Slovenica, Vol.54, pp. 144-148, **2007**

- **Fletcher** R.A.; MacKenzie K.J.D.; Nicholson C.L.; Shimadac S., T*he composition range of   aluminosilicate geopolymers*, Journal of the European Ceramic Society, vol. 25, pp. 1471–1477, **2005**

-G-

- **Gaan** S.; Rupper P.; Salimova V.; Heuberger M.; Rabe S.; Vogel F., *Thermal decomposition and burning behavior of cellulose treated with ethyl ester phosphoramidates: Effect of alkyl substituent on nitrogen atom*, Polymer Degradation and Stabilty, vol. 94, pp. 1125–1134, **2009**

- **Geppi** M.; Borsacchi S.; Mollica G., *Solid-State NMR of Organic/Inorganic Multi-Component Materials. In Solid-State NMR of Organic/Inorganic Multi-Component Materials,* Encyclopedia of Magnetic Resonance, Wiley: New York, **2008.**

- **Geppi** M.; Borsacchi S.; Mollica G.; Veracini C.A., *Applications of Solid-State NMR to the Study of Organic/ Inorganic Multicomponent Materials*, Applied Spectroscoscopy Reviews, vol. 44, pp.1−89, **2008**

- **Girardi** F.; Maggini S.; Della Volpe C.; Cappelletto E.; Mueller K.; Siboni S.,; Di Maggio R., *Hybrid organic–inorganic materials on paper: surface and thermo-mechanical properties*, Journal of Sol-Gel Science Techology, vol. 60, pp 315-323, **2011**

103

- **Graziola** F.; Girardi F.; Di Maggio R.; Callone E.; Miorin E.; Negri M.; Mueller K.; Gross S., *Three-components organic- inorganic hybrid materials as protective coatings for wood: optimisation, synthesis, and characterisation*, Progress of Organic Coating, vol. 74, pp. 479–490, **2012**

- **Grexa** O.; Lubke H., *Flammability parameters of wood tested on a cone calorimeter, Polymer Degradation Stability*, vol. 74, pp. 427–432, **2001**
- **Guo** Z.; Liu W., *Biomimic from the Superhydrophobic Plant Leaves in Nature: Binary Structure and Unitary Structure*, Plant Science, vol. 172, pp. 1103 1112, **2007**

-H-

- **Hager** R., *Waterbone silicones as wood preservatives*, International Research Group on Wood Preservation, Doc. No IRG/WP 95-30062, **1995**

- **Hansen** M.; Jakobsen H.; Skibsted J., *^{29}Si Chemical Shift Anisotropies in Calcium Silicates from High-field 2^9Si MAS NMR Spectroscopy*, Inorganic Chemistry, vol. 42, pp. 2368−2377, **2003**

- **Harada** T., *Time to ignition, heat release rate and fire endurance time of wood in cone calorimeter test*, Fire Material, vol. 25, pp. 161–167, **2001**

- **Hardjito** D.; Rangan B.V., *Fly Ash-Based Geopolymer Concrete Develoment and properties of low-calcium fly ash-based geopolymer concret*, Research Report GC 1, **2005**

- **Haufe** H.; Thron A.; Fiedler D.; Mahltig B.; Böttcher H., *Biocidal nanosol coatings*, Surface Coatings International Part B: Coatings Transactions, vol. 88, pp. 55–60, **2005**

- **Havlínová** B.; Katuščák S; Petrovičová M; Maková A, *Study of mechanical properties of papers exposed to the different methods of accelerated ageing. Part I. Effect of heat and humidity on unprocessed papers*, Journal of Cultural Heritage, vol. 10, pp. 222-231, **2009**

- **He** C.; Makovicky E.; Osbæck B., *Thermal stability and pozzolanic activity of calcined kaolin*, Applied Clay Science, vol. 9, pp.165–18, **1994**

- **He** C.; Osbæck B.; Makovicky E., *Pozzolanic reactions of six principal clay minerals: activation, reactivity assesments and technological effects*, Cement and Concrete Research, vol. 25, pp. 1691–1702, **1995a**

- **He** C.; Osbæck B.; Makovicky E., *Thermal stability and pozzolanic activity of calcined illite*, Applied Clay Science, vol. 9, pp. 337–354, **1995b**

- **He** C.; Osbæck B.; Makovicky E., *Thermal stability and pozzolanic activity of raw and calcined mixed-layer mica/ smectite*, Applied Clay Science, vol. 17, pp. 141–16, **2000**

- **Heikal** M; Morsy S.M.; Aias I., *Effect of polycarboxylate superplasticizer on hydration characteristics of cement pastes containing silica fume*, Ceramics, vol 50, pp 5-14, **2006**

- **Heller-Kallai** L., *Thermally modified clay minerals*, In: Bergaya F., Theng B.K.G., Lagaly G. (Eds.), Handbook of clay science. Development in Clay science. Elsevier, Amsterdam, pp. 289–308, **2006**

- **Hill** C.A.S.; Cetin N.S.; Quinney R.F.; Derbyshire H; Ewen RJ, A*n investigation of the potential for chemical modification and subsequent polymeric grafting as a means of protecting wood against photodegradation,* Polymer Degradation Stability, vol. 72, pp. 133–139, **2001**

- **Hill** C.A.S; Farahani M.R.M, Hale M.D.C., The use of organo alkoxysiilane coupling agents for wood preservation, Holzforshung, vol. 58, pp. 318-325, **2004**

- **Hill** C.A.S., *Wood modification: chemical, thermal and other processes,* John Wiley & Sons, West Sussex, **2007**

- **Hook** R.J., *A ^{29}Si NMR study of the sol-gel polymerization rates of substituted ethoxysilanes*, Journal of Non-Crystalline Solids, vol. 195, pp. 1-15, **1996**

- **Hou** A.; Wang X.; Yu Y., *Preparation of the cellulose/silica hybrid containing cationic groups by sol–gel crosslinking process and its dyeing properties*, Carbohydrate Polymers, vol. 77, pp.201-205, **2009**

- **Hozumi** A.; Takai O., *Effect of hydrolysis groups in fluoro-alkyl silanes on water repellency of transparent two-layer hard-coatings*, Applied Surface Science, vol. 103, pp. 431–441, **1996**

- **Huang** S.I.; Shen Y.J.; Chen H., *Study on the hydrophobic surfaces prepared by two-step sol–gel process*, Applied Surface Science, vol. 255, pp. 7040–7046, **2009**

-J-

- **Jain** R.K.; Lal K.; Bhatnagar H.L., *Thermal degradation go cellulose and its phosphorylated profucts in air and nitrogen*, Journal of Applied Polymer Science, vol. 30, pp. 897–903, **2003**

- **Jennings** H. M., *Refinements to Colloid Model of CSH in Cement: CM-II*, Cement and Concrete Research, vol. 38, pp. 275−289, **2008.**

- **Johansson** K.; Larsson C.; Antzutkin,O.N.; Forsling W.; Kota H.R.; Ronin V., K*inetics of the Hydration Reactions in the Cement Paste with Mechanochemically Modified Cement 29Si Magic-Angle- Spinning NMR Study,* Cement and Concrete Research, vol. 29, pp. 1575−1581, **1999**

- **Jung** H.Y.; Gupta R.K.; Oh E.O.; Kim Y.H.; Whang C.M.; *Vibrational spectroscopic studies of sol-gel derived physical and chemical bonded ORMOSILs*, Journal of Non Crystalline Solids, vol. 351, pp. 372–379, **2005.**

-K-

- **Kakali** G.; Perraki T.; Tsivilis S.; Badogiannis E., *Thermal treatment of kaolin: the effect of mineralogy on the puzzolanic activity*, Applied Clay Science, vol. 20, pp. 73–80, **2001**

- **Kandelbauer** A.; Petek P.; Medved S.; Pizzi A; Teischinger A.; *On the perfomance of a melamine-urea-formaldehyde resin for decorative coatings*, European Journal of Wood and Wood Products, vol 68, pp 63-75, **2010**

- **Kannangara** D.; Shen W., *Liquid-paper interactions during liquid drop impact and recoil on paper surfaces; Colloids and Surfaces A: Physicochemical Engineering Aspects*, vol. 280, pp. 203-215, **2006**

- **Kannangara** D.; Zhang H.; Shen W., *Roughness effects of cellulose and paper substrates on water drop impact and recoil*, Colloids and Surfaces A: Physicochemical Engineering Aspects, vol. 330, pp. 151–160, **2008**

- **Kiguchi** M., *Chemical modification of wood in Japan:research and commercial applications*, Wood Science Digest, vol. 55, pp. 3-4, **1995**

- **Klemenčič** D.; Simončič B.; Tomašič B.; Orel B., *Biodegradation of silver functionalised cellulose fibres*, Carbohydrate Polymers, Vol. 80, pp 426–435, **2010**

- **Klibanov** A.M., *Permanently microbicidal materials coatings*, Journal of Material Chemistry, Vol. 17, pp. 2479–2482, **2007**

-L-

- **Larsson** P.T.; Hult E.L.; Wickholm; Pettersson E.; Iversen T., *CP/MAS13C-NMR spectroscopy applied to structure and interaction studies on cellulose I*, Solid State Nucl. Magn., vol. 15, pp. 31–40, **1999**

- **Le Saoût** G.; Lothenbach B.; Hori A.; Higuchi T.; Winnefeld, F., *Hydration of Portland Cement with Additions of Calcium Sulfoaluminates*, Cement and Concrete Research, vol. 43, pp. 81−94, **2012**

- **Lee** B.H., Kim H.S., Kim S., Kim H.J., Lee B., Deng Y., Feng Q, Luo J., *Evaluating the flammability of wood-based panels and gypsum particleboard using a cone calorimeter*, Construction Build Materials, vol. 25, pp.3044–3050, **2011**

- **Liao** Y.C.; Huang C.Y., *Effects of CaO addition on lightweight aggregates produced from water reservoir sediment*, Construction Building Materials, vol. 25, pp 2997–3002, **2011a**

- **Liao** Y.C.; Huang C.Y., *Effects of heat treatment on the physical properties of lightweight aggregate from water reservoir sediment*, Ceram. Int., vol. 37, pp. 3723–3730**, 2011b**

- **Lu** J.Z., Wu Q., McNabb H.S., *Chemical coupling in wood fiber and polymer composites: a review of coupling agents and treatments,* Wood Fiber Science, vol. 32, pp. 88–104, **2000**

- **Lukowsky** D.; Peek R.D.; Rapp A.O., *Water-based silicones on wood*, International Research Group on Wood Preservation, Doc. No. IRG/WP 98-40108, **1997**

-M-

- **MacKenzie** J.D.; Bescher E.; *Some Factors Governing the Coating of Organic Polymers by Sol-Gel Derived Hybrid Materials*, Journal of Sol-Gel Technology, vol. 27, pp. 7–14, **2003.**

- **Maggini** S.; Feci E., Cappelletto E.; Girardi F.; Palanti S.; Di Maggio R., *(I/O) hybrid alkoxysilane/zirconium-oxocluster copolymers as coatings for wood protection*, Applied Material Interfaces, vol. 4, pp.4871–4881, **2012.**

- **Mahltig** B.; Fiedler D.; Böttcher H., *Antimicrobial sol-gel coatings, Journal of Sol-Gel Science and Tecnology*, vol. 32, pp. 219-222**, 2004**

- **Mahltig** B.; Swaboda C.; Roessler A.; Bottcher H., *Functionalising wood by nanosol application*, Journal of Material Chemistry, vol. 27, pp. 3180–3192, **2008.**

- **Mai** C.; Militz H.; *Modification of wood with silicon compounds.Treatment systems based on organic silicon compounds. A review*, Wood Science Technology, vol. 37, pp. 453–461**, 2004.**

- **Maneerung** T.; Tokura S.; Rujiravanit R., *Impregnation of silver nanoparticles into bacterial, Carbohydrate Polymers*, vol.73, pp. 43-5, **2008.**

- **Martin** T.P.; Kooi S.E.; Chang S.H.; Sedransk K.L.; Gleason K.K., *Initiated chemical vapor deposition of antimicrobial polymer coarings, Biomaterials*, vol. 28, pp. 909-915, **2007.**

- **Matsuyama** H.; Young J., *Synthesis of Calcium Silicate Hydrate/Polymer Complexes: Part II. Cationic Polymers and Complex Formation with Different Polymers*. Journal of Materials, vol. 14, pp. 3389−3396, **1999**

- **Mendelovici** E.; *Comparative study of the effects of thermal and mechanical treatments on the structures of clay minerals*, Journal of Thermal Analysis, vol. 49, pp. 1385–1397, **1997**

- **Milea** C.A.; Bogatu C.; Duta A., *The influence of parameters in silica sol-gel process*, Bulletin of the Transilvania University of Brasov, Engineering Sciences,vol. 4, pp. 53-61, **2011**

- **Militz H.,** Beckers E.P.J., Homan W.J., *Modification of solid wood:research and pratical potential,* International Research Group on Wood Preservation, Doc. No. IRG/WP 97-40098, **1997**

- **Miyake** N.; Ando T.; Sakai E., *Superplasticized concrete using refined lignosulfonate and its action mechanism*, Cement and Concrete research, vol 15, pp 295-302**, 1985**

- **Moudrakovski** I.L.; Alizadeh R.; Beaudoi J.J., *Natural Abundance High Field 43Ca Solid State NMR in Cement Science*, Physical Chemistry Chemical Physics, vol. 12, pp. 6961−6969, **2010**

-N-

- **Nicholas** D.D, *Wood deterioration and its prevention by preservative treatments*, vol 1. Syracuse University Press, Syracuse, **1973**

- **Norimoto** M.; Hon D.N.S.; Shiraishi N., *Wood and cellulosic chemistry*, 2nd edn Dekker, pp. 573-598, **2001**

-O-

- **Oudadesse** A.C.; Derrien; Davidovits J., *MAS-NMR studies of geopolymers heat-treated for applications in biomaterials field*, Journal of Material Science, vol. 42, pp. 3092–3098, **2007**

-P-

- **Palanti** S.; Predieri G.; Vignali F.; Feci E.; Casoli A.; Conti E., *Copper complexes grafted to functionalized silica gel as wood preservatives against the brown rot fungus Coniophora puteana*, Wood Science Technology, vol. 45, pp. 707–718, **2011**

- **Palomo** A.; Macias A.; Blanco M.T.; Puertas F., *Physical, chemical and mechanical characterization of geopolymers*, Proc. 9th Cong. on 'Chemistry of cement', New Delhi, India, pp. 505-511, **1992**

- **Palomo** A.; Grutzeck M.W.; Blanco M.T., *Alkali-activated fly ashes a cement for the future*, Cement and Concrete Research, vol. 29, 1323–1329, **1999**

- **Panagiotopoulou** K. E.; Perraki T.; Kakali G, *Dissolution of aluminosilicate minerals and by-products in alkaline media*, Material Science, vol. 42, pp. 2967-2973, **2007**

- **Pardal** X.; Brunet F.; Charpentier T.; Pochard I.; Nonat A., *^{27}Al and ^{29}Si Solid-State NMR Characterization of Calcium-Aluminosilicate-Hydrate*, Inorganic Chemistry, vol.51, pp. 1827−1836, **2012**

- **Pellenq** R.J.M.; Kushima A.; Shahsavari R.; Vliet K.J.V.; Buehler M.J.; Yip S.; Ulm F.-J., *A Realistic Molecular Model of Cement Hydrates,* Proc. Natl. Acad. Sci. U.S.A., vol. 106, 16102− 16107, **2009**

- **Podgorski** L.; Chevet B.; Onic L.; Merlin A., *Modification of wood wettability by plasma and corona treatments*, International Journal of Adhesion and Adhesive, vol. 2, pp. 103–111**, 2000**

- **Porteneuve** C.; Zanni H.; Vernet C.; Kjellsen K.O.; Korb J.-P.; Petit D., Nuclear Magnetic Resonance Characterization of High and Ultrahigh-Performance Concrete: Application to the Study of Water Leaching, Cement and Concrete Research, vol. 31, pp. 1887−1893, **2001**

- **Puertas** F.; Santos H.; Palacios M.; Martínez-Ramírez S., *Polycarboxylate Superplasticiser Admixtures: Effect on Hydration,* Microstructure and Rheological Behaviour in Cement Pastes. Advanced Cement Research, vol. 17, pp. 77−89, **2005**

-R-

- **Rawal** A.; Smith B.J.; Athens G.L.; Edwards C.L.; Roberts L.; Gupta V.; Chmelka B. F., *Molecular Silicate and Aluminate Species in Anhydrous and Hydrated Cements*, Journal of American Chemical Society, vol. 132, pp. 7321−7337, **2010**

- **Richardson** I.G., *The Nature of the Hydration Products in Hardened Cement Pastes*, Cement and   Concrete Composite, vol. 22, pp. 97−113, **2000**

- **Ridi** F.; Fratini E.; Milani S.; Baglioni P., *Near-Infrared Spectroscopy Investigation of the Water Confined in Tricalcium Silicate Pastes,* Journal of Physical Chemistry B, vol. 110, pp. 16326−16331, **2006**

- **Ridi** F.; Luciani P.; Fratini E.; Baglioni P., *Water Confined in Cement Pastes as a Probe of Cement Microstructure Evolution*, Journal of Physical Chemistry B, vol. 113, pp. 3080−3087, **2009.**

- **Ridi** F.; Fratini E.; Baglioni P., Cement: A Two Thousand Year Old Nano-colloid, Journal of Colloid Interface Science, vol. 357, pp. 255−264, **2011**

- **Rottstegge** J.; Wilhelm M.; Spiess H.W., *Solid State NMR Investigations on the Role of Organic Admixtures on the Hydration of Cement Pastes*, Cement and Concrete Composite, vol. 28, pp. 417−426, **2006**

- **Sabir** B.B.; Wild S.; Bai J., *Metakaolin and calcined clays as pozzolans for concrete: a review*, Cement and Concrete Composites, vol. 23, pp. 441–454, **2001**

- **Saka** S.; Sasaki M.; Tanahashi M., W*ood-inorganic composites prepared by the sol-gel process I. Wood-inorganic composites with porous structure*, Mokuzai Gakkaishi, vol. 38, pp. 1043-1049, **1992**

- **Sakai** E.; Yamada K.; Ohta A., *Molecular structure and dispersion-adsorption mechanism of comb-type superplasticizers used in Japan*, Journal of Advance Concrete Technology, vol. 1, pp16-25, **2003**

- **Salgaonkar** L.P.; Jayaram R.V., *Thermal and flame-retardant properties of polyester fabric grafted with polyanilines*, Journal of Applied Polymer Science, vol. 93, pp. 1981–1988, **2004**

- **Satoh** K.; Urban M.W., *Stratification of polysiloxanes at the film-air and film-substrate interfaces in silicone-modified acrylic coatings; an ATR FT-IR spectroscopic study*, Progress of Organic Coating, vol.29, pp. 195–199, **1996**

- **Schmidt** H., *Chemistry of material preparation by sol-gel process, Journal of Non-Crystalline Solids*, vol.100, pp. 51-64, **1988.**

- **Sebe** G.; Brook M., *Hydrophobization of wood surfaces: covalent grafting of silicone polymers*, Wood Science and Technology, vol. 35, pp. 269-282, **2001**

- **Shahraki** B.K.; Mehrabi B.; Gholizade h K.; Mohammadinasab M., *Thermal behavior of calcite as expansive agent*, Journal of Mining and Metallurgy B, vol. 47B, pp. 89–97, **2011**

- **Sheen** Y.C.; Chang W.H.; Chen W.C.; Chang Y.H.; Huang Y.C.; Chang F.C., *Non-Fluorinated Superamphiphobic Surfaces Through Sol–Gel Processing of Methyltriethoxysilane and Tetraethoxysilane,* Journal of Material Chemistry and Physics, vol. 114, pp. 63-68, **2009.**

- **Schmücker** M.; MacKenzie K.J.D., *Microstructure of sodium polysialate siloxo geopolymer*, Ceramics International, vol. 31, pp. 433–437, **2005**

- **Shultz** T., et al., *Development of commercial wood preservatives,* ACS Symposium Series, American Chemical Society, Washington DC, **2008**

- **Skibsted** J.; Hall C., Characterization of Cement Minerals, *Cements and Their Reaction Products at the Atomic and Nano Scale*, Cement and Concrete Research, vol. 38, pp. 205−225, **2008**

- **Sobolev** K., *The effect of complex admixture on cement properties and development of a test procedure for the evaluation of high strength cement,* Advances in cement research, vol. AC15, pp 65-75, **2003**

- **Sobolev** K., *Mechano-chemical modification of cement with high volume of blast furnace slag*, Cement e Concrete Composites, vol. 27, pp 848-853, **2005**

- **Son**Y.A.; Kim B.S.; Ravikumar K.; Lee S.G., *Imparting durable antimicrobial properties to cotton fabrics using quaternary ammonium salt through a 4-aminobenzenesulfonic acid-chloro-triazine adduct*, European Polymers Journal, vol. 42, pp. 3059-3067, **2006**

- **Stejskal** J.; Trchova M.; Sapurina I., *Flame-retardand effect of polyaniline coating deposited on cellulose fibers, Journal of Applied Polymer Science*, vol. 98, pp. 2347–2354, **2005.**

-T-

- **Tang** C.W.; Chen H.J.; Wang S.J.; Spaulding J.; *Production of synthetic lightweight aggregate using reservoir sediments for concrete and masonry*, Cement and Concrete Composite, vol. 33, pp. 292–300**, 2011**

- **Taylor** H.F.W.; *Hydrated Calcium Silicates. Part I. Compound Formation at Ordinary Temperatures*; „Journal of the Chemical Society, pp. 3682−3690, **1950**

- **Temiz** A.; Terziev N.; Jacobsen B., *Weathering, water absorption, and durability of silicon, acetylated, and heat-treated wood*, Journal of Applied Polymer Science, vol. 102, pp. 4506-4513, **2006**

- **Tyagi** B.; Chudasama C.D.; Jasra R.V.; *Determination of structural modification in acid activated montmorillonite clay by FT-IR spectroscopy*, Spectrochim. Acta A, vol. 64A, pp. 273–278, **2006**

- **Trey** S.M.; Netrval J.; Berglund L.; Johansson M.; *Electron-beam-initiated polymerization of poly(ethylene glycol)-based wood impregnants*, Applied Material Interfaces, vol. 2, pp. 3352–3362, **2010**

- **Trey** S.M.; Jafarzadeh S.; Johansson M.; *In situ polymerization of polyaniline in wood veneers*, Applied Material Interfaces, vol. 4, pp.1760–1769, **2012.**

- **Tritt-Goc** J.; Pisĺewski N.; Kosćielski S.; Milia F., *The Influence of the Superplasticizer on the Hydration and Freezing Processes in White Cement Studied by 1H Spin-lattice Relaxation Time and Single Point Imaging*, Cement and Concrete Research, vol. 30, pp. 931−936, **2000**

- **Tsai** Y.L.; Hanna J.V.; Lee Y.L.; Smith M.E.; Chan J.C.C., *Solid-state NMR study of geopolymer prepared by sol–gel chemistry*, Journal of Solid State Chemistry, vol. 12, pp. 3017-3022, **2012**

-V-

- **Van Jaarsveld** J.G.S.; Van Deventer J.S.J., *Effect of the alkali metal activator on the properties of fly-ash-based geopolymers*, Industrial Engineering Chemistry Research, vol. 38, pp. 3932–3941, **1999**

- **Verdolotti** L.; Iannace S., *Geopolymerization reaction to consolidate incoherent pozzolanic soil*, Journal of Material Science, vol. 43, pp. 865-873, **2008**

- **Vicini** S.; Princi E.; Luciano G.; Franceschi E.; Pedemonte E.; Oldak D.; Kaczmarek H.; Sionkowska A., *Thermal analysis and characterisation of cellulose oxidised with sodium methaperiodate*, Thermochimica Acta, vol. 418, pp. 23–130, 2**004**

-W-

- **Wang** R.; Li X.-G.; Wang P.-M., *Influence of Polymer on Cement Hydration in SBR-modified Cement Pastes*, Cement and Concrete Research, vol. 36, 1744−1751, **2006**

- **Wickholm** K.; Larsson P.T.; Iversen T., *Assignment of non-crystalline forms in cellulose I by CP/MAS ^{13}C-NMR spectroscopy*, Carbohydrate Research, vol. 312, pp. 123-129, **1998**

- **Winnefeld** F.; Becker S.; Pakusch J.; Götz T., *Effects of the Molecular Architecture of Comb-Shaped Superplasticizers on Their Performance in Cementitious Systems*, Cement and Concrete Composite, vol. 29, pp. 251−262, **2007**

-X-

- **Xu** H.; Deventer J.S.J.; *The geopolymerisation of alumino-silicate minerals. International Journal of Mineral Processing*, vol. 59, pp. 247–266, **2000**

- **Xu** H.; Van Deventer J.S.J., *Geopolymerisation of multiple minerals*, Minerals Engineering, vol. 15, pp. 1131-1139**, 2002**

- **Xu** F.; Ding H.; Tejirian A., *Detrimental effect of cellulose oxidation on cellulose hydrolysis by cellulsase*, Enzyme Microbial Technology, vol. 45, pp.203–209, **2009**

- **Xie** K., Yu Y., Shi Y., *Synthesis and characterization of cellulose/silica hybrid materials with chemical cross linking*, Carbohydrate Polymers, vol. 78, pp.799–805, **2009**

-Y-

- **Yamagushi** Y., *Low molecular weight silicic acid-inorganic compound complex as wood preservative*, Wood Science and Technology, vol. 36, pp. 399-417, **2002**

- **Yoshiola** K.; Sakai E.; Daimon M.; Kitahara A., *Role of steric hindrance in the perfomance of superplasticizer for concrete*, Journal of American Ceramic Society, vol. 80, pp 2667-2671**, 1997**

- **Yousuf** M.; Mollaht A.; Padmavathy Palta; Hess T.R.; Vempati R.K.; Cockef D., C*hemical and physical effect of sodium lignosulfonate superplsticizers of the hydration of Portland cement and solidification/stabilization consequences*, Cement and Concrete research, vol. 25, pp 671-682, **1995**

- **Yu** P.; Kirkpatrick R.; Poe B.; McMillan P.; Cong X., *Structure of Calcium Silicate Hydrate (C-S-H): Near-, Mid-, and Far-Infrared Spectroscopy,* Journal of American Ceramic Society, vol. 82, pp. 742−748, **1999**

-Z-

- **Zhang** D.F.; Ju B.Z.; Zhang S.F.; He L.; Yang J.Z., *The study on the dispersing mechanism of starch sulfonate as a water-reducing agent for cement*, Carbohydrate Polymers, vol. 70, pp 363-368, **2007**

- **Zibouche** F.; Kerdjoudj H.; d'Espinose de Lacaillerie J-B.; Van Damme H., Geopolymers from Algerian metakaolin. Influence of secondary minerals, Applied Clay Science, vo. 43, pp. 453-458, **2009**

- **Ziegler** I.M.; Marosi G.; Matko` S.; Horvolgyi Z.; Toth A., *Silylation of wood for potential protection against bio-degradation. An ATR-FTIR, ESCA and contact angle study*, Polymer Adv. Technology, vol. 14, pp. 790–795, **2003**

- **Ziegler** I.M.; Oszlanczi A.; Somfai B.; Horvolgyi Z.; Paszli I.; Holmgren A.; Forsling W., *Surface free energy of natural and surface-modified tropical and European wood species*, Journal of Adhesion Science Technology, vol. 18, pp. 687–713, **2004**

- **Ziegler** I.M.; Horvolgyi Z.; Toth A.; Forsling W.; Holmgren A., *Wettability and spectroscopic characterization of silylated wood samples*, Polymer Adv. Technology, vol. 17, pp. 932–939, **2006**
- **Ziegler** I.M.; Tanczos I.; Horvolgyi Z.; Agoston B., *Water-repellent acylated and silylated wood samples and their surface analytical characterization*, Colloids Surface A Physicochem Engineering Aspects, vol. 319, pp. 204–212, **2008**

- **Zingg** A.; Winnefeld F.; Holzer L.; Pakusch J.; Becker S.; Gauckler L., *Adsorption of Polyelectrolytes and Its Influence on the Rheology, Zeta Potential, and Microstructure of Various Cement and Hydrate Phases*, Journal of Colloid Interface Science, vol. 323, pp. 301−312, **2008**

- **Zingg** A.; Winnefeld F.; Holzer L.; Pakusch J.; Becker S.; Figi R.; Gauckler L., *Interaction of Polycarboxylate-Based Superplasticizers with Cements Containing Different C_3A Amounts,* Cement and Concrete Composite, vol. 31, pp. 153−162, **2009**

CHAPTER V

PUBLICATIONS and CONGRESS PARTECIPATION

SCIENTIFIC PUBBLICATION

- E. **Cappelletto**, Callone, Emanuela; Campostrini, Renzo; Girardi, Fabrizio; Maggini, Simona; Volpe, Claudio; Siboni, Stefano; Di Maggio, Rosa, Hydrophobic siloxane paper coatings: the effect of increasing methyl substitution, J.Sol-Gel Tech., June 2012, 441-452

- E. **Cappelletto**, F. Girardi, B. Tessadri, G. Bochiccio, R. di Maggio, Wood surface protection with different alkoxysilanes: a hydrophobic barrier, Cellulose, September 2013

- E. **Cappelletto**, S. Borsacchi, M. Geppi, F. Ridi, E. Frattini, P. Baglioni, Comb-Shaped Polymers as Nanostructure Modifiers of Calcium Silicate Hydrate: a 29Si Solid-State NMR Investigation, Journal of Physical Chemistry C, October 2013

- B. Liguori, C. Ferone, I. Capasso, F. Colangelo, R. Cioffi, E. **Cappelletto**, R. di Maggio, Thermally treated clay sediments as geopolymer precursors, Applied Clay Science, *submitted*.

- F. Girardi, E. **Cappelletto**, J. Sandak, G. Bochicchio, B. Tessadri, S. Palanti, E. Feci and R. Di Maggio, Hybrid organic-inorganic coatings for protecting wood, Organic Coatings, under review

- F. Girardi, S. Maggini, C. Della Volpe, E. **Cappelletto**, K. Mueller, S. Siboni, R. Di Maggio, Hybrid organic–inorganic materials on paper: surface and thermo-mechanical properties, J.Sol-Gel Tech., August 2013; 60(3)

- S. Maggini, E. **Cappelletto**, F. Girardi, W. Vaona, R. Di Maggio, Cellulose nanocomposites based on silane reinforced 3-butynoate-substituted zirconium-oxocluster copolymers: Mechanical, thermal and hydrophobic properties, Organic Coatings 76(1), September 2012, 173-180

- S. Maggini, E. **Cappelletto**, R. Di Maggio, High Temperature Resistant Silane/Zirconium-Oxocluster Hybrid Copolymers Containing "Free" Thiol/Ene Functionalities in the Polymer Matrix, Applied Materials & Interfaces, May 2012, 2435-2441

- S. Maggini, E. Feci, E. **Cappelletto,** F. Girardi, S. Palanti, R. Di Maggio, (I/O) hybrid alkoxysilane/zirconium-oxocluster copolymers as coatings for wood protection., Applied Materials & Interfaces September 2012; 4(9): 4871-81

- B. M. Tofanica, E. **Cappelletto**, D. Gavrilescu, K. Mueller, Properties of Rapeseed (Brassica napus) Stalks Fibers, Journal of Natural Fibers; 8(4):241-262, 2011

CONGRESS PARTICIPATION

E. Callone, E. Cappelletto, R. Campostrini, C. Della Volpe, K. Mueller, **Production and characterization of protective coatings for paper based on siloxane mateix obtained via sol gel route**, 3° Forum Nazionale Giovani Ricercatori di Scienza e Tecnologia dei Materiali, 22-24 March 2010, Padova, Italy (Poster)

E. Cappelletto, E. Callone, C. Della Volpe, R. Campostrini, S. Siboni, K. Mueller, **Rivestimenti protettivi ed ecocompatibili per materiali a base di cellulosa (carta e legno),** IV convegno Monitoraggio e conservazione preventiva dei Beni Culturali, 27-29 May 2010, Cassino, Italy (Oral Presentation)

E. Cappelletto, Klaus Müller, Emanuela Callone, Renzo Campostrini, **Hydrophobic silica-based coating for cellulosic materials: paper and wood**, E-WISPOC (EuropeanWinter School Physical Organic Chemistry), 30 Jenuary- 4 February 2011, Bressanone, Italy (Poster and short oral presentation)

E. Cappelletto, R. Di Maggio, **Self-assembled based monolayers for the modification of paper and wood surfaces,** 14th International Union of Pure and Applied Chemistry Conference on Polymers and Organic Chemistry (POC 2012), 6-9 January 2012, Doha, Qatar (Poster)

E. Cappelletto, R. di Maggio, **A systematic investigation on organofunctional silanes for surface treatment of paper**, VIII Italian Sol-Gel Workshop, 21-22 June 2012, Trento, Italy (Oral Presentantion).

E. Cappelletto, R. di Maggio, **Surface modification of wood with functionalized alkoxisilanes**, COST Action FP1006, 25 – 27 April 2012, Kuchl/Salzburg, Austria (Oral Presentation)

E. Cappelletto, L. Bergamonti, C. Graiff, G. Predieri, R. di Maggio, **NMR Investigation of functionalized (PAA)s**, XIL National Congress on Magnetic Resonance, 17-19 September 2012, Pisa, Italy (Poster).

CHAPTER VI

ACKNOWLEDGEMENTS

I would like to thank all people who supported me in different ways during the elaboration of this thesis.

First of all I want to thank Prof. Dr. Klaus Müller for all the support he gave me from the very beginning of my work, but also for his encouragements and advices during the little time I could work together with him.

I would like to express my utmost gratitude and appreciation to my advisor, Prof. Rosa di Maggio, for giving me the opportunity to continue this research. It is mainly due to her help that I was able to finish my thesis in a good way. She has been a great teacher and a wonderful person, I am pleased to have worked with her for the last years.

I would like to thanks my colleagues (and not only) Fabrizio and Wilma for their assistance and guidance in laboratory.

My sincere thanks go to Prof. Sandra Dirè and Dr. Emanuela Callone (Klaus Müller NMR Lab) for giving me the possibility to use the instruments.

Part of this work was performed in collaboration with Marco Geppi at the University of Pisa. He offered me a unique opportunity and a precious contribution to improve my knowledge on Solid State NMR. I would like to thanks also Silvia, Elisa and Francesca. They made me feel part of the group since day one.

Thousand thanks to my friends who supported me since ever and made my life more enjoyable especially during of my PhD: Matteo S., Claudia, Amaia, Thiago, Matteo T., Alexia, Eleonora, Michele, Marta, Lorenzo, "the guys of smarz cup" and many others. A special thanks to Stefania who bears (like a bear) and supports me always.

Last but not least, thanks to my family, Mom, Dad, Martina, Cristian and grandmothers. Thanks for all that you have done, none of this would have possible without you. I love you all.